Title

A Genetic and Genomic Perspective on the Microbiology and Distribution of Dissimilatory Iodate Reducing Microorganisms

Author

Reyes Umana, Victor Manuel

Publication Date

2021

Peer reviewed|Thesis/dissertation

A Genetic and Genomic Perspective on the Microbiology and Distribution of Dissimilatory Iodate Reducing Microorganisms

By

Victor Manuel Reyes-Umaña III

A dissertation submitted in partial satisfaction of the

requirements for the degree of

Doctor of Philosophy

in

Microbiology

in the

Graduate Division

of the

University of California, Berkeley

Committee in charge:

Professor John D. Coates, Chair
Professor Matthew Traxler
Professor Robert Rhew

Fall 2021

Abstract

A Genetic and Genomic Perspective on the Microbiology and Distribution of Dissimilatory Iodate Reducing Microorganisms

By

Victor Manuel Reyes-Umaña III

Doctor of Philosophy in Microbiology

University of California, Berkeley

Professor John D. Coates, Chair

Iodine plays a largely unrecognized yet essential function in the history of life globally. It is the 53rd most common element in Earth's crust and one of the heaviest biologically relevant elements for animals and marine plants. While some iodine is present in terrestrial environments, it is generally enriched in marine ecosystems. In these environments, it is engaged in a prolific biogeochemical cycle, oscillating through multiple distinct oxidation states depending on the location and chemistry of the environment. The most common forms found are its most oxidized form (IO_3^-) and reduced forms like iodide (I^-) and volatile organic iodines (VOI). Emerging evidence demonstrates that algae produce VOIs, which play an essential role in regulating climate at a local level. These VOIs impact climate by destroying tropospheric ozone, resulting in greater albedo (from cloud formation) and reduced radiative forcing. Numerous studies examining the iodine geochemical cycle exist; however, many stop short of describing the biological contribution to the observed geochemical phenomena. This dissertation opens by expanding on the current knowledge surrounding the iodine geochemical cycle. It describes the genetic toolkit certain microorganisms use to interact with iodine at different redox states and proposes a role for these microorganisms based on their presence globally. The story then shifts focus to a hitherto poorly characterized group of bacteria known as dissimilatory iodate reducing microorganisms (DIRM). I examine the physiology of these microorganisms by demonstrating their ability to grow on IO_3^- as the sole terminal electron acceptor. I show that this phenotype is enabled by a mobile genetic element known as the iodate reduction island (IRI) and demonstrate its distribution among numerous bacterial phyla. I conclude this dissertation by examining the geochemical variables associated with DIRM habitats and exploring various marine and non-marine environments where DIRM are expected to live. In its totality, this work seeks to demonstrate that DIRM are a ubiquitous class of microorganisms that derive energy from IO_3^- reduction and contribute to global iodine cycling in the process.

Dedication

This dissertation is dedicated to the next generation of scientists, and everyone who provided inspiration, love, and support throughout this journey.

Esta disertación está dedicada a la próxima generación de científicos, y a todos quienes sirvieron de inspiración, y a los quien me han apoyado con su cariño a lo largo de esta experiencia.

Cette dissertation est dédiée à la prochaine génération de scientifiques, et toutes les personnes qui m'ont aidé avec leur amour et leur soutien dans tout mon voyage.

أُود أن أكرِّس هذه الأطروحة للجيل القادم من العلماء ولجميع الأشخاص الذين دعموني بحبهم و وزودوني بالإلهام خلال هذه الرحلة العلمية

Crescat scientia vita excolatur

Table of Contents

Table of Figures

Abbreviations/Definitions

DIR—Dissimilatory iodate reduction/reducing
DIRM—Dissimilatory iodate reducing microorganisms
VOI—Volatile organic iodine
I^-—Iodide ion
I_2—elemental iodine
HOI—Hypoiodous acid
IO_3^-—Iodate ion
IRI—Iodate Reduction Island
MBL—marine boundary layer
DMSO—Dimethylsulfoxide
DMSOR—Dimethylsulfoxide oxidoreductase
MBL—marine boundary layer
VHP—vanadium haloperoxidase
Idr—IO_3^- reductase
Cld—chlorite dismutase
MAG—Metagenome assembled genome
HMM—hidden Markov model

Preface

To acquaint the reader with the intricacies of the iodine cycle, the **FIRST CHAPTER** of this dissertation opens with an abridged history of iodine and the early work done to understand its essentiality in human health. I discuss research from the 20th century that established our current understanding of the iodine cycle and its ubiquity in the environment. As a corollary, I delve into the early research describing the biological mechanisms potentiating the iodine biogeochemical cycle. It is from here where our story begins. I emphasize the biology and distribution surrounding a novel class of microorganism known as DIRM. Before writing this dissertation, only one DIRM had been vaguely described in the literature; it represented an enigmatic class of organism hypothesized to reduce IO_3^- to I^- in the environment.

The **SECOND CHAPTER**, which includes part of a **published** article, embarks on a journey to explore the paucity of DIRM in the literature. I begin by isolating *Denitromonas* sp. IR-12, a novel DIRM from a tidal mud flat enrichment from the Berkeley Marina. I describe the isolation process for this DIRM and establish a framework upon which new DIRM can be isolated. I conduct numerous experiments to assess the organism's physiology, learn about the energetics of DIR, and investigate the co-factors enabling the metabolism. I then proceed by describing the genes composing the iodate reductase and demonstrate their mobility across a taxonomically diverse cohort of *Proteobacteria*. The chapter then delineates the distribution of the iodate reduction island (IRI) among several organisms and proposes these organisms as putative DIRM. Future researchers may use this list as a starting point in verifying whether putative DIRM from culture collections grow by DIR. This chapter addresses several knowledge gaps surrounding the nutrient requirements and distribution of DIR as well. More importantly, it defines the metabolism as dependent on the presence of genes on this mobile genomic island.

The **THIRD CHAPTER** takes a closer look at the genetic mechanisms potentiating DIR. I begin by describing the curation of a genetic system in the model DIR organism *Denitromonas* sp. IR-12. I leverage several molecular biology tools to develop a set of targeted knockouts and demonstrate the essentiality of four core genes on the IRI to enable DIR. I demonstrate that these four genes form a core component of the IRI, each being necessary to enable DIR. These data also allow me to propose a model by which DIR occurs, and it unlocks multiple avenues upon which future scientists can explore the minutiae of DIR chemistry. While this chapter does not conclusively describe the function of all the genes composing the iodate reductase, it lays the framework upon which future research into this topic may build.

A lingering question stemming from the previous chapters is: Where do dissimilatory iodate reducing bacteria live? The fourth chapter, which includes part of a **published** article, addresses this question by gleaning information from taxonomic descriptions to paint an ecological portrait of DIRM as symbionts of coastal marine fauna and flora. However, with the dawn of metagenomics over the past several decades, I unlatched a treasure trove of data and searched for the presence of DIRM across multiple global environments. I ultimately identify multiple environments where DIRM may persist and describe the biogeochemistry of one of these environments in detail. I demonstrate that DIRM are overrepresented in metagenomes arising from marine environments and propose an ecological model for DIR in these environments.

While I established that DIR predominates in marine environments, the **FIFTH CHAPTER** expands on the observation that some DIRM are present in freshwater environments. I open by

describing *Aromatoleum toluclasticum* sp. TC-10, which was isolated from a freshwater creek in San Gregorio, California. I characterize *A. toluclasticum* sp. TC-10 as a DIRM and show that the IRI is present in its genome. When I compare *A. toluclasticum* sp. TC-10 to the type strain *A. toluclasticum* sp. MF63, I show the latter does not reduce iodate nor grows by DIR. Investigating DIR in *A. toluclasticum* provides the opportunity to delineate the boundaries of the IRI and identify the core genes and accessory genes on the genomic island. I also present the third cultured DIRM and the first isolate arising from a freshwater environment. This chapter provides confirmatory evidence that DIRM also exist in specific freshwater environments, and it expands the potential ecosystems where researchers can identify DIRM.

I **CONCLUDE** by describing how the data collected during this dissertation has enhanced our understanding of iodate respiration in bacteria. I expand on the known types of dedicated bacterial metabolisms by presenting a new class of organisms growing on IO_3^- as a terminal electron acceptor. I demonstrate the distinctiveness of DIR and describe how future protein biochemists can leverage the results of our genetic screen. I explore how the distribution of the IRI and DIRM may impact iodine biogeochemistry and discuss how future research can parameterize the results from this dissertation into iodine cycling models. While our understanding of iodate respiration is at its infancy, this dissertation seeks to provide the foundation for others to learn why and how the metabolism came to exist.

EXCURSUS

While writing the publication Genetic and phylogenetic analysis of dissimilatory iodate-reducing bacteria identifies potential niches across the world's oceans, a reviewer brought to my attention that the genus *Denitromonas* was not validly published. Therefore, this dissertation includes an addendum describing the genus *Denitromonas*.

Agradecimientos/Acknowledgements

Me gustaría comenzar con agradeciendo a toda mi familia. A mi padre, Víctor Manuel Reyes-Umaña, por todo su apoyo. Usted ha sido una inspiración para mí, desde el principio. Siempre me leías libros sobre química y ciencia y me inculcaste la pasión por la investigación y un amor por lo lindo de nuestra vida. A mi mamá, por enseñarme cómo ser una buena persona y cómo prosperar en mi vida. Usted siempre está a mi lado ayudándome, y apoyándome con su cariño. Mis abuelos, María Alicia Umaña, Trinidad Alas Aguilar y Víctor Manuel Alas. Aunque ya no están aquí, siempre admiré todo el cariño y apoyo que me dieron, y no hubiera hecho esto sin ustedes. Los extraño bastante, y siempre andan conmigo en mi corazón. And to my brother Luis Edgardo Reyes-Umaña, thanks for always being around and for being a great younger brother for me. We have been through a lot together, and I am fortunate to have you as my brother. I also would like to thank my best friend and partner Tiffany Ann Quach for all your love and support these five years. You have always been there to support me and provide a helping hand when the times get tough at work. You are caring and understanding at how difficult this process can be, and I am forever grateful and appreciative for the patience and encouragement you have provided. Querida familia, con todo su apoyo, le eché ganas a esto, ¡y lo logré! Sin ustedes no estaría aquí.

This dissertation would also not have been possible without all the professional support I have received along the way. I would love to thank my professional and industry mentors Tahar Ait-Ali, William Throndset, Bob Kuczenski. You were all highly supportive over the years, and your belief in me inevitably inspired me to seek new opportunities and return to graduate school. Likewise, I would like to thank my Ph.D. advisor, John D. Coates, for all your support throughout this project. I am forever grateful for the opportunity to research this project in your lab and for all the help you provided along the way.

Similarly, I would like to thank all the members of the Coates Lab: Hans Carlson, Anna Engelbrektson, Yi Liu, Tyler Barnum, Sophia Ewens, Maggie Stoeva, Anchal Mehra, Ouwei Wang, Israel Figueroa, Kyle Metcalfe, and David Meier. The past five years were great, and your support at every step along the way was a source of power. You all helped me persevere even on the hardest of days. Likewise, many thanks to Arash Komeili, Mitchell Thompson, Hector Trujillo, and Carson Bickley, who were all indispensably supportive with their advice and guidance on genetics. To my undergraduate mentees: Rachael Peng, Kristina Lee, Javier Cabrales, Dylan Dang, and Mariana Shalit, thank you so much for all the work and effort you put into this project. With your support, we were able to really build something cool, and learn a lot in the process. A special thanks to Jessica Kretschmer and Zachary Henning for providing your indispensable support throughout the COVID-19 pandemic. It was a truly difficult time working in the lab with all the restrictions, but we were able to push through it.

I want to thank the National Science Foundation for providing support for this dissertation through the Graduate Research Fellowship Program (Base Award: DGE1752814). The funding you provided allowed me to explore a topic I have come to love; I am forever grateful. To the PMB community, thanks for being around and providing such a supportive environment, it's been a blast getting to know everyone. To my close friends from my other walks of life, thanks for your support and understanding throughout this process, I've been fortunate to have you all close by. Y últimamente, espero que esto inspire a mi pueblo salvadoreño a que persiguen las cosas nuevas, exploran lugares nuevos, y experimentan con las ideas extravagantes.

Chapter One: Re-examining the global iodine cycle: An investigation of emerging iodine metabolisms

Abstract

Since the discovery of iodine in 1811 by Barnard Courtois, researchers have learned a lot about its biological significance to humans and other organisms. Unlike other elements, iodine persists almost exclusively in marine environments. Across the world's oceans, nearly 95% of iodine persists as iodate (IO_3^-) and must be reduced to iodide (I^-) to become bioavailable. Once reduced, iodine bioaccumulates in kelp to produce several volatile iodine species (VOIs). These VOIs, in turn, form aerosols at the marine boundary layer and contribute to the destruction of tropospheric ozone (a greenhouse gas). Early research into the iodine cycle often suggested a biological component but never thoroughly explained the impact of microorganisms on iodine mobilization. Emerging evidence demonstrates that diverse taxa actively participate in the iodine cycle, facilitating iodide oxidation, iodate reduction, and hydrocarbon iodination in marine environments. This work seeks to define the controls on iodine metabolisms and the microbial physiology, biogeography, enzymology, and microbial ecology of the iodine cycle. This chapter discusses the recent advances in iodine biogeochemistry research, emphasizing the biological mechanisms influencing marine biogeochemical processes. I discuss the current biological evidence behind phenomena such as the chemical disequilibrium of iodide/iodate in seawater and the microbial potential to produce VOI compounds. I also explore the current knowledge on the biochemistry and genetics of metabolic processes involving iodine compounds. Lastly, I examine emerging evidence on the impact of iodine on global climate and explore the role of microorganisms in iodine geochemistry.

1.1 History of iodine

Iodine (as ^{127}I) is the heaviest stable element of biological importance and an essential component of the human diet because of its role in thyroxine hormone production in most vertebrates[1-3]. Knowledge surrounding the effects of iodine dates back to the ancient Chinese who used burnt sponge and seaweed to treat goiter[4]. Although elemental iodine remained undiscovered, European scholars like Hippocrates and Galen prescribed similar suggestions to treat goiter, presumably adopting ancient Chinese medicine[4]. The pure element was discovered incidentally by the French scientist Bernard Courtois in 1811 while purifying potassium nitrate from seaweed. Initially believed to be a manifestation of either chlorine or oxygen, chemists Joseph Louis Gay-Lussac and Humphrey Davy separately confirmed that iodine was a new element in 1813[4,5]. By 1819, Andrew Fyfe, a lecturer at the University of Edinburgh, and the Swiss physician Jean François Coindet separately observed iodine accumulation in sea sponges and seaweed ash. Notably, Coindet made the crucial connection that a tincture of pure iodine significantly reduced the size of goiters[6]. News of health benefits linked to iodine supplementation led to a natural interest in the geochemistry of the element. French scientist Gaspard Adolphe Chatin first studied the distribution of iodine in the environment. He observed iodine in numerous freshwater plants and noticed a lack in goiter-endemic areas, allowing him to link iodine insufficiency to goiter[7]. As evidence linking iodine to human health emerged, the League of Nations established institutions like the World Health Organization to monitor global iodine prevalence[8]. The dawn of the atomic era further encouraged scientists to understand the health implications of radioiodine[9] by examining the global iodine cycle for radioiodine mobility[10-12]. Such research prefaced studies demonstrating the impacts of marine iodine on cloud formation and climate[13,14]. These studies revealed the importance of the iodine cycle in regulating climate and examined a previously underappreciated aspect of the global climate[15-17].

1.2 Iodine in nutrition

In mammals, iodine is involved in the synthesis of thyroid hormones like thyroxine and triiodothyronine[2]. These hormones regulate metabolism throughout the body, and their dysregulation may cause numerous metabolic disorders[3]. At the dawn of the atomic age, a rise in health concerns surrounding radioactive iodine isotopes (^{131}I and ^{129}I) prompted the investigation of mechanisms involved in the fate and transport of iodine[18]. Of significant concern is the ^{131}I radioisotope, which undergoes beta decay with a half-life of ~8 days[19]. Sub-acute exposures to ^{131}I pose a significant thyroid cancer[20] risk through contact with aerosols or contaminated food[12], especially in the days following the inadvertent release of nuclear materials such as those associated with Chernobyl or Fukushima Daiichi[12]. While management practices mitigate short-term ^{131}I risk, the ^{129}I radioisotope poses a chronic issue due to its longer half-life of 15.7 million years[21]. ^{129}I is strictly anthropogenic and has remained relatively rare throughout Earth's 4.5 billion year history[22]. However, since the beginning of the atomic era, the inadvertent release of ^{129}I by nuclear reprocessing has added a significant amount of radioiodine to the environment, resulting in the highest $^{129}I/I$ ratios ever observed.

Despite the effects of iodine on human health, relatively little is known about the natural iodine biogeochemical cycle. It is unique amongst elemental cycles and exists almost entirely in marine and marine-proximal environments (Figure 1.1), where it is predominantly found as either IO_3^- or I^-. It is highly soluble and variably sorbed onto soils or sediments, and, in the absence of any biological interactions, its mobility and fate are primarily influenced by environmental hydrology resulting in iodine accumulation in oceans[23,24]. Due to its antioxidant properties, iodine (as I^-) is often bioconcentrated in algae and marine life by several orders of magnitude above seawater levels (450-600 nM). For example, *Laminaria digitata* is one of many kelp species known to bioconcentrate iodine and accumulate up to 50 mM I^-[25]. Similarly, marine sediments rich in organic matter also accumulate iodine at concentrations significantly greater (up to 200 µg per gram of sediment) than that found in the open ocean[26].

1.3 Iodine in the atmosphere

The intricate and obscure marine iodine geochemical cycle forms one part of a geochemical cycle with a significant atmospheric cycle characterized by the oxidation of numerous reduced organic and inorganic iodine species. Early work implicated the role of wind in aerosolizing and delivering halogens from sea salt into the atmosphere at the marine boundary layer (MBL) and beyond[27,28]. The ionic composition of this sea spray differs from that of ocean waters, and an inverse correlation exists between the atomic weight of a particular ion and its concentration in sea spray. Consistent with this, iodine is concentrated nearly 100-fold more in sea spray compared to seawater[29-31]. The primary mechanism of iodine delivery ("evaporation" of volatile species) from the ocean to the atmosphere accounts for up to $5x10^{11}$g iodine/year of which sea spray contributes $5x10^9$g iodine/year[29]. Although the mechanisms delivering iodine from the ocean to the atmosphere are not clearly defined, substantial amounts of iodine likely enter the troposphere as either IO_3^-, I^-, or elemental I_2[31].

In the MBL, photochemical breakdown of iodinated gases produces iodine oxide radicals that may lead to substantial surface ozone loss and the formation of cloud condensation nuclei[13,32]. The surface I^- ozonolysis ultimately yields I_2 and hypoiodous acid (HOI)-containing particles; however, the formation of VOI gases to the MBL remains enigmatic[33]. A diversity of organic iodine species contributes significantly to the iodine flux from seawater into the atmosphere, including methyl iodide (CH_3I) and the lesser studied dihalomethanes CH_2I_2 and CH_2ICl. Ongoing research into haloalkanes and their effects on the ozone layer identified several halomethanes as a byproduct of marine algae[34]. These compounds likely enable various biological processes in algae, with the most likely function being a response to oxidative stress[25]. Notably, I^- seemingly predominates in kelp and algae, and these organisms oxidize I^- to a chemically reactive hypoiodite intermediate by using a vanadium haloperoxidase, resulting in the non-specific iodination of numerous carbon compounds[35,36]. Several studies have associated *Laminaria* and *Fucus* kelp species with the production of halomethanes and indicate that these kelp with their associated microbiomes produce up to $1.2x10^{-7}$ ml of gaseous CH_3I per milliliter of water[35]. Further studies looking at axenic kelp cultures and the MBL noted a diurnal cycle of organic iodine production, suggesting that variables such as luminosity or temperature may impact production[37]. Additionally,

organic iodine production may exhibit an element of seasonal variability with warmer months showing lower concentrations of IO_3^- in kelp forests, likely associated with increased I^- assimilation as kelp reach their peak biomass[38].

Although the atmospheric concentrations of these halogenated molecules are relatively low, they play an essential and significant role in the atmospheric chemistry near the MBL, global ozone destruction, and ultimately terrestrial iodine deposition. At the MBL, organic iodine reacts and releases I^- or iodine oxides, which can interact with ozone, reactive oxygen species, and nitrous oxides in the atmosphere[37,39]. This interaction between iodine and ozone is now recognized as an essential aspect of the iodine cycle that impacts global climate models. Since the 1860s, the total concentration of tropospheric ozone has increased, produced primarily from anthropogenic sources[17]. While in the troposphere, ozone causes numerous health effects even at low concentrations and significantly contributes to the total radiative forcing of the troposphere, causing global warming via a net solar energy gain[17]. Recent evidence suggests that halogens, including iodine, are involved in the beneficial destruction of ozone in the troposphere[40,41]. Additionally, the cloud nuclei formed by iodine oxides increase cloud cover, resulting in greater albedo around areas of high iodine flux[1]. This effect is particularly prevalent at tropical latitudes between 10° and 40° N, presumably due to enhanced kelp growth in warmer climates[40,41]. Since the mid-20th century, the increased ozone concentrations may have significantly impacted the deposition of iodine terrestrially[40,41]. More importantly, climate models have not generally included the atmospheric effects of marine halogens on tropospheric ozone; hence, understanding the biogeochemistry and microbiology that interact with dominant atmospheric halogens such as iodine is imperative to model climate change predictions successfully[40].

1.4 The iodine redox cycle

Geochemical analysis revealed that global oceanic iodine concentrations are relatively consistent; however, the iodine speciation (as IO_3^- or I^-) is variable and correlates to environmental parameters[24,42]. Thermodynamically, iodine should exist entirely as IO_3^- in fully oxygenated seawater (pH 8.05, pε 12.5)[24]. However, I^- is often found in surface seawater at significant concentrations (50-150 nM)[43]. Interestingly, both the oxidative and reductive mechanisms of the iodine cycle in seawater remain somewhat enigmatic. While Luther *et al.* have shown that oxidative neogenesis of IO_3^- from I^- can occur through various abiotic reactions, the authors discount many of these in seawater environments[42]. Geochemical investigations have revealed that I^- concentration in the marine environment correlates to depth and latitude[42,44-47]. Counter-intuitively, the highly oxidizing environment of surface waters subject to the maximum light intensity shows a higher I^-:IO_3^- ratio than the deeper zones[43].

Similarly, marine regions with higher water temperatures closer to the equator also show a higher I^-:IO_3^- ratio[43]. Conversely, the I^-:IO_3^- ratio decreases with depth, and IO_3^- predominates in deeper waters[43]. These results suggest that I^- formation primarily occurs in regions of maximum microbial activity near the surface exposed to abundant solar radiation[43]. Given that IO_3^- is the thermodynamically stable iodine form in fully oxygenated seawater, this has led to questions about the underlying cause of the I^-:IO_3^- disequilibrium[42,46]. Preliminary evidence suggests that iodine

redox cycling involves a biological component that potentiates the reductive cycle in the ocean, driving it against thermodynamic expectations. This observation is supported by the examination of seafloor sediments in the Mediterranean, which showed that the sediment serves as an iodine sink and maintains an active iodine redox cycle[48]. It has been proposed that sediment pore waters consist of four "layers": The oxic sediment is stratified with the first layer mainly containing I^-, followed by a transition zone that preceded a zone containing mostly IO_3^-[48]. Iodide accumulation occurs in the anoxic zone below the final layer of IO_3^-, suggesting that additional IO_3^- reduction occurs in this zone. It was concluded that these oxic and anoxic sediments serve as an essential source of I^-, and biological processes are responsible for the observed I^-:IO_3^- disequilibrium[48].

Recent research focused on the littoral zone of oceans suggests that conversion of IO_3^- to I^- occurs in proximity to kelp and that several VOIs emanate from these coastal waters. Truesdale[49] noted that culturing kelp (*Laminaria digitata* or *Fucus serratus*) resulted in IO_3^- reduction and concomitant I^- formation. Furthermore, several subsequent studies indicated that various seaweeds (e.g., *Macrocystis, Laminaria,* and *Fucus* species) sequester I^-, and subsequently release VOI compounds[38,49]. Although kelp beds may play an essential role in the biogeochemical iodine cycle[38], no role in the enzymatic reduction of IO_3^- to I^- has been ascribed to the possible involvement of the microbial content of kelp associated biofilms[50].

1.5 Biology of iodine redox cycling

The average concentration of total dissolved iodine in seawater is 0.45 μM[51], and thermodynamics predicts that the IO_3^-:I^- concentration ratio should be 3.2×10^{13} in oxygenated seawater[24]. However, I^- concentrations up to 0.3 μM are observed in surface waters[44,52,53], and previous studies have indicated a correlation between IO_3^- reduction and organic matter decomposition in the Northwest Arabian Sea[54]. This observation supports the speculation that the I^-:IO_3^- disequilibrium is caused by active and passive biological reduction of IO_3^- to I^-, and marine bacteria[24,55,56] and phytoplankton[57-59] may play significant roles in the process. It has been known for more than 50 years that bacteria can reduce IO_3^- [24]. The high reduction potential (IO_3^-/I^- E_h = +0.72V at pH 8.1)[24,42] makes IO_3^- an ideal electron acceptor for microbial metabolism. Early studies by Tsunogai and Sase indicated that numerous microorganisms, including *Escherichia coli,* and *Shewanella putrefaciens,* reduce IO_3^- to I^-[24,56]. Researchers believed this metabolism is mediated by the promiscuous nitrate reductase in these bacteria, and subsequent biochemical studies demonstrating that endogenous nitrate and perchlorate reductases could also reduce IO_3^- *in vitro* further supported this observation[24,60]. Following the reduction of iodate to iodide, various organisms either assimilate or oxidize iodide for various reasons. Reports of kelp[61], phytoplankton[62], and various proteobacteria[63-65] show numerous mechanisms whereby these organisms can oxidize iodide. Below, I discuss various biological mechanisms enabling iodate reduction and iodide oxidation and how these biological processes contribute to iodine cycling globally.

1.5.1 Iodide oxidation in algae

Haloperoxidases are ubiquitous across the tree of life, enabling the oxidation of reduced halogens like iodide and subsequent iodination of a diverse set of molecules[66,67]. Early haloperoxidases were primarily mammalian and generally used a heme cofactor to oxidize halogens[68]. The first non-heme haloperoxidase described was in the brown algae *Ascophyllum nodosum* and used a vanadium cofactor[69,70]. The vanadium haloperoxidase (VHP) showed demonstrable activity against both iodide and bromide, suggesting similar substrate specificities compared to other haloperoxidases[70]. VHPs are widely distributed in marine environments[68,71] and have been found in brown algae[72], green algae[73], red algae[74], and select terrestrial organisms like lichen[75]. These enzymes function by oxidizing halide ions with hydrogen peroxide and the vanadium cofactor to generate free hypohalous acid, which reacts non-specifically with various small molecules to generate halogenated versions of them[71,76]. While the reaction is seemingly non-specific, VHPs stabilize hypohalous acids to halogenate the carbon substrate at specific sites and maintain chirality[76,77]. Iodide oxidation in algae ultimately contributes to the production of various volatile organic iodines, which has important implications for atmospheric chemistry, and results in the loss of iodine to the atmosphere.

1.5.2 Iodide oxidation in bacteria

Like algae, bacteria also contribute to iodine redox cycling through the oxidation of iodide. *Pseudomonas iodooxidans* was one of the first isolates demonstrating the production of free iodine using an extracellular heme peroxidase[63,78]. Subsequent studies showed the ubiquity of iodide oxidation globally by identifying several *Alphaproteobacteria* in natural gas brines and seawater in Japan that oxidized upwards of 1.2 mM of iodide to elemental iodine (I_2)[65]. Unlike algal haloperoxidases, bacterial iodide oxidation generally uses oxygen instead of hydrogen peroxide[65]; however, these organisms produce similar VOIs like CH_2I_2 and CH_2ClI, suggesting that they may contribute to global iodocarbon emissions[65]. More recently, researchers have identified *Iodidimonas sp.* Q1, *R. denitrificans* 116-2, and *Roseovarius sp. A-2* as three organisms with dedicated iodide oxidation pathways[79,80]. *Iodidimonas sp.* Q1 and *Roseovarius sp. A-2* possesses this multicopper oxidase-like protein consisting of at least two subunits: IoxA and IoxC[64]. These multicopper oxidases oxidize $2I^-$ to I_2, and perform a two-electron transfer to reduce O_2 to H_2O in the process[80]. This multicopper oxidase has a higher K_M and catalytic efficiency to iodide than other known multicopper oxidases, suggesting that this is a specialized enzyme in its ability to oxidize iodide[64]. Other proteins produced by the *iox* gene cluster (*ioxABCDEF*) seemingly bind copper or assemble the cytochrome c oxidase complex in yeast[64], but their functions ultimately remain hypothetical. Mechanisms describing hydrogen peroxide mediated iodide oxidation in bacteria have also been described[81]. Observations suggest that organic acids secreted by bacteria enhance iodide oxidation by lowering the pH of the environment, which enables the formation of peroxycarboxylic acids that interact with iodide to form tri-iodide (I_3^-)[81]. More recently, researchers have observed that marine nitrifying bacteria can oxidize I^- to IO_3^-, describing the first link between marine nitrification and iodate formation[82]. The authors posit if one were to generalize this link, changes in nitrification could potentially impact iodate formation with subsequent impacts on atmospheric chemistry. Nonetheless, bacteria possess multiple mechanisms

to oxidize iodide to either I_2 or triiodide, which ultimately contributes to iodine redox cycling globally.

1.5.3 Cell senescence mediated iodate reduction

The cell senescence hypothesis traces its origins back to the observation that iodate is biophilic, and the euphotic zone, a zone with high biological productivity, is consistently enriched for iodide[43,45,83]. Researchers attribute iodide enrichments at these zones to phytoplankton or algae that reduce micromolar quantities of iodate when grown in culture[84]. For instance, iodate reduction in the presence of the red marine algae *Isochrysis galbana* continues when the nitrate reductase is deactivated by tungstate supplementation in the growth media[58]. Similar observations were made in diatoms that show increasing rates of iodate reduction upon late growth phase and cell senescence[85]. Notably, researchers observed that iodate reduction occurs independently of growth rate, suggesting that cellular processes do not necessarily potentiate iodate reduction[58]. Ultimately, researchers determined that the decoupling between iodate reduction and growth was due to a non-specific cell-senescence-driven process, as the iodate reduction rate increases when the algae are no longer growing[86]. Reduced sulfur released from dying cells in the form of glutathione is believed to be the primary mechanism behind phytoplankton-mediated iodate reduction[86]. Time series data across Antarctica corroborates the association between summer algal blooms and increased iodide concentrations[87]. Thus, the cell senescence contributes to the IO_3^-:I^- disequilibrium observed at zones of high biological productivity such as coastal zones and photic zones near the sea surface.

1.5.4 Reductant-mediated iodate reduction

Iodate reduction mediated by the metabolic byproducts of anaerobic respiration such as bisulfide[88] and ferrous iron[89] were first observed in marine environments but were not directly linked to any specific organism. *Desulfovibrio desulfuricans* and *Shewanella putrefaciens* were among the first demonstrated iodate reducing microorganisms that reduced up to 100 μM iodate under anoxic conditions[56]. Cell suspensions of these organisms abiotically reduce IO_3^- to I^- with reactive end-products (HS^- & Fe^{2+}) of the respiratory metabolisms of these organisms[56,90]. Later studies affirmed the contribution of *S. putrefaciens* to iodate reduction in an Arabian Sea oxygen minimum zone by connecting marine iodate reduction and *S. putrefaciens* mediated iodate reduction[55]. However, MR-4 growth in artificial seawater shows that the organism conserves energy by iodate reduction through the removal of 250 μM of iodate[55]. Notably, researchers demonstrated that iodate reduction requires lactate and occurs independently of sulfide production in seawater, suggesting that bacteria can directly mediate iodate reduction[55]. Further studies addressing the mechanism potentiating iodate reduction in *Shewanella* demonstrated that numerous *S. oneidensis* subspecies could reduce up to 250μM iodate to iodide and knocking out the only nitrate reductase (NapA) does not preclude iodate reduction[91].

Researchers ultimately noted that several proteins associated with the extracellular electron conduit (EEC), specifically MtrA and MtrB, were associated with iodate reduction in *S. oneidensis* MR-1[92]. MtrA and MtrB are putatively involved in the metal-mediated reduction of oxidants in MR-1, suggesting a possible metal-mediated mechanism for iodate reduction[93]. However,

deletions of the EEC proteins OmcA and/or MtrC still reduce iodate despite their essentiality in iron or manganese reduction[92]. Ultimately, further studies are needed to fully understand how different metal cofactors contribute to iodate reduction under environmental concentrations in the ocean. Nonetheless, multiple lines of evidence suggest that bacteria can indirectly reduce iodate during the anaerobic respiration of metals.

1.5.5 DMSO reductase mediated iodate reduction

Dimethyl sulfoxide reductases (DMSORs) are a diverse class of molybdenum containing enzymes broadly found throughout bacteria and archaea[94] that use a bis(molybdopterin guanine dinucleotide) cofactor with a bound molybdenum atom (Figure 1.2). Although DMSORs maintain a high degree of similarity in their tertiary structure, these enzymes commonly perform a two-electron transfer onto a diversity of oxyanion substrates[94]. Early studies speculated that iodate reduction to iodide was likely mediated by these type II DMSORs given their involvement in reducing numerous other oxyanions[94,95]. Nitrate reducing heterotrophic bacteria in oceanic surface waters like *Achromobacter*, *Bacillus*, *Pseudomonas*, and *Vibrio* showed demonstrable iodate reduction to varying degrees[96]. Upon adding nitrate to these cell cultures, iodate reduction activity would cease, suggesting preferential usage of nitrate over iodate in these bacteria[96]. Iodate reduction was observed over four hours with purified nitrate reductase from *E. coli*, suggesting the enzyme has a weak affinity towards iodate[96]. Since nitrate concentrations in oceanic surface waters are relatively low[97], Tsunogai and Sase concluded that nitrate reductase facilitates iodate reduction in ocean surface waters[96]. Likewise, an *Agrobacterium*/*Rhizobium*-related strain DVZ35 also demonstrates promiscuity towards iodate via its nitrate reductase by concurrent reduction of iodate and nitrate[98]. Without nitrate present, DVZ35 does not reduce IO_3^-, thus implying a role for the nitrate reductase in iodate reduction[98]. Whether nitrate reductase activity towards IO_3^- is significant remains unclear, as conflicting data reports no IO_3^- reduction by the purified *E. coli* NarGHI *in vitro*[99]. Like nitrate reductases, reports of IO_3^- reduction by perchlorate reductases (PcrAB) have been made. Purified PcrAB from *Azospira oryzae* GR-1 demonstrated IO_3^- reduction when assessed *in vitro*, identifying another DMSOR capable of iodate reduction[100,101]. Similar observations were made in *Azospira suillum* PS PcrAB, suggesting that the perchlorate reductase shows activity against multiple oxyanions and has a particularly high affinity towards iodate over nitrate[95,100,102].

While evidence of non-specific IO_3^- reduction by various DMSORs mounts, evidence demonstrating a dedicated IO_3^- reductase is emerging. Isolation of *Pseudomonas stutzeri* sp. SCT provided the first conclusive evidence of a dedicated dissimilatory iodate reducing microorganism (DIRM)[103]. *Pseudomonas* sp. SCT grows anaerobically with millimolar quantities of IO_3^- as its sole electron acceptor while concomitantly producing equimolar amounts of I^- during growth[104]. The IO_3^- reducing phenotype is seemingly inducible, as soluble periplasmic fractions of *Pseudomonas* sp. SCT will only reduce iodate if previously grown on iodate[104]. Taken together this evidence suggests that a dedicated enzyme potentiating dissimilatory iodate reduction exists. Further, this enzyme seems specific to iodate, since cells grown on nitrate and tested for iodate reduction will not reduce iodate[104]. Combined with observations that PcrAB can reduce iodate, the observation in *Pseudomonas* sp. SCT is suggestive of a dedicated iodate-specific DMSO reductase.

1.6 Preamble

Here, I demonstrate that microorganisms interface with the global iodine cycle at multiple points. I outline the current understanding of how microorganisms interface with the iodine cycle and discuss the open question of the IO_3^-:I^- disequilibrium. Among the many theories explaining this disequilibrium, we turn our attention to certain microorganisms that reduce millimolar quantities of IO_3^-. *Pseudomonas* sp. SCT is not publicly available for researchers to study, so I begin by searching for an organism with the same iodate reducing phenotype. My goal is to corroborate observations made in *Pseudomonas* sp. SCT and identify mechanisms enabling the phenotype. My approach seeks to leverage modern genetic and genomic tools to examine the isolate's physiology and assess the distribution of any identified genetic markers among existing bacterial isolates. I then plan to assess the distribution of these types of microorganisms and establish their connection to the global iodine cycle. Ultimately, this work aims to characterize the mechanisms at play in this new class of microorganisms and discuss the potential impacts on our environment and our understanding of microbial physiology.

1.7 Figures

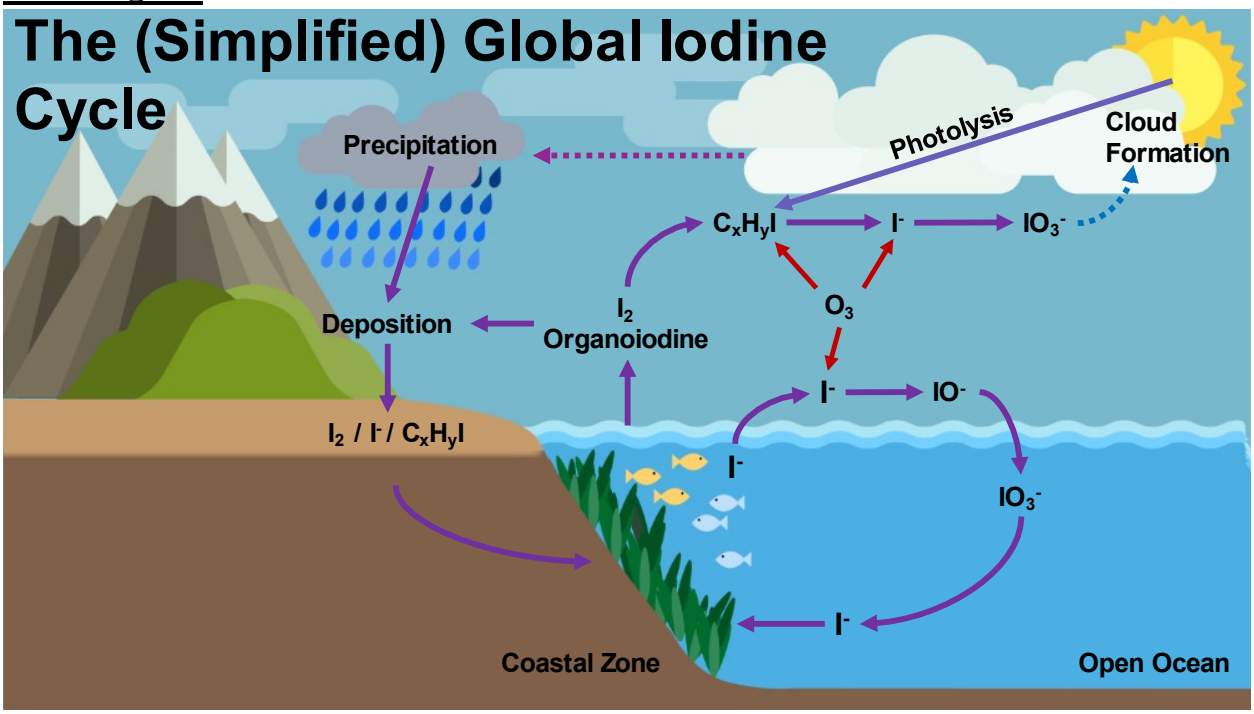

FIGURE 1.1: A SIMPLIFIED DIAGRAM DEMONSTRATING THE GLOBAL IODINE GEOCHEMICAL CYCLE. The above diagram shows the major iodine redox shifts that occur globally. Purple arrows denote the dominant directionality of the iodine cycle. Red arrows denote the effect of ozone on iodine species at the marine boundary layer. Blue dotted arrows show the physical manifestation of iodine oxyanions on cloud formation.

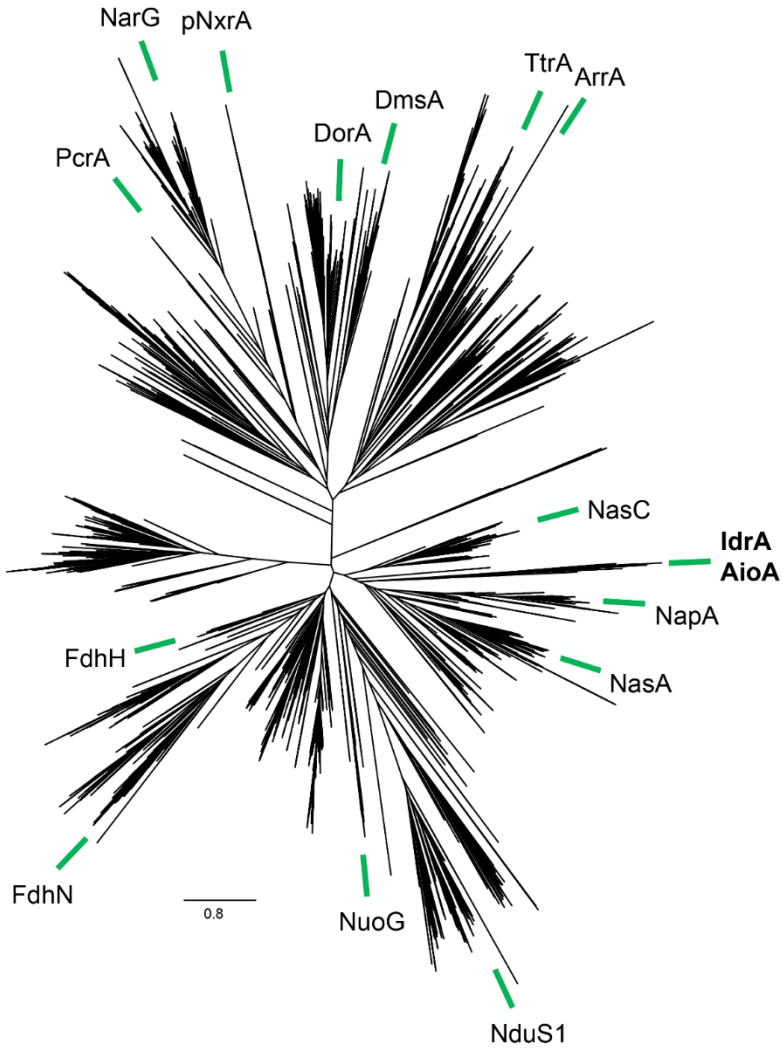

FIGURE 1.2: AN UNROOTED TREE SHOWING THE DIVERSITY OF THE MOLYBDOPTERIN OXIDOREDUCTASE SUPERFAMILY OF ENZYMES. The unrooted tree shows the pre-aligned representative proteome 55 set of proteins in the molybdopterin oxidoreductase superfamily of enzymes. Abbreviations: *fdh*—formate dehydrogenase, *nar*—dissimilatory nitrate reductase, *pcr*—dissimilatory perchlorate reductase, *nas*—assimilatory nitrate reductase, *nap*—periplasmic nitrate reductase, *nxr*—nitrite oxidoreductase, *dor*—TMAO reductase, *dms*—DMSO reductase, *ttr*—tetrathionate reductase, *arr*—arsenate reductase, *nuo*—NADH:Quinone oxidoreductase, *ndu*—NADH:Ubiquinone oxidoreductase, *aio*—arsenite oxidase, *idr*—iodate reductase.

Chapter Two: Genetics, physiology, and phylogenetic analysis of dissimilatory iodate-reducing bacteria

Abstract

Iodine is oxidized and reduced as part of a biogeochemical cycle that is especially pronounced in the oceans, where the element naturally concentrates. The use of oxidized iodine in the form of iodate (IO_3^-) as an electron acceptor by microorganisms is poorly understood. Here, I outline genetic, physiological, and ecological models for dissimilatory IO_3^- reduction to iodide (I^-) by a novel estuarine bacterium, *Denitromonas* sp. IR-12. Our results show that dissimilatory iodate reduction (DIR) by strain IR-12 is molybdenum-dependent and requires an IO_3^- reductase (*idrA*) and likely other genes in a mobile cluster with a conserved association across known and predicted DIR microorganisms (DIRM). Based on genetic and physiological data, I propose a model where three molecules of IO_3^- are likely reduced to three molecules of hypoiodous acid (HIO), which rapidly disproportionate into one molecule of IO_3^- and 2 molecules of iodide (I^-), in a respiratory pathway that provides an energy yield equivalent to that of nitrate or perchlorate respiration.

2.1 Introduction

Iodine (as ^{127}I) is the heaviest stable element of biological importance and an essential component of the human diet due to its role in thyroxine biosynthesis in vertebrates[3,105,106]. Iodine is enriched in marine environments where it exists in several oxidation states, reaching average concentrations of 450 nM[107]. In these environments, organisms such as kelp bioconcentrate iodine as iodide (I^-) and produce volatile iodine species such as methyl iodide[108]. These volatile iodine species contribute to the destruction of tropospheric ozone (a major greenhouse gas) and aerosol formation at the marine boundary layer, consequently resulting in cloud formation and other local climatic effects[12,105]. Despite the global biological and geochemical importance of iodine, little is known about its biogeochemistry in the ocean[107]. For instance, the biological mechanism accounting for the unexpected chemical disequilibrium between I^- and iodate (IO_3^-) in seawater (I^-:IO_3^- disequilibrium) remains unknown[107]. At the physicochemical conditions of seawater, iodine is most stable as IO_3^-[109], yet measurements of IO_3^- and I^- in regions with high biological productivity (e.g., marine photic zones, kelp forests, or sediments), reveal an enrichment of the I^- ion beyond what can be explained through abiotic reduction[109,110] with ferrous iron[111] or sulfide.

Among numerous explanations proposed for I^- enrichment, microbial IO_3^- reduction is particularly compelling. The high reduction potential (IO_3^-/I^- E_h = 0.72 V at pH 8.1)[96,109] makes IO_3^- an ideal electron acceptor for microbial metabolism in marine environments. Early studies indicated common microorganisms such as *Escherichia coli* and *Shewanella putrefaciens,* reduce IO_3^- to I^- [96,112]. Subsequent studies associated this metabolism with the inadvertent activity of DMSO respiratory reductase enzymes in marine environments, along with specific enzymes (i.e., perchlorate reductase, nitrate reductase) that reduce IO_3^- *in vitro* [96,113,114]. However, there is little evidence that organisms hosting these enzymes are capable of growth by IO_3^- reduction. While inadvertent IO_3^- reduction might be mediated by marine bacteria possessing DMSO reductases, until recently, no definitive evidence existed that global IO_3^- reduction is a microbially assisted phenomenon.

In support of a microbial role for the observed I^-:IO_3^- disequilibrium, previous studies demonstrated that at least one member each of the common marine genera *Pseudomonas* and *Shewanella* are capable of IO_3^- reduction[104,114,115]. More recently, IO_3^- reduction by *Pseudomonas* sp. strain SCT was associated with a molybdopterin oxidoreductase closely related to arsenite oxidase[115]. As part of this work, a dedicated biochemical pathway was proposed involving two peroxidases associated with a heterodimeric IO_3^- reductase (Idr)[115]. The putative model proposes a four-electron transfer mediated by Idr, resulting in the production of hydrogen peroxide and hypoiodous acid[115]. Two peroxidases detoxify the hydrogen peroxide while a chlorite dismutase (Cld) homolog dismutates the hypoiodous acid into I^- and molecular oxygen, which is subsequently reduced by the organism[115]. The proposed pathway involving a molecular O_2 intermediate is analogous to canonical microbial perchlorate respiration[116]. By contrast, Toporek *et al.*[117] using the IO_3^- respiring *Shewanella oneidensis* demonstrated the involvement of an unidentified reductase associated with the *mtrAB* multiheme cytochrome, suggesting an alternative DIR pathway. The disparate mechanisms underscore the potential diversity of IO_3^- respiratory processes. As such, identification of additional DIR microorganisms (DIRM) would clarify which

genes are required for this metabolism and enable identification of IO_3^- respiratory genes in metagenomes.

With this as a primary objective, I identified a novel marine DIRM, *Denitromonas* sp. strain IR-12, that obtained energy for growth by coupling IO_3^- reduction to acetate oxidation. Taxonomic analysis placed this organism in the *Denitromonas* genus commonly associated with marine environments[118]. I used comparative genomics to identify the core genes involved in IO_3^- respiration, which formed a distinct mobile genomic island. Reverse genetics, physiology, and comparative genomic data were used to propose a new model for DIR, with a confirmed role for a molybdopterin-dependent IO_3^- reductase (IdrAB)[115]. A phylogenetic analysis was used to establish the distribution of this metabolism across the tree of life and measure the degree to which the genomic island is subject to horizontal gene transfer. These results together enabled the proposed model for the global distribution of the DIR metabolism and the ecology of the microorganisms involved.

2.2 Methods

2.2.1 Media, chemicals, and culture conditions

Anaerobic enrichment cultures from marine environments were grown at 30°C using a minimal media containing the following per liter: 0.54 g NH_4Cl, 0.14 g KH_2PO_4, 0.20 g $MgCl_2 \cdot 6 H_2O$, 0.14 g $Na_2SO_4 \cdot 10 H_2O$, 20.0 g NaCl, 0.24 g Na_2MoO_4 0.20 g, and 2.5 g $NaHCO_3$ with an added vitamin mix and mineral mix (see section 2.2.7). Oxygen was removed from the media and bottles were dispensed in an 80% N_2/20% CO_2 atmosphere. Anaerobic subcultures for isolation were grown in Artificial Pore Water (APM) medium at 30°C (30.8 g NaCl, 1.0 g NH_4Cl, 0.77 g KCl, 0.1 g KH_2PO_4, 0.20 g MgSO4·7H2O, 0.02 g $CaCl_2 \cdot 2 H_2O$, 7.16 g HEPES, along with vitamin and mineral mixes. A post sterile addition of 34.24 mL 0.4 M $CaCl_2$ and 26.07 mL 2 M $MgCl_2 \cdot 6H_2O$ was added to each liter of APM media. Conditions with lactate, acetate, iodate, and nitrate all used the sodium salts of these compounds. Conditions without molybdenum omitted Na_2MoO_4 from the mineral mixes. Aerobic cultures were all grown either on APM, R2A (HiMedia, USA), or R2A agar (BD Biosciences, USA). Kanamycin concentrations when used were at one tenth the standard concentrations on plates (5 mg/L, Sigma Aldrich, USA) and at one fourth the standard concentration in liquid (12.5 mg/L). All compounds were purchased through Sigma Aldrich (Sigma Aldrich, USA). Growth of tubes were measured either using the Thermo Scientific GENESYS 20 or the TECAN Sunrise 96-well microplate reader set at a wavelength of 600 nm. For growth measurements in Hungate tubes, a special adapter was built to measure the tubes on the GENESYS 20. Growth experiments using the microplate reader were run in an anerobic glove bag under an atmosphere of 97.8% N_2 and 2.2% H_2.

2.2.2 Strain characterization experiments

Imaging of *Denitromonas* sp. IR-12 was performed on a Technai-12 transmission electron microscope by the staff at the University of California Berkeley Electron Microscope Laboratory. Motility was made by visual observation of a wet mount under a compound microscope at 100x

magnification. Inhibitory concentrations of iodate and iodide were determined by using the fitting a dose response curve over a wide range of iodate/iodide concentrations (in halving concentrations between 0.39-200 mM) in APM with 10 mM lactate and using the peak OD_{600} as the response variable. Optimal salinity was measured by calculating the max growth rate during the exponential phase at salinities of 0%, 0.125%, 0.25%, 0.5%, 1.0%, 2.0%, 3.0%, 4.0%, 5.0%, 7.5%, and 10%. The GraphPad Prism software suite (version 8.4.0) was used to calculate the IC_{50} values. Temperature range was determined by growth of *Denitromonas* sp. IR-12 on R2A agar plates at 20°C, 25°C, and 30°C. Evaluation of antibiotic resistance was performed by dissolving antibiotics tetracycline (10 μg/μL) and chloramphenicol (25 μg/μL) into R2A agar plates, and streak plating *Denitromonas* sp. IR-12. Kanamycin sensitivity was determined similarly by testing concentrations of 50.0 μg/μL, 25.0 μg/μL, 12.5 μg/μL, and 5.0 μg/μL.

2.2.3 Isolation of dissimilatory iodate-reducing bacteria

Sediment from the top two inches of a tidal flat in the San Francisco Bay estuary at the Berkeley Marina (37°86'56.4" N, -122°30'63.9" W) was added to anaerobic media bottles at 25 g sediment/100 mL for isolation of dissimilatory iodate-reducing bacteria. Samples were degassed and amended with 200 μM iodate for three days, and subsequently amended with 10 mM acetate and 2 mM iodate to enable growth of heterotrophic iodate reducing bacteria. Enrichments that showed iodate reduction to iodide were then passaged at least five times into fresh minimal media with 10 mM acetate and 2 mM iodate. To ensure purity of the passaged enrichment culture, the organism was plated aerobically onto an agar plate containing the minimal media, and a single colony was isolated from this plate.

2.2.4 Strains and plasmids

All plasmids, primers and strains constructed are listed in Table 2.1. The *E. coli* strain used for plasmid propagation was XL1-Blue, while WM3064 was used to perform conjugations. Plasmid pNTPS138, a generous gift from the Kathleen Ryan Lab at UC Berkeley, was used for the SacB counterselection. Plasmid pBBR1-MCS2 is a low copy expression vector and was used for complementation experiments. All expression plasmids and deletion vectors were constructed using the Benchling software suite (San Francisco, USA). Plasmids were assembled from genomic DNA either by Gibson assembly or restriction digestion and ligation using standard procedures. Gibson assembly was carried out using NEB HiFi 2x Master Mix, and remaining enzymes and master mixes were ordered from New England Biosciences (NEB, USA). Additional plasmids were built using primers to remove unwanted sequences by site directed mutagenesis and re-circularizing the resulting product with the KLD Enzyme Mix (NEB, USA). Plasmids were routinely isolated using the Qiaprep Spin Miniprep kit (Qiagen, USA), and all primers were ordered from Integrated DNA Technologies (IDT, Coralville, IA). Since most sequences in the iodate reduction cluster contain at minimum 60% GC content, amplification is relatively challenging. Amplification of these challenging portions of the genome were optimized as follows: Amplification of DNA for generating assembly products was performed using Q5 DNA Polymerase 2x Master Mix (NEB, USA) with 3% DMSO. Annealing temperatures for each reaction was determined by subtracting the Tm provided by the NEB Tm calculator

(https://tmcalculator.neb.com) for each primer pair by 1.8°C. All *Denitromonas* sp. IR-12 strains (pre- or post-transformation) were propagated from glycerol stocks (25% glycerol) stored at -80°C, grown on a plate for up to 72 hours, picked and then grown for an additional 48-72 hours in liquid R2A. For additional information on plasmid construction, performing transformations, and conjugations in *Denitromonas* sp. IR-12 see supplemental methods.

2.2.5 Expression vector transformation

Electroporator model GenePulser XCell (BioRad, USA) was used for high efficiency transformation of expression vectors into *Denitromonas* sp. IR-12. The procedure in short: 40 mL of *Denitromonas* sp. IR-12 was grown for 72 hours and spun down at 4000 RPM at 4°C for 15 minutes in 6 mL of cold, sterile deionized H_2O, followed by a wash and spin down in 6mL of cold, sterile 10% glycerol for an additional 15 minutes. The supernatant is decanted, and the pellet is resuspended to a final volume of 600 µL of 10% glycerol. Purified plasmid DNA is added at a concentration of 10ng/µL, and cells sit on ice for a minimum of 10 minutes. Electroporator is then pulsed once at 1750V, 25µF, and 400Ω for a 1mm GenePulser cuvette (BioRad, USA). Cells are then transferred to 500 µL of R2A media and are recovered for 4 hours at 30°C. After outgrowth 100µL of cells are plated out on R2A plates with 5 µg/µL kanamycin and allowed to grow at 30°C for three days. A 1:10 dilution is recommended due to high transformation efficiency. Since the concentration of kanamycin is relatively low, all colonies are screened for the presence of the kanamycin resistance marker via PCR.

2.2.6 Suicide vector transformation

WM3064 *E. coli* was used to efficiently deliver suicide vectors into *Denitromonas* sp. IR-12. 50mL of *Denitromonas* sp. IR-12 is grown aerobically in R2A at 30°C for 30 hours, and *E. coli* is grown from an overnight culture for 4-6 hours at 37°C. Cultures are harvested and spun down at 7000 RCF at room temperature for 5 minutes. Cultures are then washed in R2A containing diaminopimelic acid (DAP) and are separately resuspended to a final volume of 250µL in R2A+DAP. The optical densities of each culture are measured, and the cells are added together and mixed at a 1:1 ratio in a final volume of 500µL. The entire conjugation is spotted onto three separate R2A+DAP plates and incubated at 30°C for 24 hours. The entire conjugation is then scraped off and resuspended in 10mL of R2A (no DAP) with 15% glycerol. 100µL of the conjugation is then spread out on two separate R2A plates with kanamycin and allowed to grow for 5 days. Transconjugants are then picked and plated again on R2A plates with kanamycin to allow for additional growth. Transconjugants are then screened by PCR for plasmid integration, and transconjugants possessing the rare integration event are picked and grown in liquid R2A for 3 days. 100µL of selected transconjugants are plated out on R2A + 7.5% sucrose, and colonies are picked and screened on R2A + 7.5% sucrose and R2A + kanamycin after 5 days. Colonies showing growth on R2A + sucrose and no growth on R2A + kanamycin are then screened for the removal of the suicide vector and the presence of the expected deletion.

2.2.7 Vitamin and mineral mixes

Vitamin and the two mineral mixes were prepared separately as stock solutions. Per liter the vitamin mix contains, 2.0 mg D-biotin, 2.0 mg folic acid, 10.0 mg pyroxidine HCl, 5.0 mg riboflavin, 5.0 mg thiamine, 5.0 mg nicotinic acid, 5.0 mg pantothenic acid, 0.1 mg vitamin B12, 5.0 mg p-amino benzoic acid, 5.0 mg D,L-6,8-thiotic acid. Per liter mineral mix one contains 1.5 mg NTA disodium salt, 3.0 g $MgSO_4 \cdot 7H2O$, 0.5 g $MnSO_4 \cdot H2O$, 1.0 g NaCl, 0.1 g $FeSO_4 \cdot 7H2O$, 0.1 g $CaCl_2 \cdot 2H2O$, 0.1 g $CoCl_2 \cdot 6H2O$, 0.13 g ZnCl, 0.1 g $CuSO_4 \cdot 5H2O$, 0.1 g $AlK(SO_4)_2 \cdot 12H2O$, 0.1 g Boric Acid, 0.025 g $Na_2MoO_4 \cdot 2H2O$, 0.024 g $NiCl_2 \cdot 6H2O$, 0.025 g $Na_2WO_4 \cdot 2H2O$, 0.02 g Na_2SeO_4. Mineral mix one is then adjusted to a pH of 6.0 with 1M NaOH. Per liter mineral mix two contains 40.0 g NaCl, 50.0 g NH_4Cl, 5.0 g KCl, 5.0 g KH_2PO_4, 10.0 g $MgSO_4 \cdot 7H2O$, and 1.0 g $CaCl_2 \cdot 2H2O$. Mineral mix two is then adjusted to pH 6.0 with KOH.

Media with vitamin and mineral mixes, add all the above mixes. Per liter of media, 10 mL of the vitamin mix, 10 mL of the mineral mix one, and 20 mL of mineral mix two are added.

2.2.8 Iodate and iodide quantification

A Dionex IonPac AS25 Anion Exchange Column was used on an ICS-1500 Ion Chromatography system (Thermo Fischer, USA) exclusively to measure the consumption of iodate and acetate, as well as the production of iodide in all samples. Briefly, all samples are diluted 1:20 in deionized water and loaded onto the autosampler for processing. Standards are made by serial dilution starting with 1 mM of the standard molecule. Iodate and iodide standards were linear across a range of 0.008-1.000 mM ($R^2 > 0.99$). Acetate standards were near linear ($R^2 > 0.98$) between 0.031-1.000 mM; however, acetate standards were fit along a quadratic model ($R^2 > 0.99$), as suggested by Brinkmann *et al.* for quantifying weak acids[119]. All samples were run in triplicate using a flow rate of 1 mL/min and a 36 mM NaOH eluent. Acetate peaks were consistently detected at 3.6 minutes, iodate peaks were consistently detected at 3.8 minutes, and iodide peaks were consistently detected at 11.5 minutes.

2.2.9 Genome sequencing, comparative genomics, and phylogenetic analysis

Genome sequencing was carried out on an HiSeq4000 using 150 bp paired end reads (Illumina, USA). This work used the Vincent J. Coates Genomics Sequencing Laboratory at UC Berkeley, supported by NIH S10 OD018174 Instrumentation Grant. FastQC 0.11 was used to assess the quality of the illumina reads and sickle 1.33 to trim the reads. The genome was subsequently assembled using SPAdes 3.9[120] and the assembly graph was assessed for completion using bandage[121]. The Prokka (version 1.14) pipeline was then used to generate the genome annotations and the general feature format file (.gff), which allowed for genome navigation and visualization on the Artemis software (available at http://sanger-pathogens.github.io)[122]. To search for the iodate reduction island, MMseqs2 was used to cluster homologous proteins in the amino acid FASTA (.faa) files from *Denitromonas* sp. IR-12 , *P. stutzeri* sp. SCT, *D. halophilus* SFB-1, and *P. stutzeri* sp. CAL by subfamily[123]. A presence and absence matrix for each subfamily was generated and represented as a four-way Venn diagram using pyvenn (https://github.com/tctianchi/pyvenn). To identify additional iodate reductase proteins in public databases, a profile-HMM was constructed using HMMER 3.0 following a multiple sequence

alignment using MUSCLE 3.8 on the molybdopterin oxidoreductase (Pfam_00384) seed set and *Denitromonas* sp. IR-12 /*P. stutzeri* SCT IdrA proteins[124,125]. A separate arsenite oxidase (AioA) profile-HMM was created using analogous methods. Genomes from high probability BLAST hits for IdrA and AioA (E value = 0) and from the AioA and AioA-like protein clades identified in Saunders *et al.*[126] were downloaded from NCBI using the ncbi-genome-download tool (https://github.com/kblin/ncbi-genome-download).

Approximately-maximum-likelihood phylogenetic trees were generated using Fasttree[127] specifying 10,000 resamples and using standard settings for everything else. For tree in figure 4A, fragmented sequences (shorter than 280aa) were removed. Visualization of resultant trees used the ete3 toolkit[128]. To perform the neighborhood frequency analysis, 10 genes upstream and downstream from the *aioA* or *idrA* locus were extracted from the associated GenBank files for each genome, and MMseqs2 was used to cluster homologous proteins as follows[123]: An all-vs.-all search using MMseqs2 was performed using e-value: 0.001, sensitivity: 7.5, and cover: 0.5. A sequence similarity network was built based on the pairwise similarities and the greedy set cover algorithm from MMseqs2 was performed to define protein subclusters as described in detail by Méheust *et al.*[129]. The resulting subclusters were defined as subfamilies. The cutoff for the IdrA HMM was ultimately determined by iteratively setting the score to a value that excludes genomes that lack the $IdrP_1$/$IdrP_2$ homologs adjacent to IdrAB and set to a threshold of 640. To search for cld in the downloaded genomes, a profile-HMM for cld, described previously, was used[130]. Frequency was calculated as number of genomes in possession of a cluster divided by the total number of genomes. Projections of this data were drawn using a custom Python 3.7 script. All tanglegram analyses used Dendroscope to load trees for processing and visualization[131].

2.3 Results and discussion

2.3.1 Isolation of *Denitromonas* sp. IR-12

Strain IR-12 was enriched from estuarine sediment samples by selective enrichment under anoxic conditions followed by single colony isolation on aerobic agar plates. Analysis of the 16S rRNA indicated an axenic culture composed of a single phylotype belonging to the *Denitromonas* genus in the class *Betaproteobacteria* identical to an uncultured *Denitromonas* clone from a metagenomic sample (GenBank: KF500791.1) (**Error! Reference source not found.**A). The closest cultured relatives were *D. indolicum* strain MPKc[132] (GenBank: AY972852.1, 99.46% similarity) and *D. aromaticus* (GenBank: AB049763.1, 99.40% similarity). Strain IR-12 is a facultative anaerobe with rod-shaped motile cells 1-2 μm long and 0.5 μm diameter containing a single polar flagellum (**Error! Reference source not found.**B).

2.3.2 Physiology and energetics of *Denitromonas* sp. IR-12

Cells of *Denitromonas* sp. IR-12 grew on basal medium with acetate and IO_3^- as the sole electron donor and acceptor, respectively (Figure 2.1C and D). Ion chromatography and growth studies revealed that IO_3^- was quantitatively reduced to I^- with concomitant cell density increase. No growth or acetate consumption occurred in the absence of IO_3^-. Similarly, no IO_3^- reduction

occurred in the absence of acetate or in heat killed controls. These results indicated that IO_3^- reduction was enzymatically mediated coupled to acetate oxidation and growth. Acetate-free control cultures reduced micromolar amounts of IO_3^- (114 ± 34 μM, mean ± standard deviation, n=3) which was attributable to residual acetate carried over from the inoculum (Figure 2.1C). *Denitromonas* sp. IR-12 consumed 2.46 ± 0.499 mM IO_3^- (mean ± standard deviation, n=3) while oxidizing 2.86 ± 0.427 mM acetate (mean ± standard deviation, n=3) with a final optical density (OD_{600}) increase of 0.109. This is equivalent to an average stoichiometry of 0.86 mol IO_3^- per mol acetate. The doubling time of cells grown under these conditions is 10.96 hours (μ=0.06) which is roughly three times longer than cells growing under aerobic conditions in analogous media (3.42 hours, μ=0.20). The morphological consistency between *Denitromonas* sp. IR-12 and *E. coli*, suggests that an OD_{600} increase of 1.0 is equivalent to 0.39 grams of cell dry weight per liter[133] and that ~50% of cell dry weight is comprised of carbon[134]. Using these numbers, the corrected stoichiometry accounting for acetate incorporation into cell mass is 93% of the theoretical value according to:

$$3\ CH_3COOH + 4\ IO_3^- \rightarrow 6\ CO_2 + 4\ I^- + 6\ H_2O$$

Our calculations indicate that 30.72% of total carbon is assimilated into biomass while the remaining is respired. Such a result is typical for highly oxidized electron acceptors such as oxygen, nitrate, or perchlorate[116,135]. In support of this, the calculated Gibb's free energy for the reduction of IO_3^- per mole of electrons transferred during iodate respiration on acetate is -97.44 kJ/mol e^- (assuming pH of 8.1, T=298.15K, and 1 atm)[136]. These values place the energy provided through IO_3^- respiration akin to that of perchlorate respiration (ClO_4^-/Cl^-, $E^{o\prime}$ = +0.797 V) [116], and between that of aerobic respiration (O_2/H_2O, $E^{o\prime}$ = +0.820 V) and nitrate reduction (NO_3^-/N_2, $E^{o\prime}$ = +0.713 V)[137]. This suggests a similar degree of carbon assimilation would be expected for IO_3^- respiration [135].

2.3.3 DIR is molybdate dependent

The reduction of oxyanions like IO_3^-, such as bromate, chlorate, perchlorate, and nitrate, is typically catalyzed by enzymes belonging to the DMSO reductase superfamily of molybdopterin oxidoreductases[138]. These enzymes require molybdenum as a cofactor in order to donate two electrons at a time to the receiving molecule[139]. To determine if phenotypic IO_3^- reduction was molybdenum-dependent, I passaged *Denitromonas* sp. IR-12 six times in aerobic, molybdate-free minimal media to remove any trace molybdenum as described in Chaudhuri *et al*[140]. As expected, and similarly to observations with perchlorate reducing microorganisms[140], omitting molybdenum from the oxic medium did not affect the aerobic growth of *Denitromonas* sp. IR-12 (data not shown). In contrast, no growth or IO_3^- reduction was observed when these cells were passaged into molybdenum-free anoxic media with IO_3^- as the electron acceptor (Figure 2.1E). When 0.1 mM sodium molybdate was added into the non-active cultures at 14 hours post inoculation, growth and IO_3^- resumed (Figure 2.1E). These results demonstrate that IO_3^- respiration by *Denitromonas* sp. IR-12 is molybdenum dependent and are consistent with the involvement of a DMSO oxidoreductase in IO_3^- reduction[140].

2.3.4 Core genes required for DIR

To identify the genes required for IO_3^- respiration I performed a comparative genomic analysis between the genomes of the IO_3^- respiring species (*Denitromonas* sp. IR-12 and *Pseudomonas* sp. SCT), and the non-IO_3^- respiring close relatives (*D. halophilus* SFB-1, and *Pseudomonas* sp. CAL). Additionally, *Pseudomonas* and *Denitromonas* are from phylogenetically distinct classes (*Gammaproteobacteria* and *Betaproteobacteria,* respectively), reducing the likelihood of shared gene content[141]. I surmised that DIRM must share a unique gene (or set of genes) that enables IO_3^- reduction. This comparison identified 26 genes uniquely shared by the two DIRM and not found in the closely related non-IO_3^- respiring species (Figure 2.2A; Table 2.2). Four of these genes were present in a gene cluster that contained genes for alpha and beta subunits of a DMSO reductase family molybdopterin enzyme related to arsenite oxidase (AioAB)[126] supporting our result of a molybdenum dependency for this metabolism. The remaining two genes in the cluster were closely related to cytochrome C peroxidases *ccp1* and *ccp2*, possibly involved electron shuttling and oxidative stress responses[142,143]. These four genes were similar to those identified by Yamazaki *et al.* under the proposed nomenclature *idrA*, *idrB*, *idrP1*, *idrP2* for *Pseudomonas* sp. SCT[115] (Figure 2.2B). A SignalP analysis showed that *idrP1* and *idrP2* possessed a signal sequence for periplasmic secretion via the Sec pathway, while *idrB* used the Tat pathway[144]. By contrast *idrA* did not have a signal peptide sequence, suggesting its protein product is co-transported with IdrB into the periplasm[145]. Based on this evidence, I concluded that dissimilatory IO_3^- reduction in *Denitromonas* sp. IR-12 occurs entirely in the periplasm, consistent with the observation by Amachi *et al*. that associated IO_3^- reductase activity in the periplasmic fractions of *Pseudomonas* strain SCT[104]. Notably, the gene cluster lacked a quinone oxidoreductase suggesting that *Denitromonas* sp. IR-12 involves the expression of a non-dedicated quinone oxidoreductase.

Evidence associating IdrAB to DIR, currently relies on the IO_3^- consuming activity of crude cell extracts of *Pseudomonas* strain SCT and differential expression of *idrABP1P2* under IO_3^- reducing conditions[115]. To validate the association between these genes and DIR in *Denitromonas* sp. IR-12, I developed a genetic system to perform targeted knockouts (see Table 2.1 and methods for details). The *idrA* gene was targeted since its associated molybdenum cofactor ultimately mediates the reduction of the oxyanion[138]. Upon introduction of an in-frame deletion at the *idrA* locus, the organism was incapable of growth via IO_3^- respiration (Figure 2.2B) while growth under oxic conditions remained unimpaired. Complementation of *idrA* on a low copy number vector (pVR065) restored the IO_3^- respiring phenotype demonstrating that the *idrA* gene is a prerequisite to enable IO_3^- respiration (Figure 2.2B). Our identification of a second DIRM, in addition to *Pseudomonas* strain SCT, with an IdrAB suggests that IO_3^- reduction requires a specialized molybdopterin oxidoreductase, and that other molybdopterin oxidoreductases in the genome cannot rescue the phenotype. Furthermore, our work demonstrates a distinct difference from IO_3^- reduction by the multiheme cytochrome associated reductase in *Shewanella* and suggests that the ability to reduce IO_3^- may have evolved at least twice independently.

2.3.5 An alternative DIR model

The current model for IO_3^- respiration by *Pseudomonas* strain SCT proposes the donation of electrons from the quinone pool via a cytochrome c to IdrAB, to initiate reduction of IO_3^- to HIO and H_2O_2. H_2O_2 is reduced to H_2O by the peroxidases $IdrP_1$ and $IdrP_2$, while a chlorite dismutase (Cld)-like enzyme converts HIO to I^- and $½O_2$, a catalytic function that has never been demonstrated for Cld or Cld-like proteins[115]. The resultant oxygen is then further respired to H_2O by a terminal oxygen reductase. The putative participation of a Cld-like protein was based on expression data rather than empirically determined activity[115]. Furthermore, comparative genomics does not support the general involvement of Cld in IO_3^- respiration, as *cld* is never co-located with the iodate reduction gene cluster and is notably absent from all but two of the 145 putative DIRM genomes identified in NCBI GenBank (see below) including the genome of *Denitromonas* sp. IR-12.

Since *Denitromonas* sp. IR-12 genome lacks *cld*-like genes, I propose that the primary mechanism of IO_3^- respiration by this organism relies on the complex and reactive chemistry of iodine oxyanions[146] and that the peroxidases $IdrP_1$ and $IdrP_2$ serve a critical detoxification role for inadvertent oxidants generated rather than being central components of the pathway itself. In the *Denitromonas* sp. IR-12 model (Figure 2.3A), IdrAB accepts electrons from cytochrome c551, and performs a four-electron transfer, similarly to the mechanism of perchlorate reductase (Pcr)[113], with a resultant production of the chemically unstable intermediate hypoiodous acid (HIO). This intermediate then undergoes abiotic disproportionation to yield I^- and IO_3^- in a 2:1 ratio as reported in alkaline aquatic environments[147,148], and is simplistically represented by the following equation:

$$3\ HIO \rightarrow 2\ I^- + IO_3^- + 3\ H^+$$

The resultant IO_3^- subsequently cycles back into the reductive pathway. In this manner, the cell completes the 6-electron reduction of IO_3^- to I^- without invoking a Cld-like enzyme with putative capacity to dismutate IO^- to I^- and O_2. This model is similar to the cryptic model for some species of perchlorate reducing microorganism which rely on the chemical reactivity of the unstable pathway intermediate chlorite (ClO_2^-) with reduced species of iron or sulfur to prevent toxic inhibition [113,149]. I propose that the initial reduction of IO_3^- at the IdrA inadvertently produces low levels of incidental toxic H_2O_2. This is analogous to the production of hypochlorite (ClO^-) by respiratory perchlorate reducing microorganisms during respiration of perchlorate or chlorate[150,151]. To protect themselves from this reactive chlorine species, perchlorate respiring organisms have evolved a detoxifying mechanism based on redox cycling of a sacrificial methionine rich peptide[151]. In the *Denitromonas* sp. IR-12 model for IO_3^- respiration the cytochrome c peroxidases play the critical detoxification role against inadvertent H_2O_2 production, rather than a central role for the reductive pathway as proposed for *Pseudomonas* strain SCT[115] (Figure 2.3A). Such a model is not only parsimonious with the predicted biochemistries and abiotic reactivities of the proteins and iodine oxyanions involved but is also consistent with the micromolar quantities of H_2O_2 observed by Yamazaki *et al.* during the reduction of millimolar quantities of IO_3^- by *Pseudomonas* strain SCT[115].

2.3.6 Evolutionary history of DIR

Core genes for DIR were used to define the phylogenetic distribution of this metabolism. Numerous homologs, some showing between 50-80% amino acid identity to the catalytic subunit of IdrA, were identified among genomes in NCBI GenBank. A phylogenetic tree of the DMSO reductase family (Figure 2.4A and 2.4B) confirms previous results indicating that arsenite oxidase alpha subunit (AioA) is the most closely related characterized enzyme to IdrA[115]. The extent of the IdrA clade was difficult to define because IdrA from *Denitromonas* sp. IR-12 and *Pseudomonas* sp. SCT are closely related. To determine whether more IdrA homologs in this clade function as IO_3^- reductases or arsenite oxidases, I performed a gene neighborhood analysis looking at the 10 genes both upstream and downstream of either the *idrA* or *aioA* locus and clustered them using MMseqs2[123] (Figure 2.5; Figure 2.6). I observed a clear distinction in neighborhood synteny between genes mostly closely to *idrA* versus those most closely related to *aioA*. All neighborhoods in the *idrA* clade showed conserved synteny at *idrABP$_1$P$_2$* (Figure 2.5), whereas organisms with an AioA, showed an alternative gene structure, notably missing the cytochrome c peroxidases. Based on this pattern, all organisms possessing *idrABP$_1$P$_2$* genes are likely DIRM. The outgroups of IO_3^- reductase in this phylogeny are homologs found in *Halorubrum* spp., which are known to oxidize arsenite[152], and a *Dehalococcodia* bacterium (GCA_002730485.1), which also lacks the cytochrome c peroxidases in its gene neighborhood (Figure 2.5; Figure 2.6). Further research into these proteins may provide more information on the transition from arsenite oxidase to IO_3^- reductase.

Genes mediating IO_3^- reduction were identified in 145 genomes from bacteria in the *Alphaproteobacteria*, *Betaproteobacteria*, and *Gammaproteobacteria* (Figure 2.4; Table 2.3). Deeper branching members included members of *Planctomycetaceae* and several others belonging to the Candidate Phyla Radiation group such as, *Ca. Rokubacteria*, *Ca. Lindowbacteria*, and NC10 (Figure 2.4B)[153-155]. DIR seemed most prevalent in the phylum *Proteobacteria*, which is a pattern that has been observed for some other rare metabolisms[156]. The discordance between the taxonomy of the host organisms and the phylogeny of IdrA (Figure 2.4B ; Figure 2.7)[131] suggested that DIR is a horizontally transferred metabolism. For example, IdrA in the *Gammaproteobacterium Pseudomonas* sp. SCT was most closely related to IdrA in *Betaproteobacteria* such as *Azoarcus* sp. DN11. Additional evidence for horizontal gene transfer in individual genomes included insertion sites at the 3' end of tRNAs, a skew in GC content, and association with other horizontally transferred genes[157,158]. In *Denitromonas* sp. IR-12, there was no significant GC skew or direct inverted repeats. However, a $tRNA^{Gly}$ was observed roughly 72 kbp downstream of the *idrABP$_1$P$_2$* locus which was previously demonstrated to be an integration site by Larbig *et al.* in *P. stutzeri*[159]. Additionally, numerous heavy metal resistance markers, like *mer* and *cus* genes, were found near the *idrABP$_1$P$_2$* locus (1.2 kbp and 22 kbp away respectively), further suggesting horizontal transfer[157,160,161]. A method to detect genomic islands in complete genomes predicted the *idrABP$_1$P$_2$* locus to be its own 5.8 kbp genomic island in *Azoarcus* sp. DN11, which has a complete genome and a closely related IdrA[162]. Therefore, while there is poor conservation of genes surrounding *idrABP$_1$P$_2$* and questions remain about its recent evolution, the high degree of conservation of *idrABP$_1$P$_2$* locus itself and the phylogenetic pattern of inheritance support its description as an iodate reduction genomic island (IRI) that is subject to horizontal gene transfer. In addition to the perchlorate reduction genomic island (PRI)[156] the IRI represents one of the few

respiratory genomic islands known that crosses large phylogenetic boundaries (class, order, and family).

2.4 Significance

Here I describe a new organism, *Denitromonas* sp. IR-12, that grows by IO_3^- respiration which is mediated by a novel molybdenum dependent DMSO reductase. The conserved core genes associated with DIR and the chemistry of iodine oxyanions are consistent with a hybrid enzymatic-abiotic pathway by which IdrAB reduces IO_3^- to HIO, which abiotically disproportionates to I^- and IO_3^-[147,148]. In this model, cytochrome c peroxidase like proteins ($IdrP_1$ and $IdrP_2$) detoxify reactive H_2O_2 byproducts. Genes for this metabolism form part of a highly conserved IO_3^- reduction genomic island (IRI). Organisms harboring the IRI belong to phylogenetically distinct taxa, many of which are associated with marine sediments or multicellular hosts, suggesting that DIR is a horizontally transferred metabolism across marine ecosystems over geologic time.

2.5 Figures and tables

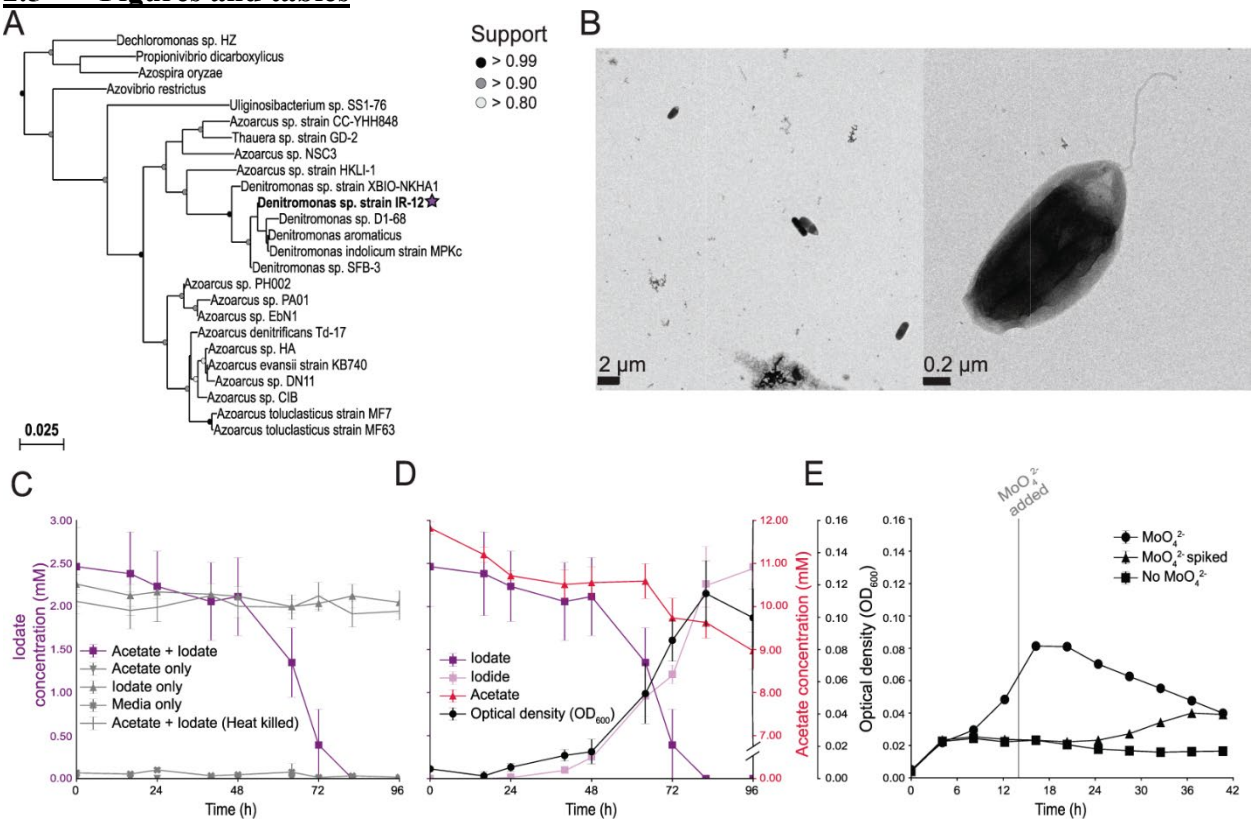

FIGURE 2.1: PHYLOGENY AND PHYSIOLOGY OF DENITROMONAS SP. IR-12. A 16S rRNA gene phylogeny of *Denitromonas* sp. IR-12 (denoted by a purple star) belonging to a subclade of *Azoarcus*, separate from other known *Azoarcus* species. **B** TEM images of an active culture of *Denitromonas* sp. IR-12 with the scale at 2 µm (left) and 0.2 µm (right) taken on a Technai 12 TEM. **C** Iodate consumption across all five conditions assessed in the growth experiment in **D**. *N* = 3 and error bars show standard deviation. **D** Iodate consumption (■), acetate consumption (▲), iodide production (■), and growth (●; measured as optical density at λ=600 nm; OD600) in an active culture of *Denitromonas* sp. IR-12 growing anaerobically. *N* = 3 and error bars show standard deviation. **E** Optical density (OD600) in the presence (■), absence (●), and amendment of MoO42- after 14 hours incubation (▲). *N* = 7 and error bars show standard deviation.

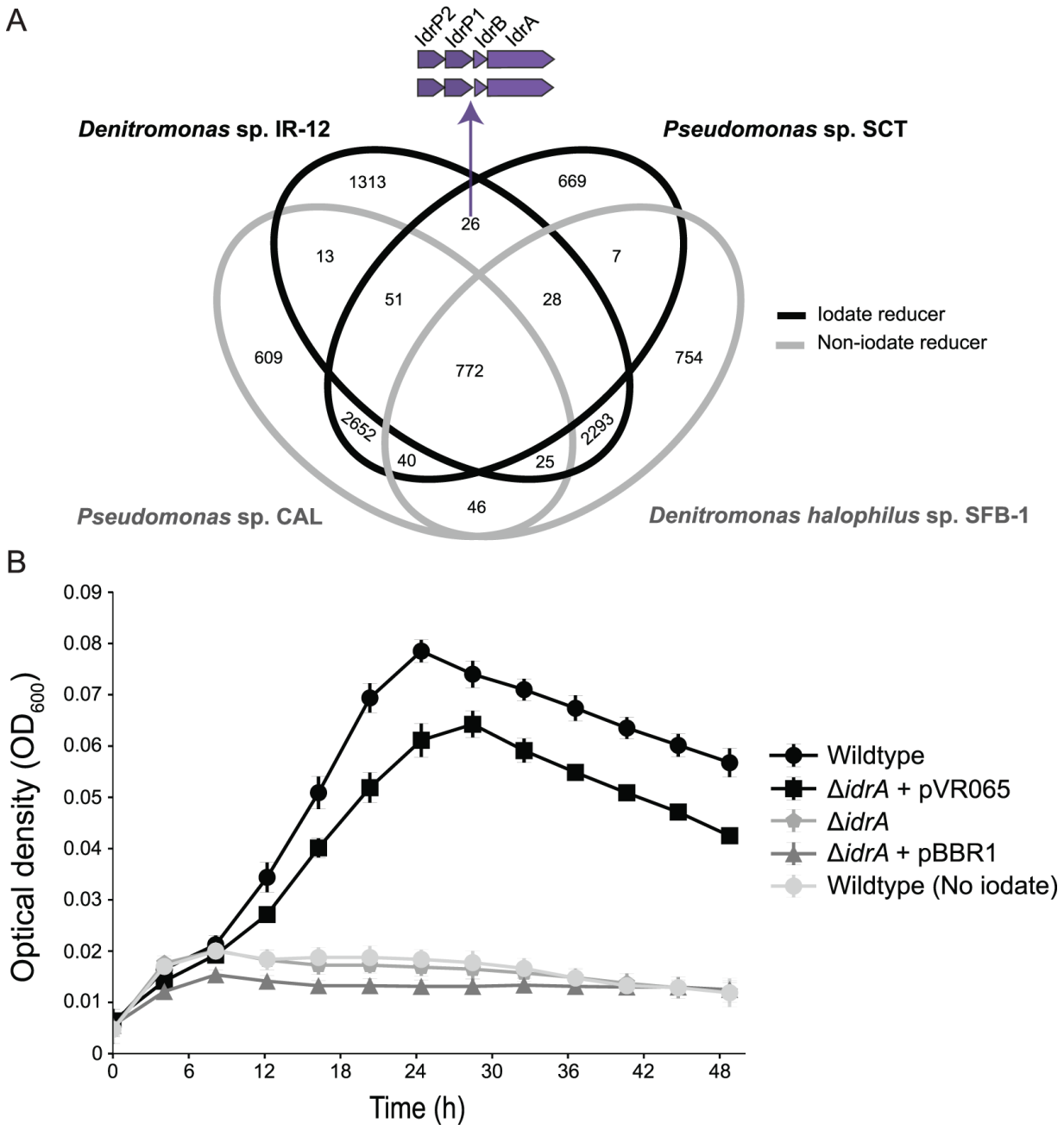

FIGURE 2.2: IDENTIFICATION OF A UNIQUE GENE CLUSTER IN IODATE REDUCING GENOMES ENABLING THE IDENTIFICATION AND CHARACTERIZATION OF THE IODATE REDUCTASE (IDRA). **A** A four-way comparison between two genomes from confirmed DIRM (black line) and two genomes from closely related non-DIRM (gray line) identifying 26 shared genes among the two taxonomically distinct iodate reducing bacteria (see Table S2). The four genes involved in DIR are shown above the Venn diagram in purple. **B** Anaerobic growth of wildtype of Denitromonas sp. IR-12 in the presence (●) or absence (○) of iodate is shown in comparison to the idrA mutant (●), the idrA mutant complemented with an empty vector (▲), or with idrA complemented in trans (■). $N = 8$ and error bars represent standard deviation.

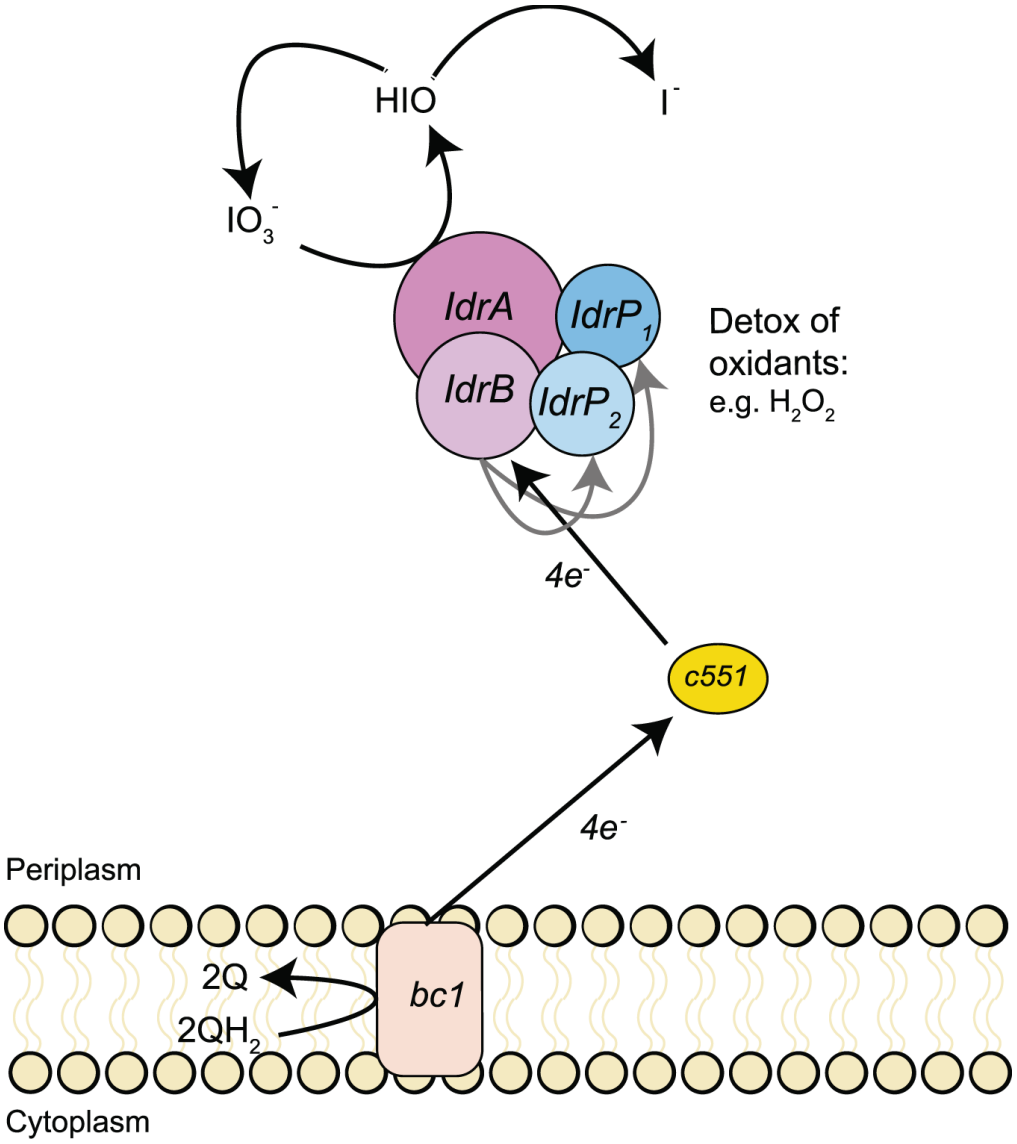

FIGURE 2.3: MECHANISTIC MODEL OF IODATE REDUCTION. A representation of the electron flow (black arrows) from the quinone pool to iodate in *Denitromonas sp.* IR-12. QH_2 reduced quinone, Q oxidized quinone, bc1 bc1 complex, IO_3 iodate, HIO hypoiodous acid, I iodide, H_2O_2 hydrogen peroxide. Gray arrows represent micromolar production of yet unknown oxidant that is detoxified by $IdrP_1$ and $IdrP_2$.

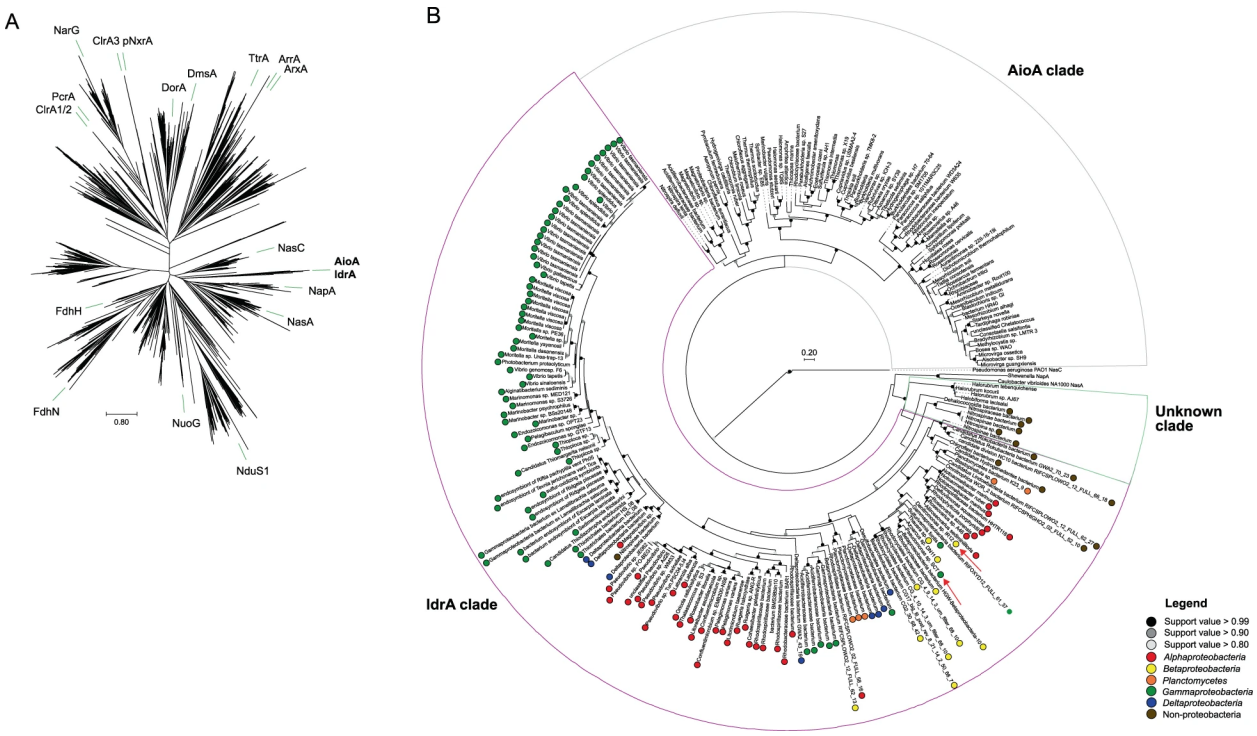

FIGURE 2.4: PHYLOGENY AND TAXONOMIC DISTRIBUTION OF IDRA. A Phylogeny of molybdopterin oxidoreductases (Pfam 00384) using pre-aligned proteins from the representative proteomes 55 dataset. Green bars indicate location of an individual protein in each branch belonging to the labeled group. **B** Phylogeny of the iodate reductase (IdrA), arsenite oxidase (AioA), and an unknown clade that contains proteins from organisms showing demonstrated arsenite oxidation abilities. Colored circles along the edges of the IdrA clade indicate the different class each organism belongs to. Arrows indicate the location of IdrA from the two confirmed iodate-reducing microorganisms.

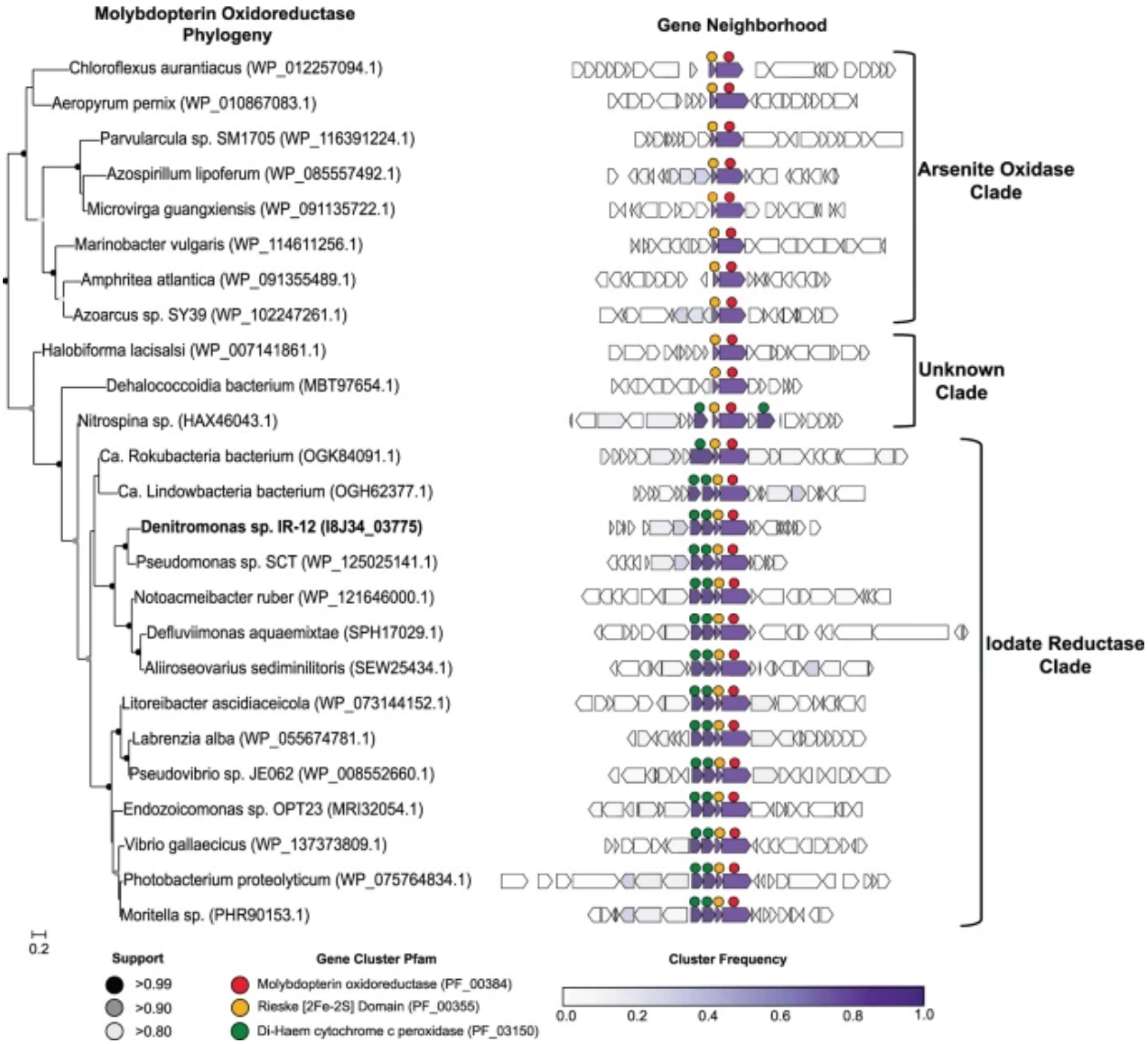

FIGURE 2.5: PHYLOGENY AND GENE NEIGHBORHOODS OF ARSENITE OXIDASE, IODATE REDUCTASE, AND THE ASSOCIATED UNKNOWN CLADE. A pruned tree of the molybdopterin oxidoreductase phylogeny (left) showing a representative subset of genomes identified from Figure 2.4B. *Denitromonas* sp. IR-12 is illustrated in bold and locus tags are provided in parentheses. Gene neighborhoods (right) show ten genes upstream and downstream (if present) from the *idrA* locus. Individual genes were clustered into groups based on amino acid similarity using MMSeqs2 and the frequency of genomes possessing an individual cluster is colored by the intensity of purple. Circles above each gene represents either the molybdopterin oxidoreductase (●), the associated Rieske containing subunit (●), or the di-haem cytochrome c peroxidase protein families (●).

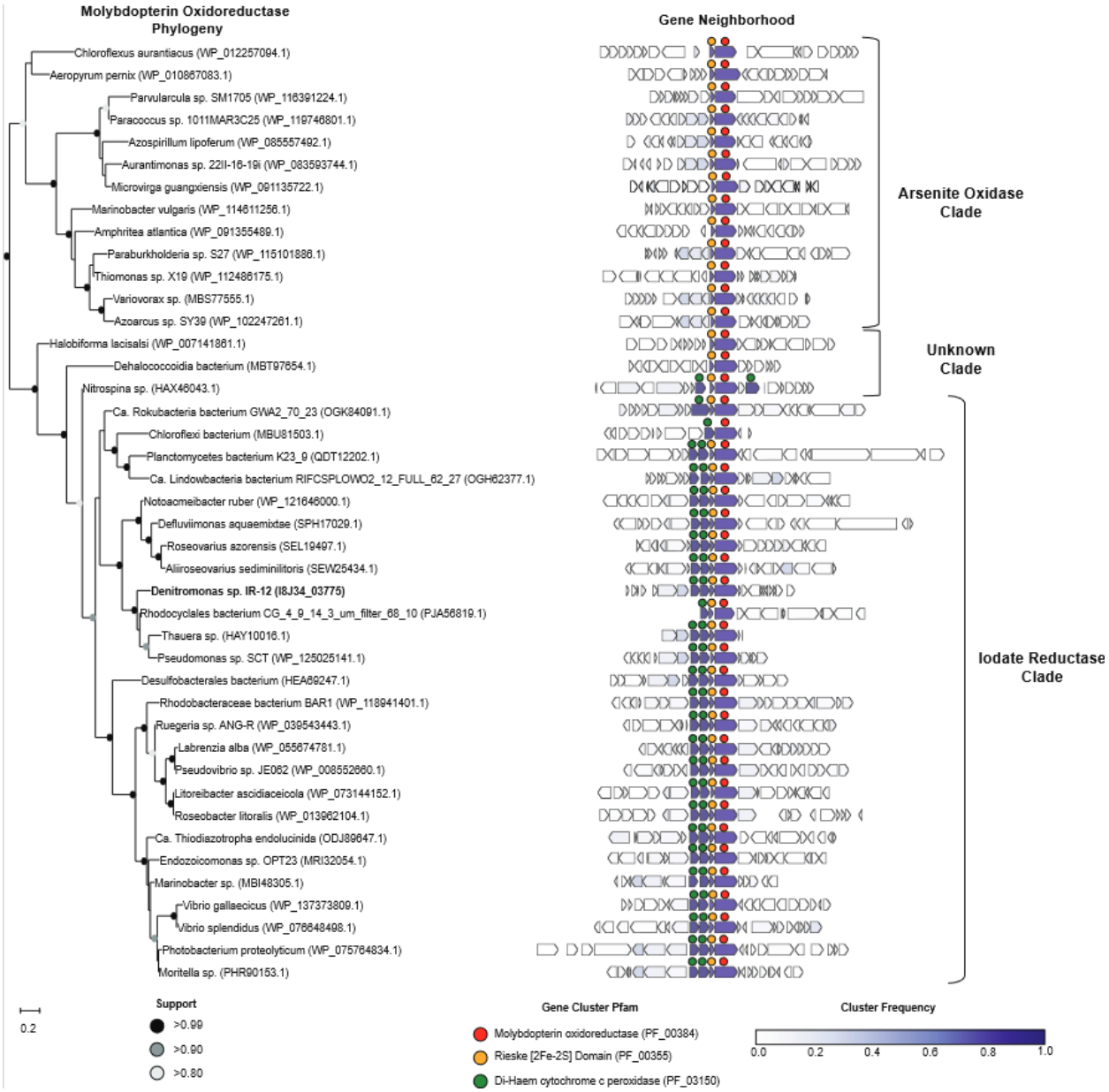

FIGURE 2.6: EXPANDED GENE NEIGHBORHOOD TREE. An expanded tree of the molybdopterin oxidoreductase phylogeny (left) showing a representative subset of genomes identified from Figure 4B. Denitromonas sp. IR-12 is illustrated in bold. Genome neighborhoods (right) show 10 genes upstream and downstream (if present) from the idrA or aioA locus. Individual genes were clustered into groups based on amino acid similarity using MMSeqs2 and the frequency of each cluster across all genomes is colored by the intensity of purple where 1.0 means the cluster is present in all genomes, and 0.0 means the cluster is absent in all genomes. Circles above each gene represents the gene cluster protein family.

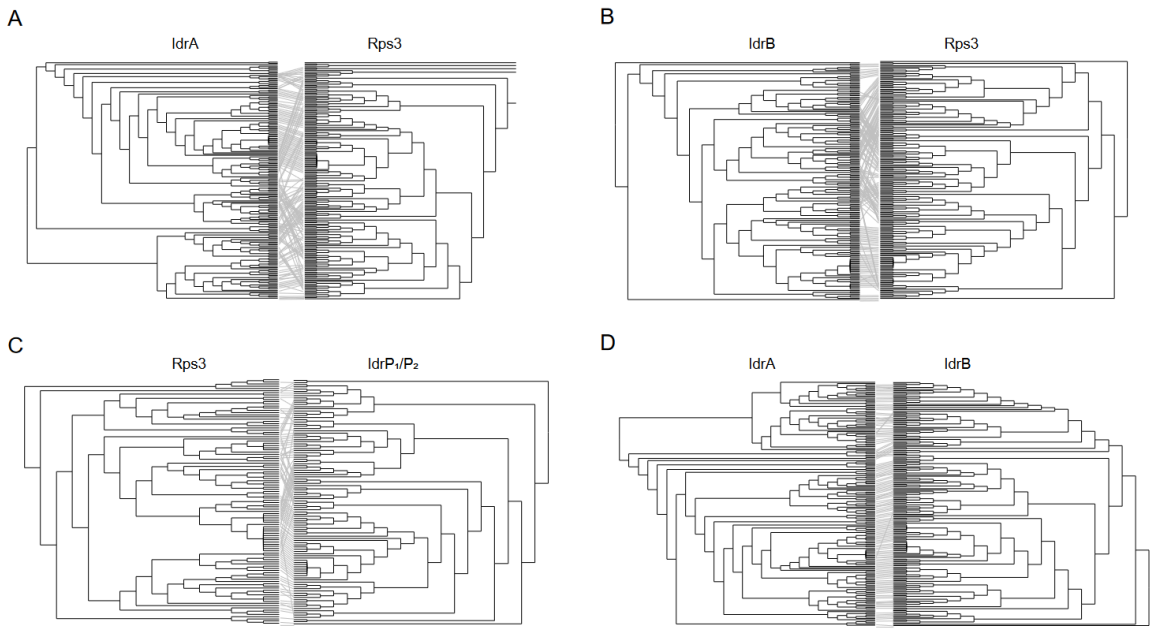

FIGURE 2.7: TANGLEGRAM ANALYSIS OF INDIVIDUAL PROTEINS IN THE IRI. A pairwise tanglegram analysis between IdrA (A), IdrB (B), and $IdrP_1/P_2$ (C), and Rps3. Labels for each tree have been removed for ease of viewing. Rps3 trees in all figures use *Halobiforma lacisalsi* as an outgroup, which is removed when corresponding IRI gene is not present in the organism (C). Lines drawn between trees represent a connection between the physical location on the left tree and the physical connection on the right tree. Entanglement in A-C demonstrates the discordant tree topology, and is suggestive of horizontal gene transfer. A comparison between IdrA and IdrB (D) is shown to demonstrate the co-evolution of these two proteins together.

TABLE 2.1: PLASMIDS, STRAINS, AND PRIMERS USED

Name	*Description*	*Source*
	Plasmid	
pBBR1-MCS2	Expression vector low copy pBBR1 *oriV* and kanamycin resistance marker	
pNTPS138	Suicide Vector containing *sacB*, *traJ*, and neomycin resistance	Gift from the Kathleen Ryan Lab
pJK073	Δ*idrA* in frame deletion on pNTPS138 backbone built by Gibson assembly using products from IR403_F/IR404_R on pNTPS138. IR405_F/IR406_R and IR407_F/IR408_R were used to amplify upstream and downstream regions flanking *idrA* from gDNA	This study
pVR032	*idrABP$_1$P$_2$* expression vector built by XbaI/SacI double digest into pBBR1 using product from IR284_F and IR285R amplification of gDNA	"
pVR035	Re-circularized *idrABP$_1$P$_2$* expression vector using product from IR278_F and IR279_R on pVR032 to remove disrupted upstream lacZα	"
pVR062	Re-circularized *idrABP$_1$P$_2$* expression vector on lac promoter using product from IR280_F and IR281_R on pVR035 to remove remaining lacZα	"
pVR065	Re-circularized *idrA* expression vector on a lac promoter using product of IR279_R and IR361_F on pVR062	"
	E. coli	
WM3064	*thrB1004 pro thi rpsL hsdS lacZΔM15 RP4-1360 Δ(araBAD)567 ΔdapA1341::[erm pir]*	William Metcalf, University of Illinois
XL1-Blue	*endA1 gyrA96(nal^R) thi-1 recA1 relA1 lac glnV44 F'[::Tn10 proAB$^+$ lacI^q Δ(lacZ)M15] hsdR17(r_K^- m_K^+)*	Stratagene
	Denitromonas sp. IR-12	
DIR12	Wildtype	This study
DIR12_27	*ΔidrA*	"
DIR12_28	*ΔidrA* + pVR065	"
DIR12_29	*ΔidrA* + pBBR1-MCS2	"
	Primers	
IR284_F	TTTTTCTAGAGTCCATTCGAGATCGACAAGGGGAAACT (5' XbaI site added)	"
IR285_R	TTTTTGAGCTCCAAGCAGGGCTGTGACGATGATTGTTTT (3' SacI site added)	"
IR278_F	CTAGAGTCCATTCGAGATCGACAAGGG	"
IR279_R	AGCTGTTTCCTGTGTGAAATTGTTATCCG	"
IR280_F	CGCGTTAAATTTTTGTTAAATCAGCTC	"
IR281_R	GAGCTCCAAATCTCCAGGGTTTCGGGG	"
IR361_F	ATGAGTGAAAACATCAAGCAAGGCG	"
IR403_F	AGCAGGAAAGCTGCTTCACATCTAGAGGGTCGACGCATGCCTGT	"
IR404_R	CCAATCGGCACCGAACACGTTCGTCAAGGCCTTAAGTGAGTCGTATTACGG	"
IR405_F	ACGACTCACTTAAGGCCTTGACGAACGTGTTCGGTGCCGATTGG	"

IR406_R	AGTTCAAGCGGCGACGGCCTCACATGATGATTCTCCTTGTGCTTAGCGG	"
IR407_F	AAGCACAAGGAGAATCATCATGTGAGGCCGTCGCCGCTTGAACT	"
IR408_R	ACAGGCATGCGTCGACCCTCTAGATGTGAAGCAGCTTTCCTGCTGCGC	"

TABLE 2.2: LIST OF PROTEINS SHARED BETWEEN DENITROMONAS SP. IR-12 AND P. STUTZERI SP. SCT. List of all 26 proteins identified as shared homologs between Denitromonas *sp. IR-12* and P. stutzeri sp. SCT. IR-12 denotes protein in Denitromonas *sp. IR-12* and SCT denotes protein in P. stutzeri. Alternating colors represents a group of homologs. Shared genes belonging to the iodate reduction island are in bold purple. Locus tags for Denitromonas sp. IR-12 correspond to Prokka annotation.

Gene ID	*Genome ID*	*Gene Product Name*
KPDAEFOI_00687	**IR-12**	**Arsenite oxidase subunit AioA**
WP_125025141.1	**SCT**	**arsenate reductase (azurin) large subunit [Pseudomonas sp. SCT]**
KPDAEFOI_00682	IR-12	Sensor histidine kinase WalK
WP_125025133.1	SCT	sensor histidine kinase [Pseudomonas sp. SCT]
KPDAEFOI_04566	IR-12	Glycine betaine transporter
WP_015278434.1	SCT	BCCT family transporter [Pseudomonas stutzeri]
KPDAEFOI_02021	IR-12	hypothetical protein
WP_125021808.1	SCT	terminase [Pseudomonas sp. SCT]
KPDAEFOI_00683	IR-12	Transcriptional regulatory protein ZraR
WP_125025135.1	SCT	sigma-54-dependent Fis family transcriptional regulator [Pseudomonas sp. SCT]
KPDAEFOI_02296	IR-12	Ktr system potassium uptake protein B
WP_125021904.1	SCT	TrkH family potassium uptake protein [Pseudomonas sp. SCT]
KPDAEFOI_02000	IR-12	Putative prophage major tail sheath protein
WP_125021774.1	SCT	phage tail sheath protein [Pseudomonas sp. SCT]
KPDAEFOI_04546	IR-12	Acyl-CoA dehydrogenase
WP_125020924.1	SCT	acyl-CoA dehydrogenase [Pseudomonas sp. SCT]
KPDAEFOI_00685	**IR-12**	**Cytochrome c551 peroxidase**
WP_125025139.1	**SCT**	**cytochrome-c peroxidase [Pseudomonas sp. SCT]**
KPDAEFOI_00684	**IR-12**	**Cytochrome c551 peroxidase**
WP_125025137.1	**SCT**	**photosynthetic protein synthase I [Pseudomonas sp. SCT]**
KPDAEFOI_00700	IR-12	Demethylmenaquinone methyltransferase
WP_125024918.1	SCT	methyltransferase domain-containing protein [Pseudomonas sp. SCT]

KPDAEFOI_01933	IR-12	hypothetical protein
WP_125024798.1	SCT	hydroxyacid dehydrogenase [Pseudomonas sp. SCT]
KPDAEFOI_02022	IR-12	hypothetical protein
WP_125021811.1	SCT	phage portal protein [Pseudomonas sp. SCT]
KPDAEFOI_00004	IR-12	1,5-anhydro-D-fructose reductase
WP_003284930.1	SCT	MULTISPECIES: pyrroloquinoline quinone precursor peptide PqqA [Pseudomonas]
KPDAEFOI_03674	IR-12	N-acetyl-alpha-D-glucosaminyl-diphospho-ditrans, octacis-undecaprenol 4-epimerase
WP_125021464.1	SCT	SDR family oxidoreductase [Pseudomonas sp. SCT]
KPDAEFOI_00704	IR-12	Phosphate import ATP-binding protein PstB 3
WP_125024929.1	SCT	phosphate ABC transporter ATP-binding protein [Pseudomonas sp. SCT]
KPDAEFOI_00701	IR-12	Phosphate-binding protein PstS 1
WP_125024920.1	SCT	phosphate ABC transporter substrate-binding protein [Pseudomonas sp. SCT]
KPDAEFOI_04543	IR-12	2,3-dehydroadipyl-CoA hydratase
WP_125020926.1	SCT	enoyl-CoA hydratase [Pseudomonas sp. SCT]
KPDAEFOI_02295	IR-12	Ktr system potassium uptake protein A
WP_015277208.1	SCT	TrkA family potassium uptake protein [Pseudomonas stutzeri]
KPDAEFOI_00680	IR-12	hypothetical protein
WP_125024906.1	SCT	carboxymuconolactone decarboxylase family protein [Pseudomonas sp. SCT]
WP_125025012.1	SCT	carboxymuconolactone decarboxylase family protein [Pseudomonas sp. SCT]
KPDAEFOI_00686	**IR-12**	**Arsenite oxidase subunit AioB**
WP_125025155.1	**SCT**	**arsenate reductase (azurin) small subunit [Pseudomonas sp. SCT]**
KPDAEFOI_04088	IR-12	Protein ArsC
WP_125021591.1	SCT	arsenate reductase ArsC [Pseudomonas sp. SCT]
KPDAEFOI_01995	IR-12	hypothetical protein
WP_125021770.1	SCT	phage tail assembly protein [Pseudomonas sp. SCT]
KPDAEFOI_01970	IR-12	hypothetical protein

WP_003294399.1	SCT	hypothetical protein [Pseudomonas stutzeri]
KPDAEFOI_02016	IR-12	hypothetical protein
WP_125021796.1	SCT	phage tail protein [Pseudomonas sp. SCT]
KPDAEFOI_01994	IR-12	hypothetical protein
WP_084899166.1	SCT	MULTISPECIES: GpE family phage tail protein [Pseudomonas]

TABLE 2.3: SELECT BACTERIA FROM FIGURE 2.4B POSSESSING THE IRI AND ASSOCIATED ENVIRONMENT

Species Name	Lifestyle	Associated Environment	Citation
Gammaproteobacterium	Endosymbiont	*Ridgeia piscesae* (Tubeworm)	[1]
Gammaproteobacterium	Endosymbiont	*Lamellibrachia satsuma* (Tubeworm)	[2]
Gammaproteobacterium	Endosymbiont	*Tevnia jerichonana* (Tubeworm)	[3]
Alginatibacterium sediminis	Free Living	Marine sediment	[4]
Aliiroseovarius sediminilitoris	Free Living	Seawater	[5]
Azoarcus sp. DN11	Free Living	Gasoline-Contaminated Groundwater	[6]
Azoarcus toluclasticus	Free Living	Coastal stream	This study
Defluviimonas aquaemixtae	Free Living	Boundary of freshwater spring and ocean	[7]
Denitromonas sp. IR-12	Free Living	Estuarine sediment	This study
Litorimicrobium taeanense	Free Living	Sandy beach	[8]
Marinobacter psychrophilus	Free Living	Arctic sea ice	[9]
Moritella dasanensis	Free Living	Seawater near glacier	[10]
Moritella yayanosiii	Free Living	Mariana trench	[11]
Oricola cellulosilytica	Free Living	Seawater	[12]
Pelagimonas varians	Free Living	Seawater	[13]
Photobacterium proteolyticum	Free Living	Estuarine sediment	[14]
Pseudomonas sp. SCT	Free Living	Marine sediment	[15]
Roseovarius azorensis	Free Living	Seawater	[16]
Sedimenticola thiotaurini	Free Living	Salt marsh sediment	[17]
Endozoicomonas sp. OPT23	Host associated	*Ophlitaspongia papilla* (Sea squirt)	[18]
Labrenzia alba	Host associated	*Ostera spp.* (Mediterranean oyster)	[19]
Litoreibacter ascidiaceicola	Host associated	*Halocynthia aurantium* (Sea squirt)	[20]
Moritella viscosa	Host associated	*Gadus morhua* (Atlantic cod)	[21]
Notoacmeibacter marinus	Host associated	*Notoacmea schrenckii* (Marine Limpet)	[22]

Notoacmeibacter ruber	Host associated	*Rhizophora stylosa* (Spotted mangrove)	[23]
Pseudovibrio axinellae	Host associated	*Axinella dissimilis* (Irish maine sponge)	[24]
Rhodophyticola porphyridii	Host associated	*Porphyridium marinum* (Red algae)	[25]
Roseobacter litoralis	Host associated	High tide seaweeds	[26]
Ruegeria halocynthiae	Host associated	*Halocynthia roretzi* (Sea squirt)	[27]
Thiomargarita nelsonii	Host associated	provannid gastropod	[28]
Vibrio gallaecicus	Host associated	*Ruditapes philippinarum* (Manila clam)	[29]
Vibrio sinaloensis	Host associated	*Lutjanus guttatus* (spotted rose snapper)	[30]
Vibrio splendidus	Host associated	*Ruditapes decussatus* (Carpet shell clam)	[31]
Vibrio tapetis	Host associated	*Ruditapes philippinarum* and *Ruditapes decussatus* (Clams)	[32]
Vibrio tasmaniensis	Host associated	*Salmo salar L.* (Atlantic salmon)	[33]
Sulfurivermis fontis	Microbial Mat	Hot spring microbial mat	[34]

References for Table S3 (Separate numbering scheme from in text references)

1. Chao LS-L, Davis RE, Moyer CL. Characterization of bacterial community structure in vestimentiferan tubeworm Ridgeia piscesae trophosomes. Mar Ecol. 2007;28(1):72-85.
2. Patra AK, Cho HH, Kwon YM, Kwon KK, Sato T, Kato C, et al. Phylogenetic relationship between symbionts of tubeworm Lamellibrachia satsuma and the sediment microbial community in Kagoshima Bay. Ocean Sci J. 2016;51(3):317-332.
3. Gardebrecht A, Markert S, Sievert SM, Felbeck H, Thürmer A, Albrecht D, et al. Physiological homogeneity among the endosymbionts of Riftia pachyptila and Tevnia jerichonana revealed by proteogenomics. ISME J. 2012;6(4):766-776.
4. Wang Z, Zhang Z, Hu Z, Zhao J, Zhao D, Zhang Y. Alginatibacterium sediminis gen. nov., sp. nov., a novel marine gammaproteobacterium isolated from coastal sediment. Int J Syst Evol Microbiol. 2019;69(2):511-516.
5. Park S, Park J-M, Kang C-H, Yoon J-H. Aliiroseovarius pelagivivens gen. nov., sp. nov., isolated from seawater, and reclassification of three species of the genus Roseovarius as Aliiroseovarius crassostreae comb. nov., Aliiroseovarius halocynthiae comb. nov. and Aliiroseovarius sediminilitoris comb. nov. Int J Syst Evol Microbiol. 2015;65(Pt_8):2646-2652.
6. Kasai Y, Takahata Y, Manefield M, Watanabe K. RNA-based stable isotope probing and isolation of anaerobic benzene-degrading bacteria from gasoline-contaminated groundwater. Appl Environ Microbiol. 2006;72(5):3586-3592.

7. Jung Y-T, Park S, Lee J-S, Yoon J-H. Defluviimonas aquaemixtae sp. nov., isolated from the junction between a freshwater spring and the ocean. Int J Syst Evol Microbiol. 2014;64(Pt_12):4191-4197.
8. Jin HM, Lee HJ, Kim JM, Park MS, Lee K, Jeon CO. Litorimicrobium taeanense gen. nov., sp. nov., isolated from a sandy beach. Int J Syst Evol Microbiol. 2011;61(6):1392-1396.
9. Zhang D-C, Li H-R, Xin Y-H, Chi Z-M, Zhou P-J, Yu Y. Marinobacter psychrophilus sp. nov., a psychrophilic bacterium isolated from the Arctic. Int J Syst Evol Microbiol. 2008;58(6):1463-1466.
10. Kim HJ, Park S, Lee JM, Park S, Jung W, Kang J-S, et al. Moritella dasanensis sp. nov., a psychrophilic bacterium isolated from the Arctic ocean. Int J Syst Evol Microbiol. 2008;58(4):817-820.
11. Nogi Y, Kato C. Taxonomic studies of extremely barophilic bacteria isolated from the Mariana Trench and description of Moritella yayanosii sp. nov., a new barophilic bacterial isolate. Extremophiles. 1999;3(1):71-77.
12. Hameed A, Shahina M, Lai W-A, Lin S-Y, Young L-S, Liu Y-C, et al. Oricola cellulosilytica gen. nov., sp. nov., a cellulose-degrading bacterium of the family Phyllobacteriaceae isolated from surface seashore water, and emended descriptions of Mesorhizobium loti and Phyllobacteriummyrsinacearum. Antonie Van Leeuwenhoek. 2015;107(3):759-771.
13. Hahnke S, Tindall BJ, Schumann P, Simon M, Brinkhoff T. Pelagimonas varians gen. nov., sp. nov., isolated from the southern North Sea. Int J Syst Evol Microbiol. 2013;63(Pt_3):835-843.
14. Li Y, Zhou M, Wang F, Wang ET, Du Z, Wu C, et al. Photobacterium proteolyticum sp. nov., a protease-producing bacterium isolated from ocean sediments of Laizhou Bay. Int J Syst Evol Microbiol. 2017;67(6):1835-1840.
15. Amachi S, Kawaguchi N, Muramatsu Y, Tsuchiya S, Watanabe Y, Shinoyama H, et al. Dissimilatory iodate reduction by marine Pseudomonas sp. strain SCT. Appl Environ Microbiol. 2007;73(18):5725-5730.
16. Rajasabapathy R, Mohandass C, Dastager SG, Liu Q, Khieu T-N, Son CK, et al. Roseovarius azorensis sp. nov., isolated from seawater at Espalamaca, Azores. Antonie Van Leeuwenhoek. 2014;105(3):571-578.
17. Jones DS, Bailey JV, Flood BE. Sedimenticola thiotaurini sp. nov., a sulfur-oxidizing bacterium isolated from salt marsh sediments, and emended descriptions of the genus Sedimenticola and Sedimenticola selenatireducens. Int J Syst Evol Microbiol. 2015;65(8):2522-2530.
18. Alex A, Antunes A. Comparative Genomics Reveals Metabolic Specificity of Endozoicomonas isolated from a marine sponge and the genomic repertoire for host-bacteria symbioses. Microorganisms. 2019;7(12):635.
19. Pujalte MJ, Macián MC, Arahal DR, Garay E. Stappia alba sp. nov., isolated from Mediterranean oysters. Syst Appl Microbiol. 2005;28(8):672-678.
20. Kim Y-O, Park S, Nam B-H, Park J-M, Kim D-G, Yoon J-H. Litoreibacter ascidiaceicola sp. nov., isolated from the golden sea squirt Halocynthiaaurantium. Int J Syst Evol Microbiol. 2014;64(Pt_8):2545-2550.

21. Colquhoun D, Hovland H, Hellberg H, Haug T, Nilsen H. Moritella viscosa isolated from farmed Atlantic cod (Gadus morhua). Bull Eur Assoc Fish Pathol. 2004;24(2):109-114.
22. Huang Z, Guo F, Lai Q, Shao Z. Notoacmeibacter marinus gen. nov., sp. nov., isolated from the gut of a limpet and proposal of Notoacmeibacteraceae fam. nov. in the order Rhizobiales of the class Alphaproteobacteria. Int J Syst Evol Microbiol. 2017;67(8):2527-2531.
23. Yan X-R, Tuo L. Notoacmeibacter ruber sp. nov., a novel endophytic bacterium isolated from leaf of Rhizophora stylosa. Antonie Van Leeuwenhoek. 2019;112(6):919-925.
24. O'Halloran JA, Barbosa TM, Morrissey JP, Kennedy J, Dobson ADW, O'Gara F. Pseudovibrio axinellae sp. nov., isolated from an Irish marine sponge. Int J Syst Evol Microbiol. 2013;63(Pt_1):141-145.
25. Jung HS, Jeong SE, Chun BH, Quan Z-X, Jeon CO. Rhodophyticola porphyridii gen. nov., sp. nov., isolated from a red alga, Porphyridium marinum. Int J Syst Evol Microbiol. 2019;69(6):1656-1661.
26. Shiba T. Roseobacter litoralis gen. nov., sp. nov., and Roseobacter denitrificans sp. nov., aerobic pink-pigmented bacteria which contain bacteriochlorophyll a. Syst Appl Microbiol. 1991;14(2):140-145.
27. Kim Y-O, Park S, Nam B-H, Kang S-J, Hur YB, Lee S-J, et al. Ruegeria halocynthiae sp. nov., isolated from the sea squirt Halocynthia roretzi. Int J Syst Evol Microbiol. 2012;62(Pt_4):925-930.
28. Flood BE, Fliss P, Jones DS, Dick GJ, Jain S, Kaster A-K, et al. Single-cell (meta-)genomics of a dimorphic candidatus Thiomargarita nelsonii reveals genomic plasticity. Front Microbiol. 2016;7(603).
29. Beaz-Hidalgo R, Doce A, Pascual J, Toranzo AE, Romalde JL. Vibrio gallaecicus sp. nov. isolated from cultured clams in north-western Spain. Syst Appl Microbiol. 2009;32(2):111-117.
30. Gomez-Gil B, Fajer-Avila E, Pascual J, Macián MC, Pujalte MJ, Garay E, et al. Vibrio sinaloensis sp. nov., isolated from the spotted rose snapper, Lutjanus guttatus Steindachner, 1869. Int J Syst Evol Microbiol. 2008;58(7):1621-1624.
31. Gómez-León J, Villamil L, Lemos ML, Novoa B, Figueras A. Isolation of Vibrio alginolyticus and Vibrio splendidus from aquacultured carpet shell clam Ruditapes decussatus larvae associated with mass mortalities. Appl Environ Microbiol. 2005;71(1):98-104.
32. Borrego JJ, Castro D, Luque A, Paillard C, Maes P, Garcia MT, et al. Vibrio tapetis sp. nov., the causative agent of the brown ring disease affecting cultured clams. Int J Syst Evol Microbiol. 1996;46(2):480-484.
33. Thompson FL, Thompson CC, Swings J. Vibrio tasmaniensis sp. nov., isolated from Atlantic Salmon (Salmo salar L.). Syst Appl Microbiol. 2003;26(1):65-69.
34. Kojima H, Watanabe M, Fukui M. Sulfurivermis fontis gen. nov., sp. nov., a sulfur-oxidizing autotroph, and proposal of Thioprofundaceae fam. nov. Int J Syst Evol Microbiol. 2017;67(9):3458-3461.

Chapter Three: A mechanistic dissection of dissimilatory iodate reduction through genetics and genomics

Abstract

Chapter two demonstrated the existence of a mobile genomic island known as the IRI, which bestows the ability to perform DIR upon bacteria possessing it. Removal of the *idrA* gene from the IRI prevents bacteria from growing on iodate, suggesting that the gene is necessary to enable DIR. However, our analysis identified multiple genes that are tentatively involved in DIR. Here I describe the potential role each of these genes likely plays in the mature iodate reductase and show that removing any single gene inhibits growth under iodate reducing conditions. I also show that nitrate or the nitrate reductase does not significantly impact the ability of a DIRM to grow by DIR and demonstrate that *Denitromonas* sp. IR-12 preferentially uses nitrate over iodate. I examine the role of the $IdrP_1$ and $IdrP_2$ proteins and show that overexpression of $IdrP_1$ in a Δ*idrP*$_2$ strain does not enable growth by DIR, suggesting different roles for $IdrP_1$ and $IdrP_2$. Together, these data support the parsimonious DIR model proposed in chapter two and demonstrate that each component of the iodate reductase is necessary to enable DIR.

3.1 Introduction

Dissimilatory iodate reducing bacteria are a recently identified class of bacteria that can conserve energy and grow by reducing iodate (IO_3^-) as a terminal electron acceptor. All isolated DIRM exhibit a generalist chemoorganotrophic lifestyle, coupling the oxidation of numerous carbon substrates to the reduction of O_2, NO_3^-, or IO_3^-. The model DIRM discussed in this dissertation, *Denitromonas* sp. IR-12 bears much in common with other members of this chemoorganotrophic marine taxa but uniquely couples growth to IO_3^- respiration, completely reducing 2.5 mM IO_3^- to iodide (I^-)[163]. *Pseudomonas* sp. SCT is another cultured DIRM belonging to the broadly distributed and metabolically versatile genus *Pseudomonas*. Like *Denitromonas* sp. IR-12, *Pseudomonas* sp. SCT grows on up to 8 mM IO_3^- coupled to acetate oxidation[115,164]. Both organisms possess a unique genomic island enabling growth by dissimilatory iodate reduction (DIR) known as the iodate reduction island (IRI)[163]. The IRI contains a core set of four genes consisting of the heterodimeric molybdopterin oxidoreductase IdrAB and two di-heme cytochrome c peroxidase-like proteins $IdrP_1$ and $IdrP_2$[163]. Outside of the IRI, only minimal preservation of synteny exists. However, the synteny of the core genes is highly conserved across all confirmed and putative DIRM, suggesting that the *idrABP$_1$P$_2$* genes are inherited jointly and share a common evolutionary history[163].

Further obfuscating the understanding of the DIR metabolism is the mechanism of the iodate reductase. The predicted stoichiometry of DIR suggests a six-electron transfer from the reduced substrate (e.g., acetate) to IO_3^-. However, most molybdopterin oxidoreductases (DMSO reductases) are generally capable of catalyzing a two-electron transfer at the molybdenum cofactor, following the general equation[139]:

$$Mo^{VI} + 2H^+ + 2e^- \leftrightarrow Mo^{IV} + H_2O$$

The only example of a DMSO reductase performing two tandem two-electron transfers is the perchlorate reductase, which uses a gating mechanism to contain the chlorate intermediate mediating the 4 electron reduction of perchlorate (ClO_4^-) to chlorite (ClO_2^-)[113]. Furthermore, in the case of IO_3^-, intermediates formed by either a two-electron transfer (IO_2^-) or a four-electron transfer (IO^-) are unstable and ultimately disproportionate back to IO_3^- and I^-[147,148]. Two proposed models of DIR exist. Both models implicate the role of the heterodimeric molybdopterin oxidoreductase IdrAB in performing two tandem two-electron transfers from IO_3^- to HOI. However, following the initial reduction, one proposal suggests DIR generates hydrogen peroxide and HOI. Transcriptomic data then suggests each molecule is reduced by the $IdrP_1$/$IdrP_2$ and a chlorite dismutase, respectively[115]. However, chlorite dismutase is only known to use ClO_2^- as a substrate, converting it into chloride (Cl^-) and dioxygen (O_2), and activity against HOI has never been demonstrated[165]. A more parsimonious model that accounts for the reactive nature of iodine species relies on aquatic chemistry, suggesting that HOI abiotically disproportionates to IO_3^- and I^-, and that $IdrP_1$/$IdrP_2$ detoxifies transient intermediates (like hydrogen peroxide)[163]. Crucially,

both models are premised on the essentiality of all genes in the IRI and assume redundancy for genes *idrP1* and *idrP2*.

Chapter three seeks to examine many of the open questions surrounding the proposed DIR models through the lens of genetics. I demonstrate the essentiality of the core genes within the IRI by performing targeted knockouts coupled to growth assays in the model DIRM *Denitromonas* sp. IR-12. I provide additional evidence that the nitrate reductase does not enable growth on IO_3^- and identify possible differential expression of the nitrate and iodate reductases. I also challenge the $IdrP_1$/$IdrP_2$ redundancy assumption by demonstrating that $IdrP_1$ is strictly self-complementary and cannot rescue *idrP2* null strains even when overexpressed. Finally, I assess the divergent evolutionary history between $IdrP_1$ and $IdrP_2$ and discuss possible functions of these proteins. Together, these data paint an increasingly coherent picture of the steps involved in DIR and presents a point from which to assess the protein biochemistry of the iodate reductase.

3.2 Methods

3.2.1 Media, chemicals, and culture conditions

Anoxic cultures were grown in Artificial Pore Water (APM) medium at 30°C (30.8 g NaCl, 1.0 g NH_4Cl, 0.77 g KCl, 0.1 g KH_2PO_4, 0.20 g $MgSO_4 \cdot 7H_2O$, 0.02 g $CaCl_2 \cdot 2\ H_2O$, 7.16 g HEPES, along with vitamin and mineral mixes[163]. A post sterile addition of 34.24 mL of 0.4 M $CaCl_2$ and 26.07 mL 2 M $MgCl_2 \cdot 6H_2O$ was added to each liter of APM media. An anoxic stock of $FeSO_4 \cdot 7\ H_2O$ was added to a final concentration of 36 μM to all media when assessing conditions with *idrP1* or *idrP2* on a plasmid. Conditions with lactate and iodate all used the sodium salts of these compounds. Kanamycin concentrations when used were at one tenth the standard concentrations on plates (5 mg/L, Sigma Aldrich, USA) and at one fourth the standard concentration in liquid (12.5 mg/L). All compounds were purchased through Sigma Aldrich (Sigma Aldrich, USA). Growth of tubes were measured either using the Thermo Scientific GENESYS 20 or the TECAN Sunrise 96-well microplate reader set at a wavelength of 600 nm. For growth measurements in Hungate tubes, a special adapter was built to measure the tubes on the GENESYS 20. Growth experiments using the microplate reader were run in an anerobic glove bag under an atmosphere of 97.8% N_2 and 2.2% H_2.

3.2.2 Strains and plasmids

All constructed plasmids, primers and strains are listed in Table 3.1. The *E. coli* strain used for plasmid propagation was XL1-Blue, while WM3064 was used to perform conjugations. Plasmid pNTPS138, a generous gift from the Kathleen Ryan Lab at UC Berkeley, was used for the SacB counterselection. Plasmid pBBR1-MCS2 is a low copy expression vector and was used for complementation experiments. All expression plasmids and deletion vectors were constructed using the Benchling software suite (San Francisco, USA). Plasmids were assembled from genomic DNA by Gibson assembly using standard procedures. Gibson assembly was carried out using NEB HiFi 2x Master Mix (NEB, USA). Additional plasmids were built using primers to remove unwanted sequences by site directed mutagenesis and re-circularizing the resulting product with

the KLD Enzyme Mix (NEB, USA). Plasmids were routinely isolated using the Qiaprep Spin Miniprep kit (Qiagen, USA), and all primers were ordered from Integrated DNA Technologies (IDT, Coralville, IA). Since most sequences in the iodate reduction cluster contain at minimum 60% GC content, amplification is relatively challenging. Amplification of these challenging portions of the genome were optimized as follows: Amplification of DNA for generating assembly products was performed using Q5 DNA Polymerase 2x Master Mix (NEB, USA) with 3% DMSO. Annealing temperatures for each reaction was determined by subtracting the Tm provided by the NEB Tm calculator (https://tmcalculator.neb.com) for each primer pair by 1.8°C. All *Denitromonas* sp. IR-12 strains (pre- or post-transformation) were propagated from glycerol stocks (25% glycerol) stored at -80°C, grown on a plate for up to 72 hours, picked and then grown for an additional 48-72 hours in liquid R2A.

3.2.3 Expression vector transformation

Electroporator model GenePulser XCell (BioRad, USA) was used for high efficiency transformation of expression vectors into *Denitromonas* sp. IR-12. The procedure in short: 40 mL of *Denitromonas* sp. IR-12 was grown for 72 hours and spun down at 4000 RPM at 4°C for 15 minutes in 6 mL of cold, sterile deionized H_2O, followed by a wash and spin down in 6mL of cold, sterile 10% glycerol for an additional 15 minutes. The supernatant is decanted, and the pellet is resuspended to a final volume of 600 µL of 10% glycerol. Purified plasmid DNA is added at a concentration of 10ng/µL, and cells sit on ice for a minimum of 10 minutes. Electroporator is then pulsed once at 1750V, 25µF, and 400Ω for a 1mm GenePulser cuvette (BioRad, USA). Cells are then transferred to 500 µL of R2A media and are recovered for 4 hours at 30°C. After outgrowth 100µL of cells are plated out on R2A plates with 5 µg/µL kanamycin and allowed to grow at 30°C for three days. A 1:10 dilution of outgrown cells is recommended due to high transformation efficiency. Since the concentration of kanamycin is relatively low, all colonies are screened for the presence of the kanamycin resistance marker via PCR.

3.2.4 Suicide vector transformation

WM3064 *E. coli* was used to efficiently deliver suicide vectors into *Denitromonas* sp. IR-12. 50mL of *Denitromonas* sp. IR-12 is grown aerobically in R2A at 30°C for 30 hours, and *E. coli* is grown from an overnight culture for 4-6 hours at 37°C. Cultures are harvested and spun down at 7000 RCF at room temperature for 5 minutes. Cultures are then washed in R2A containing diaminopimelic acid (DAP) and are separately resuspended to a final volume of 250µL in R2A+DAP. The optical densities of each culture are measured, and the cells are added together and mixed at a 1:1 ratio in a final volume of 500µL. The entire conjugation is spotted onto three separate R2A+DAP plates and incubated at 30°C for 24 hours. The entire conjugation is then scraped off and resuspended in 10mL of R2A (no DAP) with 15% glycerol. 100µL of the conjugation is then spread out on two separate R2A plates with kanamycin and allowed to grow for 5 days. Transconjugants are then picked and plated again on R2A plates with kanamycin to allow for additional growth. Transconjugants are then screened by PCR for plasmid integration, and transconjugants possessing the rare integration event are picked and grown in liquid R2A for 3 days. 100µL of selected transconjugants are plated out on R2A + 7.5% sucrose, and colonies are

picked and screened on R2A + 7.5% sucrose and R2A + kanamycin after 5 days. Colonies showing growth on R2A + sucrose and no growth on R2A + kanamycin are then screened for the removal of the suicide vector and the presence of the expected deletion.

3.2.5 Vitamin and mineral mixes

Vitamin and the two mineral mixes were prepared separately as stock solutions. Per liter the vitamin mix contains, 2.0 mg D-biotin, 2.0 mg folic acid, 10.0 mg pyroxidine HCl, 5.0 mg riboflavin, 5.0 mg thiamine, 5.0 mg nicotinic acid, 5.0 mg pantothenic acid, 0.1 mg vitamin B12, 5.0 mg p-amino benzoic acid, 5.0 mg D,L-6,8-thiotic acid. Per liter mineral mix one contains 1.5 g NTA disodium salt, 3.0 g $MgSO_4 \cdot 7H2O$, 0.5 g $MnSO_4 \cdot H2O$, 1.0 g NaCl, 0.1 g $FeSO_4 \cdot 7H_2O$, 0.1 g $CaCl_2 \cdot 2H_2O$, 0.1 g $CoCl_2 \cdot 6H_2O$, 0.13 g ZnCl, 0.1 g $CuSO_4 \cdot 5H_2O$, 0.1 g $AlK(SO_4)_2 \cdot 12H_2O$, 0.1 g Boric Acid, 0.025 g $Na_2MoO_4 \cdot 2H_2O$, 0.024 g $NiCl_2 \cdot 6H_2O$, 0.025 g $Na_2WO_4 \cdot 2H_2O$, 0.02 g Na_2SeO_4. Mineral mix one is then adjusted to a pH of 6.0 with 1M NaOH. Per liter mineral mix two contains 40.0 g NaCl, 50.0g NH_4Cl, 5.0 g KCl, 5.0 g KH_2PO_4, 10.0g $MgSO_4 \cdot 7H_2O$, and 1.0g $CaCl_2 \cdot 2H_2O$. Mineral mix two is then adjusted to pH 6.0 with KOH. Media with vitamin and mineral mixes, add all the above mixes. Per liter of media, 10 mL of the vitamin mix, 10 mL of the mineral mix one, and 20 mL of mineral mix two are added.

3.2.6 $IdrP_1$ and $IdrP_2$ tree building

HMMER 3.0 was used to create a profile hidden Markov model (HMM) to search for cytochrome c peroxidase like proteins in a curated database previously containing genomes with Idr or Aio[163]. The Pfam_03150 seed set was used to create the profile HMM, and a previously curated dataset of genomes with Aio/Idr[163] was searched using a threshold of 45 as the cutoff. The profile HMM was then used to search the representative proteome dataset (https://www.ebi.ac.uk/Tools/hmmer/search/hmmsearch), and ten representative sequences from hits with different architectures were downloaded. Any sequence architecture with 5 or fewer sequences were not added onto the dataset. All 999 sequences were concatenated into a single fasta file, deduplicated, and aligned using MUSCLE 3.8 at standard settings. The unrooted phylogenetic tree was the built from aligned sequences using Fasttree[127], specifying 10,000 resamples and using standard settings for everything else. A rooted tree using a subset of sequences containing only $IdrP_1$ and $IdrP_2$ sequences from the Aio/Idr genome was made using the same methodology. Visualization of resultant trees used the iTOL web app.

3.3 Results

3.3.1 *idrAB* is necessary for growth by DIR

Targeted deletions at the *idrABP$_1$P$_2$* locus were carried out to assess the essentiality of individual genes. Cell growth under IO_3^- reducing conditions was used to determine whether individual gene deletions significantly impact growth and energy conservation. Consistent with observations presented in chapter two, an in-frame deletion of *idrA* prevents *Denitromonas* sp. IR-12 from growing when IO_3^- is the sole terminal electron acceptor (Figure 3.1A)[163]. When *idrA* is

expressed on a low copy vector in *trans,* the growth phenotype recovers; likewise, removal of the Reiske 2Fe-2S containing protein produced by *idrB* quenches the activity of the cell to conserve energy by DIR (Figure 3.1B). When *idrB* is provided in *trans*, the phenotype fully recovers to wildtype, taking longer to reach the peak OD_{600}. Providing an empty vector to either the *idrA* or the *idrB* null mutants does not recover the growth phenotype, suggesting that only the presence of either gene in *trans* is ultimately responsible for phenotype recovery.

Wildtype and mutant *Denitromonas* strains were grown with IO_3^-, NO_3^-, or both acceptors to assess the potential contribution of nitrate reductase on Δ*idrA* growth during DIR (Figure 3.2). The wildtype and Δ*idrA* attained similar optical densities when 2 mM nitrate was provided as the sole electron acceptor (OD_{600} ~ 0.03). Conditions where no electron acceptor was provided, showed no growth. When provided 2 mM IO_3^- as the sole terminal electron acceptor, the wildtype strain grew to an OD_{600} of 0.078 ± 0.001 by 24 hours (mean ± standard deviation; N=4). Δ*idrA* showed no significant growth, consistent with our earlier observation and highlighting the prerequisite nature of *idrA* for dissimilatory IO_3^- respiration. When both IO_3^- and NO_3^- were provided as terminal electron acceptors, the mutant and wildtype strains grew during the first 12 hours. The wildtype condition then grew over the ensuing 12 hours to an OD_{600} of 0.092 ± 0.001, whereas Δ*idrA* exhibits no significant growth. Thus, the wildtype condition shows a distinct diauxic growth curve, first peaking at the max optical density of the NO_3^- only condition, with a diauxic lag ensuing before growth continues. Diauxie is generally indicative of a phase of metabolic adaptation where the cells produce the enzymes necessary to grow on a non-preferred alternative substrate when more than one is available. However, emerging evidence shows more complex regulatory networks are at play during the diauxic shift, including heterogenous population responses and stochastic gene expression[166,167]. These results ultimately indicate that *Denitromonas* preferentially utilizes NO_3^- over IO_3^- when both are provided, and some type of metabolic adaptation occurs when switching between either substrate. Crucially, removal of IdrA does not impact growth on nitrate, suggesting that IdrA is required for growth on IO_3^-, and the nitrate reductase cannot replace its function.

3.3.2 $IdrP_1$ and $IdrP_2$ are necessary for growth by DIR

The *idrP₁* and *idrP₂* genes produce phylogenetically distinct proteins that precede every *idrAB* gene in characterized DIRM[163]. In *Denitromonas* sp. IR-12, the two IdrP proteins share 42.43% amino acid sequence identity between themselves, suggesting $IdrP_1$ and $IdrP_2$ may play separate roles. Consistent with the low sequence identity between either protein, removal of either *idrP₁* or *idrP₂* individually inhibits growth when IO_3^- is the sole terminal electron acceptor (Figure 3.1C and 3.1D). Initial attempts at complementing the growth phenotype were unsuccessful. Since both *idrP₁* and *idrP₂* are di-heme cytochrome c peroxidases, I hypothesized that the limiting iron concentrations in the media (1 μM) caused excess apoprotein formation resulting in inactive iodate reductase complexes. After adding 36 μM $FeSO_4$ to the minimal media, both *idrP₁* and *idrP₂* complementation vectors rescued the growth phenotype. Under the iron supplemented conditions, all control conditions were left unaffected, and the empty vector controls were still unable to rescue the phenotype. These data suggest that both *idrP₁* and *idrP₂* are needed individually for growth on IO_3^- as the terminal electron acceptor. Furthermore, I surmise that the "low-copy" expression vectors likely produce protein at levels higher than the wildtype.

3.3.3 IdrP$_1$ overexpression in a Δ*idrP$_2$* mutant does not rescue DIR phenotype

Both Δ*idrP$_1$* and Δ*idrP$_2$* conditions retain a functional IdrP homolog; however, the remaining *idrP$_1$* or *idrP$_2$* gene in either background insufficiently enables growth by DIR. Using the Δ*idrP$_2$* mutant as an example, I tested whether increasing the copy number of IdrP$_1$ under iron-enriched conditions enables growth by DIR. Under IO_3^- reducing, iron-enriched conditions, the Δ*idrP$_2$* mutant does not grow compared to the wildtype condition, consistent with previous observations (Figure 3.3). While Δ*idrP$_2$* with excess IdrP$_1$ grew to an OD_{600} significantly higher than the Δ*idrP$_2$* only condition, the excess IdrP$_1$ condition did not grow significantly more than the empty vector control. These data suggest that increasing the IdrP$_1$ copy number does not affect the cell's growth by DIR when IdrP$_2$ is missing. Thus, the inability for IdrP$_1$ to rescue the DIR growth phenotype in the Δ*idrP$_2$* is indicative of separate roles for these two IdrP proteins.

3.3.4 Phylogeny of IdrP$_1$ and IdrP$_2$

An unrooted phylogenetic tree drawn from the alignment of numerous cytochrome c peroxidase-like proteins provides a glimpse into the evolutionary history of IdrP$_1$ and IdrP$_2$. The *E. coli*, *Paracoccus*, and *Burkholderia* cytochrome c peroxidases are provided as reference proteins with characterized functions. Cytochrome c peroxidase in *E. coli* (Figure 3.4A—green) and *Burkholderia* (Figure 3.4A—yellow) function as respiratory oxidases that use H_2O_2 as a terminal electron acceptor under anoxic conditions[168,169]. The closely related di-heme cytochrome c peroxidases in *Paracoccus denitrificans* (Figure 3.4A—purple) aids in the synthesis of methylamine dehydrogenase (MADH), enabling the synthesis of a MADH cofactor, tryptophan tryptophylquinone. Moreover, *Paracoccus* di-heme cytochrome c peroxidase seemingly has weak peroxidase activity, suggesting a primary role in cofactor synthesis.

Both IdrP$_1$ and IdrP$_2$ are distantly related to any of the previously characterized di-heme cytochrome c peroxidases. Both protein subfamilies form a unique superclade with divergent evolutionary histories (Figure 3.4A). Some members of the superclade include deep branching IdrP$_2$-like genes belonging to the marine genera *Nitrospina* and *Chloroflexi*. These IdrP$_2$ like branches often show different gene synteny than IdrP$_2$ in DIRM, and in *Chloroflexi* are much larger proteins than IdrP$_2$ in DIRM. A closer look at the IdrP$_1$/IdrP$_2$ superclade shows that the IdrP$_2$ clade is deep branching, and the proteins are highly conserved compared to IdrP$_1$ (Figure 3.4B). IdrP$_1$ arises from a later evolutionary event and forms a more diverse group of proteins. To date, all cultured DIRM possess an IdrP$_1$ and an IdrP$_2$ protein, suggesting both are necessary for DIR. However, some putative DIRM have two copies of IdrP$_1$ (e.g., *Pseudovibrio axinellae* or *Vibrio splendidus*), calling to question whether these organisms grow by DIR or whether the more recently evolved IdrP$_1$ proteins perform different functions altogether.

3.4 Discussion

The data presented herein addresses fundamental questions about the essentiality of the iodate reductase components in *Denitromonas* sp. IR-12. I demonstrate that all four core genes on the IRI are necessary to enable growth by DIR. Combined with a reexamination of the structure

and function, these data refine the current proposed model for DIR. I determine that both IdrA and IdrB are necessary to enable cell growth on IO_3^-. Structural predictions and prior cofactor limitation analyses indicate that IdrAB is a molybdopterin oxidoreductase[163]. IdrB is phylogenetically like the arsenite oxidase B subunit, AioB, which enables the cell to shuttle electrons from the molybdoenzyme AioA to soluble cytochromes in the periplasm[170,171]. IdrB is predicted to have a Reiske [2Fe-2S] cofactor and possess a $CXHX_{18}CX_2H$ motif, characteristic of Aio type reductases[115,170]. Thus, a mature iodate reductase without IdrB would lack the necessary components to transfer electrons from the soluble cytochromes onto the IdrA subunit, ultimately inhibiting growth in Δ*idrB* strains. Likewise, IdrA was previously shown to be phylogenetically similar to the arsenite oxidase A subunit, AioA. The IdrA in *Denitromonas* possesses the same $CX_2CX_3CX_{70}S$ motif found in *Pseudomonas* sp. SCT, suggesting a close phylogenetic relationship to both Aio and previously characterized IdrA subunits[115,172]. A mature iodate reductase lacking the IdrA subunit will ultimately not pass electrons onto IO_3^-, thus preventing growth by DIR in a Δ*idrA* strain. While sequence conservation suggests a role for the conserved residues, emerging evidence shows that the *Pseudomonas* sp. SCT iodate reductase is unable to oxidize arsenite[115]. The lack of arsenite oxidation activity suggests that Aio and Idr may share a similar backbone, but the redox potential of the iron-sulfur clusters on IdrAB causes electrons to move in opposite directions. Additional analyses to determine the key residues enabling electron flow in a particular direction will be necessary. Mutational analyses and comparative genomics may shed light on how residues coordinating the iron-sulfur clusters change the direction of electron flow between Aio and Idr[173]. Nonetheless, these results are consistent with prior observations showing that both subunits of a molybdopterin oxidoreductase are essential for its function[163,174].

The alternative electron acceptor usage analysis seeks to address questions surrounding the preferred electron acceptor and possible synergistic interactions between respiratory nitrate reductases and iodate reductase. A comparison of the wildtype and Δ*idrA* strains suggests that *Denitromonas* preferentially uses nitrate over iodate. Additionally, the wildtype strain shows diauxic growth, suggesting it may regulate the expression of the iodate reductase upon nitrate depletion. A regulated iodate reductase is consistent with observations in *Pseudomonas* sp. SCT, where iodate reductase activity is only induced when IO_3^- is provided[104,115]. Alternatively, preferential consumption of nitrate from constitutively expressed enzymes may result in the diauxic growth curve as both enzymes may show greater affinity to NO_3^- over IO_3^-. Interestingly, iodate is theoretically a marginally better electron acceptor (IO_3^-/I^- E_h = +0.72V; ΔG^0 = −97.44 kJ/mol e^-) than nitrate (NO_3^-/N_2, $E^{o\prime}$ = +0.71 V; ΔG^0 = −96.48 kJ/mol e^-), meaning that *Denitromonas* would theoretically attain more energy from the former. However, since the product of DIR is likely HOI, and while the half-cell for IO_3^-/HOI has never been measured, it is presumably less favorable than growth by denitrification. Furthermore, comparatively lower environmental concentrations of IO_3^- compared to NO_3^- potentially explain why the latter is consumed first in *Denitromonas*. Similar observations have been made in dissimilatory perchlorate reducing bacteria, where these organisms preferentially use nitrate over the more energetically favorable perchlorate[140]. Like iodate, perchlorate is comparatively much rarer in the environment compared to nitrate[175,176]. Thus, bacteria that preferentially use nitrate ahead of more energetically favorable electron acceptors potentially account for the energy expenditure of producing reductase machinery when not necessary. Further insights examining the regulation of the iodate reductase,

or its enzymology can delineate what causes diauxie in *Denitromonas*, and potentially aid in understanding the specialization of the iodate reductase.

Prior studies implicate the involvement of the respiratory nitrate reductase (NarGHI) in reducing IO_3^-[96]. I show here that the removal of *idrA* has no impact on growth by nitrate reduction, meaning the iodate reductase is not necessary for growth on NO_3^-. Likewise, I demonstrate that nitrate reductase components do not complement either Δ*idrA* or Δ*idrB* strains when IO_3^- is the sole terminal electron acceptor. Thus, the iodate reductase forms a distinct DMSO reductase that specifically turns over IO_3^- as its substrate. Our experiments describing the diauxic growth of *Denitromonas* also open several questions about the regulation (or lack thereof) of the iodate reductase. Analyses of the IRI in *Denitromonas* indicate the presence of an *fnr*-like regulator near the *idr* cluster[163]. The IRI associated *fnr* may regulate the iodate reductase independently from the *fnr*/ArcA system or provide an additional level of control[177]. Also plausible is that no regulation exists, and the iodate reductase is competitively inhibited by nitrate; however, data showing NO_3^- and IO_3^- consumption is needed in order to affirm this supposition. Further investigations into iodate reductase and nitrate reductase regulation and kinetics will shed light on the interplay of these enzymes in *Denitromonas*.

Somewhat enigmatic is the role of $IdrP_1$ and $IdrP_2$. Removing either $IdrP_1$ or $IdrP_2$ from the genome inhibits DIR in *Denitromonas*, suggesting that both proteins execute alternate functions. Moreover, when multiple $IdrP_1$ copies are expressed in the Δ*idrP2* strain, the cell does not grow by DIR, meaning $IdrP_1$ activity cannot substitute for $IdrP_2$ activity. The evolutionary history of $IdrP_1$ and $IdrP_2$ shows that they clade separately, with $IdrP_2$ forming a more conserved deeper branching clade than the more recently evolved $IdrP_1$. Furthermore, all cultured DIRM representatives possess both $IdrP_2$ and $IdrP_1$, supporting the alternate function hypothesis. Intriguingly, some putative DIRM like *Pseudovibrio axinellae* and *Vibrio splendidus* share the same core IRI genes as cultured DIRM but lack an $IdrP_2$ homolog. Instead, they possess two copies of the more recently evolved $IdrP_1$ homologs. Given the necessity of both $IdrP_1$ and $IdrP_2$, it is likely that $IdrP_2$ deficient organisms may not reduce IO_3^-. Such an observation is consistent with $IdrP_2$ functioning as a key determinant of DIR. Alternatively, subtle sequence differences between the $IdrP_1$ homologs in *P. axinellae* and *V. splendidus* may sufficiently enable DIR. Additional research is needed to validate whether the $IdrP_2$ deficient IRIs can grow by DIR. If so, alignments of these $IdrP_1$ homologs could identify key residues on each homolog needed for DIR. While $IdrP_2$ is seemingly a determinant of DIR, further validation of DIR activity in distantly related DIRM is needed to assess whether *P. axinellae* or *V. splendidus* $IdrP_1$ homologs complement $IdrP_1$ activity in Δ*idrP1* DIRM.

Equally puzzling is the substrate specificity of either $IdrP_1$ or $IdrP_2$. Di-heme cytochrome c peroxidases are periplasmic calcium-dependent proteins, roughly 300 amino acids long, possess a low potential c type heme (where H_2O_2 is reduced), and a high potential heme that shuttles electrons from cytochromes or azurins[178]. Primary sequence similarity between $IdrP_1$, $IdrP_2$, and cytochrome c peroxidase (CCP) suggests that both $IdrP_1$ and $IdrP_2$ possess peroxidase activity. Possible H_2O_2 production and consumption during DIR in *Pseudomonas* sp. SCT supports IdrP mediated peroxidase activity[115] against periplasmically generated H_2O_2. However, the true nature of the oxidant produced during DIR remains an open question, as the method of H_2O_2 detection does not distinguish between H_2O_2 and other oxidants[115,163]. The data I present indicates unique

roles for each homolog, questioning whether either homolog is strictly a peroxidase. Furthermore, I demonstrate that bacterial CCPs form a phylogenetically diverse group of proteins and that $IdrP_1$ and $IdrP_2$ together form a distant superclade of CCP-like proteins. Bacterial di-heme cytochrome c peroxidases are poorly characterized and display various functions determined by either activity assays or gene neighborhood analyses[179]. The most widely characterized CCPs are the canonical CCPs associated with the detoxification of exogenous H_2O_2. Examples include *Burkholderia* and *Neisseria*, which possess demonstrable peroxidase activity, and its removal results in greater sensitivity to exogenous H_2O_2[169,180]. Other CCPs like the *E. coli* type shuttle electrons from soluble cytochromes to H_2O_2. These CCPs enable *E. coli* to conserve energy and grow while using H_2O_2 as the sole electron acceptor[168]. MauG-like CCPs form another class of CCP with weak peroxidase activity. Unlike canonical CCPs, MauG plays a specialized role in cofactor synthesis for methylamine dehydrogenase[181]. Characterized CCPs clade separately from the $IdrP_1$ or $IdrP_2$ type CCPs, suggesting a different evolutionary history between them. Furthermore, some characterized CCPs exhibit different substrate specificities. The gram-negative bacterium *Bacteroides fragilis* possesses a CCP with increased sensitivity towards peroxide stress from cumene hydroperoxide or *tert*-butyl peroxide but not from H_2O_2 mediated peroxide stress[182]. CCPs with activity towards alternate substrates are sometimes found near CCP homologs that clade separately. For instance, the CCP homologs in the avian commensal, *C. jejuni*, presents the clearest example of tandem, H_2O_2 insensitive, CCPs with seemingly separate roles[183]. These CCPs separate into phylogenetically distinct clades, and removal of either CCP has distinct impacts on cecum colonization[183]. Since $IdrP_2$ and $IdrP_1$ seemingly play separate roles in DIR, at least one of these proteins likely possesses substrate specificity to something other than H_2O_2. Ultimately, biochemical assays assessing the substrate specificity for either enzyme will be necessary to understand the separate roles of $IdrP_1$ and $IdrP_2$ in *Denitromonas* sp. IR-12.

Data presented in this chapter provides additional insight into the proposed model for DIR. Our data supports the parsimonious DIR model described in chapter two that proposes IdrAB performs a four-electron transfer to HIO, and HIO disproportionates to I^- and IO_3^-. The $IdrP_1$ and $IdrP_2$ then function in parallel to detoxify yet uncharacterized DIR intermediates. These data suggest that deletion of either *idrA* or *idrB* hinders DMSO reductase mediated electron transfer, while *idrP1* or *idrP2* deletions stymie toxic intermediate detoxification. Consistent with the proposed function for each component of the iodate reductase, all single mutants present an inhibited growth phenotype during DIR. I also demonstrate that beyond essentiality, $IdrP_1$ and $IdrP_2$ likely play different roles during DIR. Future endeavors should prioritize the purification of the mature iodate reductase and its components and assess the activity of $IdrP_1$ and $IdrP_2$ towards H_2O_2 and other oxidants. Such experiments will further refine the proposed model for DIR and address the perplexing chemistry performed by DIRM during iodate reduction.

3.5 Figures and tables

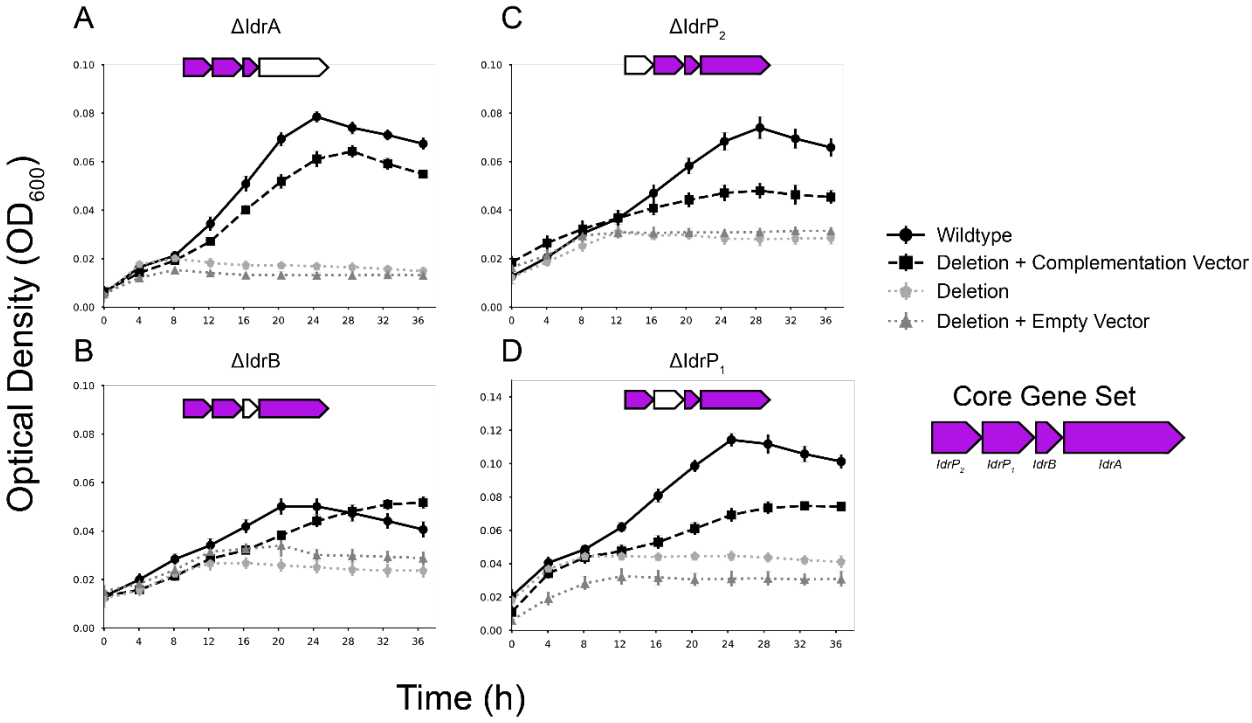

FIGURE 3.1: ALL GENES AT THE IDR LOCUS ARE REQUIRED FOR DISSIMILATORY IODATE REDUCTION. Time courses showing the effect of in-frame gene deletions of individual *idr* genes over the course of 36 hours. All conditions show growth with iodate as the sole terminal electron acceptor. Growth of the wildtype (●), in-frame deletion (⬟), mutant with empty vector (▲), or mutant complemented in trans (■) shown as the OD_{600}.

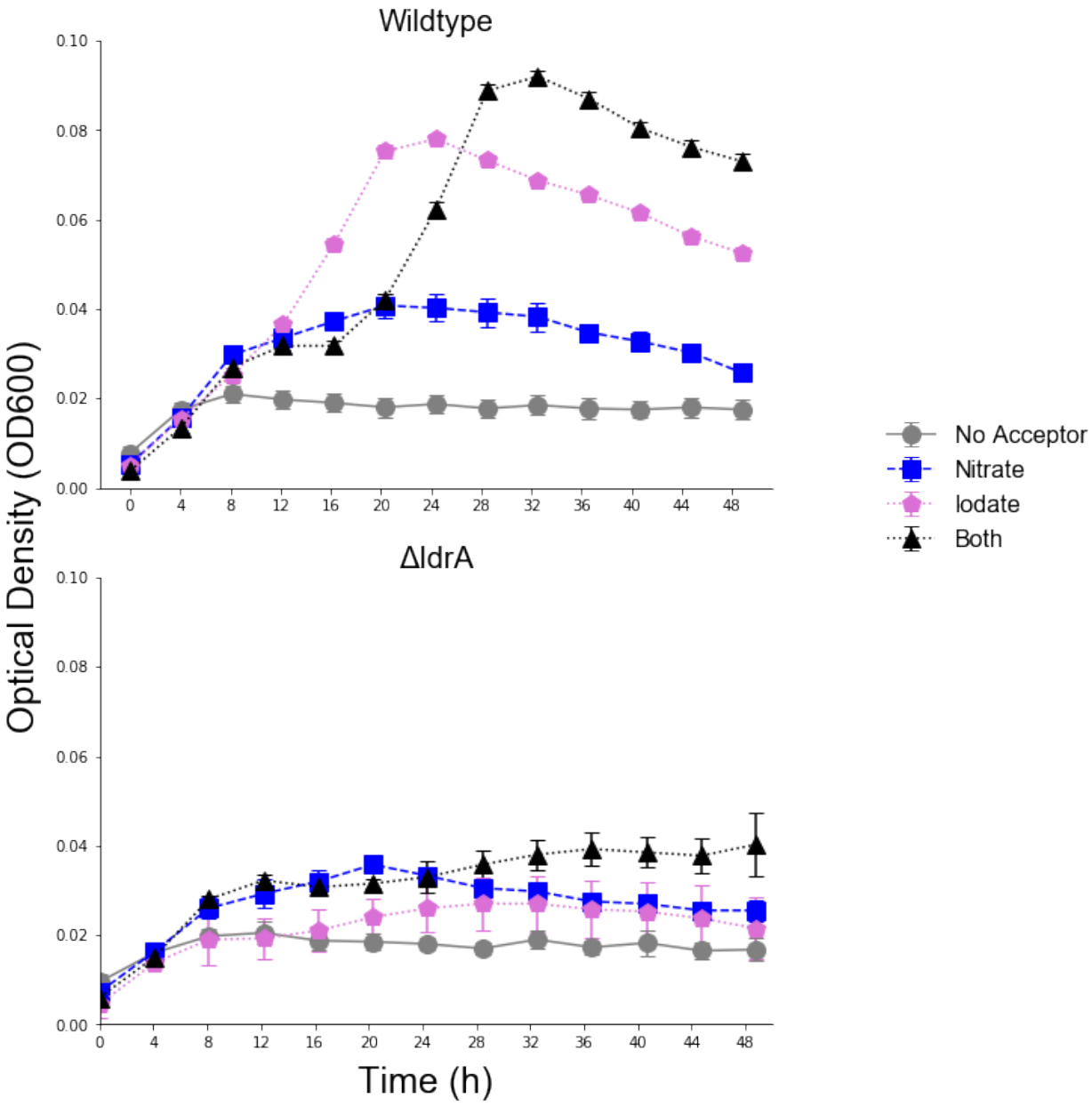

FIGURE 3.2: TERMINAL ELECTRON ACCEPTOR UTILIZATION FOR WILDTYPE AND IDRA NULL MUTANT. Time courses showing growth on different terminal acceptors for the wildtype and Δ*idrA*. All data is presented as mean ± standard deviation with an n=4.

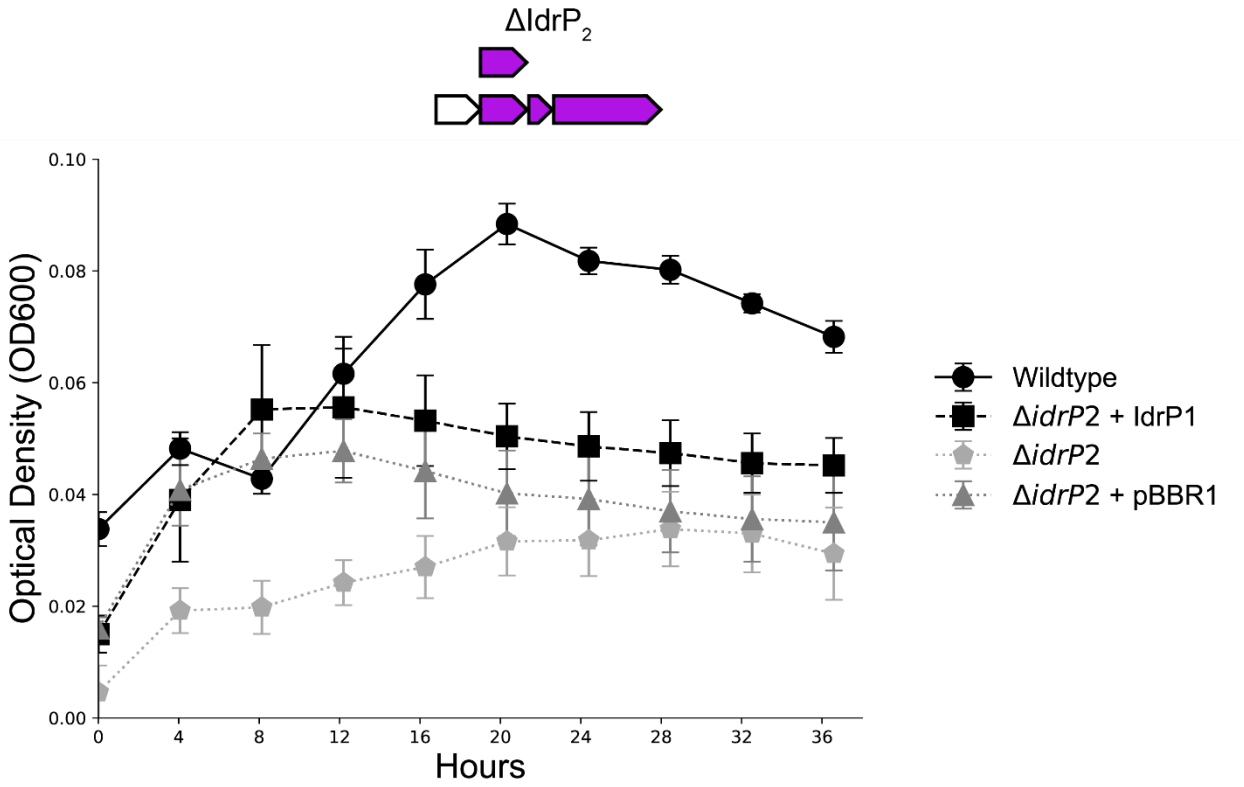

FIGURE 3.3: OVEREXPRESSION OF IDRP1 DOES NOT COMPLEMENT PHENOTYPE. Time courses showing the effect of $IdrP_1$ overexpression over the course of 36 hours. All conditions show growth with iodate as the sole terminal electron acceptor. Growth of the wildtype (●), in-frame deletion (⬟), mutant with empty vector (▲), or mutant complemented in trans (■) shown as the OD_{600}.

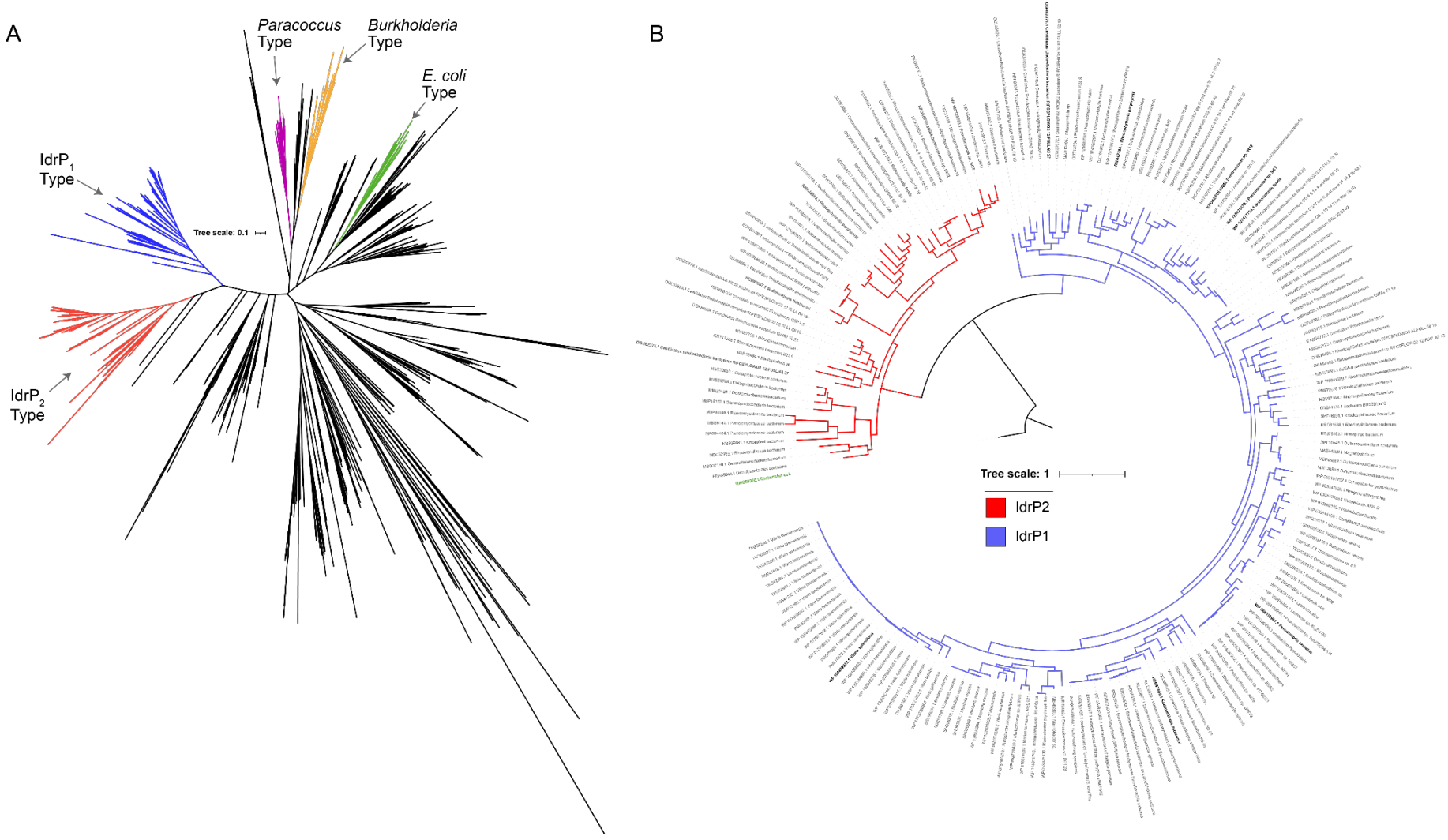
A
Paracoccus Type
Burkholderia Type
E. coli Type
IdrP1 Type
IdrP2 Type
Tree scale: 0.1
B
Tree scale: 1
IdrP2
IdrP1

FIGURE 3.4: PHYLOGENY OF IDRP1 AND IDRP2. A. Shows an unrooted tree of all cytochrome c peroxidase like proteins found in the Idr/Aio dataset, plus additional cytochrome c peroxidases from the representative proteome dataset. The *E. coli*, *Paracoccus*, and *Burkholderia* type cytochrome c peroxidases are provided for reference. Clades colored in black are IdrP-like proteins that were not associated with an iodate reductase. **B.** Shows a rooted tree with the *E. coli* cytochrome c peroxidase as the outgroup (Green). Tree is color coded by the clade of IdrP.

TABLE 3.1: PLASMIDS, STRAINS, AND PRIMERS

Name	*Description*	*Source*
	Plasmid	
pBBR1-MCS2	Expression vector low copy pBBR1 *oriV* and kanamycin resistance marker	
pNTPS138	Suicide Vector containing *sacB*, *traJ*, and neomycin resistance	Gift from the Kathleen Ryan Lab
pJD002	Suicide Vector containing *sacB*, neomycin resistance, and pMB1 ori	Gift from the Jay Keasling Lab
pJK073	Δ*idrA* in frame deletion on pNTPS138 backbone built by Gibson assembly using products from IR403_F/IR404_R on pNTPS138. IR405_F/IR406_R and IR407_F/IR408_R were used to amplify upstream and downstream regions flanking *idrA* from gDNA	[163]
pJK074	Δ*idrB* in frame deletion on pNTPS138 backbone built by Gibson assembly using products from IR409_F/IR410_R on pNTPS138. IR413_F/IR414_R and IR411_F/IR412_R were used to amplify upstream and downstream regions flanking *idrB* from gDNA	This study
pVR051	Δ$idrP_2$ in frame deletion with a residual 14aa peptide sequence on pJD002 backbone built by Gibson assembly using products from IR322_F/IR323_R on pJD002. IR326_F/IR327_R and IR324_F/IR325_R were used to amplify upstream and downstream regions flanking $idrP_2$ from gDNA	"
pVR104	Backbone swap between pVR051 to pNTPS138 built by Gibson assembly using products from IR534_F/IR535_R on pNTPS138. IR536_F/IR537_R were used to amplify the flanking $idrP_1$ region from pVR051	"
pJK076	Δ$idrP_1$ in frame deletion on pNTPS138 backbone built by Gibson assembly using products from IR421_F/IR422_R on pNTPS138. IR425_F/IR426_R and IR423_F/IR424_R were used to amplify upstream and downstream regions flanking $idrP_1$ from gDNA	"
pVR032	*idrABP*$_1$*P*$_2$ expression vector built by XbaI/SacI double digest into pBBR1 using product from IR284_F and IR285R amplification of gDNA	[163]
pVR035	Re-circularized *idrABP*$_1$*P*$_2$ expression vector using product from IR278_F and IR279_R on pVR032 to remove disrupted upstream lacZα	[163]
pVR062	Re-circularized *idrABP*$_1$*P*$_2$ expression vector on lac promoter using product from IR280_F and IR281_R on pVR035 to remove remaining lacZα	[163]
pVR065	Re-circularized *idrA* expression vector on a lac promoter using product of IR279_R and IR361_F on pVR062	[163]
pVR082	Re-circularized *idrAB* expression vector on a lac promoter using product of IR363_F and IR279_R on pVR062	This study
pVR066	Re-circularized *idrB* expression vector on a lac promoter using product of IR400_F and IR445_R on pVR082	This study
pVR068	Re-circularized *idrP*$_2$*P*$_1$ expression vector on a lac promoter using product of IR400_F and IR279_R on pVR062	This study
pVR070	Re-circularized *idrP*$_2$ expression vector on a lac promoter using product of IR400_F and IR290_R on pVR068	This study
pVR069	Re-circularized *idrP*$_1$ expression vector on a lac promoter using product of IR402_F and IR279_R on pVR068	This study
	E. coli	

WM3064	*thrB1004 pro thi rpsL hsdS lacZΔM15 RP4-1360 Δ(araBAD)567 ΔdapA1341::[erm pir]*	William Metcalf, University of Illinois
XL1-Blue	*endA1 gyrA96(nal^R) thi-1 recA1 relA1 lac glnV44 F'[::Tn10 proAB$^+$ lacI^q Δ(lacZ)M15] hsdR17(r_K^- m_K^+)*	Stratagene
	Denitromonas sp. IR-12	
DIR12	Wildtype	[163]
DIR12_27	*ΔidrA*	[163]
DIR12_28	*ΔidrA* + pVR065	[163]
DIR12_29	*ΔidrA* + pBBR1-MCS2	[163]
DIR12_54	*ΔidrB*	This study
DIR12_57	*ΔidrB* + pVR066	"
DIR12_59	*ΔidrB* + pBBR1-MCS2	"
DIR12_73	*Δ$idrP_1$*	"
DIR12_82	*Δ$idrP_1$* + pVR069	"
DIR12_99	*Δ$idrP_1$* + pBBR1-MCS2	"
DIR12_93	*Δ$idrP_2$ (with 14aa)*	"
DIR12_111	*Δ$idrP_2$ (with 14aa)* + pVR070	"
DIR12_112	*Δ$idrP_2$ (with 14aa)* + pBBR1-MCS2	"
DIR12_129	*Δ$idrP_2$ (with 14aa)* + pVR069	"
	Primers	
IR284_F	TTTTTCTAGAGTCCATTCGAGATCGACAAGGGGAAACT (5' XbaI site added)	[163]
IR285_R	TTTTTGAGCTCCAAGCAGGGCTGTGACGATGATTGTTTT (3' SacI site added)	"
IR278_F	CTAGAGTCCATTCGAGATCGACAAGGG	"
IR279_R	AGCTGTTTCCTGTGTGAAATTGTTATCCG	"
IR280_F	CGCGTTAAATTTTTGTTAAATCAGCTC	"
IR281_R	GAGCTCCAAATCTCCAGGGTTTCGGGG	"
IR361_F	ATGAGTGAAAACATCAAGCAAGGCG	"
IR403_F	AGCAGGAAAGCTGCTTCACATCTAGAGGGTCGACGCATGCCTGT	"
IR404_R	CCAATCGGCACCGAACACGTTCGTCAAGGCCTTAAGTGAGTCGTATTACGG	"
IR405_F	ACGACTCACTTAAGGCCTTGACGAACGTGTTCGGTGCCGATTGG	"
IR406_R	AGTTCAAGCGGCGACGGCCTCACATGATGATTCTCCTTGTGCTTAGCGG	"
IR407_F	AAGCACAAGGAGAATCATCATGTGAGGCCGTCGCCGCTTGAACT	"
IR408_R	ACAGGCATGCGTCGACCCTCTAGATGTGAAGCAGCTTTCCTGCTGCGC	"
IR363_F	ATGACAACGCATCCGATTCATCTG	This study

IR445_R	GATGATTCTCCTTGTGCTTAGCGGC	"
IR400_F	GGCCGTCGCCGCTTGAAC	"
IR290_R	GGCGTTCTCCTCAGTTCTTGCC	"
IR402_F	ATGGGACACATTCGATCCATTCG	"
IR409_F	TCGAGAAGGGCAACTACTGGTAGAGGGTCGACGCATGCCT	"
IR410_R	CGCTTCGAGGAATGCCACCAGTCAAGGCCTTAAGTGAGTCG	"
IR411_F	CAGTAAGGAGATCAACCATGTAAGCACAAGGAGAATCATCA	"
IR412_R	AGGCATGCGTCGACCCTCTACCAGTAGTTGCCCTTCTCGA	"
IR413_F	GACTCACTTAAGGCCTTGACTGGTGGCATTCCTCGAAGCG	"
IR414_R	GATGATTCTCCTTGTGCTTACATGGTTGATCTCCTTACTGGGT	"
IR322_F	GGTGGCCTTCAACCAGCAATGCCGATAAGCTAGCTTCACGCTGCCG	"
IR323_R	GCACCAGGTCGACCCGCCGGTGGCGCTCACTGCCCGCTTTCCAG	"
IR324_F	CTGGAAAGCGGGCAGTGAGCGCCACCGGCGGGTCGACCTGGTGC	"
IR325_R	CTCAGTTCTTGCCGAATTGGCGGCGGATGGATTGATGCGTTGTCATGAGTT TCC	"
IR326_F	GACAACGCATCAATCCATCCGCCGCCAATTCGGCAAGAACTGAG	"
IR327_R	GCAGCGTGAAGCTAGCTTATCGGCATTGCTGGTTGAAGGCCACC	"
IR534_F	GCCTTCAACCAGCAATGCTAGAGGGTCGACGCATGC	"
IR535_R	CAGGTCGACCCGCCGGTGGTCAAGGCCTTAAGTGAGTCG	"
IR536_F	CTCACTTAAGGCCTTGACCACCGGCGGGTCGACCTG	"
IR537_R	GCATGCGTCGACCCTCTAGCATTGCTGGTTGAAGGCCACC	"
IR421_F	CACCGGTCTCGACGACGCCGTAGAGGGTCGACGCATGCCT	"
IR422_R	AGCGAGTGCCGGCAATCCGTGTCAAGGCCTTAAGTGAGTCG	"
IR423_F	GACTCACTTAAGGCCTTGACACGGATTGCCGGCACTCGCT	"
IR424_R	TGTCATGGTTGATCTCCTTACATGGCGTTCTCCTCAGTTCTTGC	"
IR425_F	GAACTGAGGAGAACGCCATGTAAGGAGATCAACCATGACAACGCATCC	"
IR426_R	AGGCATGCGTCGACCCTCTACGGCGTCGTCGAGACCGGTG	"

Chapter Four: A holistic description of dissimilatory iodate reducing bacteria habitats identifies niches in marine and low oxygen environments

Abstract

While DIRM like *Denitromonas* sp. IR-12 and *Pseudomonas* sp. SCT serve as model organisms to study DIR, it is challenging to extrapolate whether their habitats are genuinely representative of DIRM broadly. Comparative genomics broadened the potential habitats where putative DIRM exist, expanding it to marine life in coastal environments. However, these results are biased towards cultured microorganisms, which potentially underrepresents these enigmatic creatures' true diversity and distribution. Here, I explore the Tara Oceans and Genomes of Earth's Metagenomes (GEM) databases to illustrate the potential diversity and distribution of DIRM. Data from the Tara Oceans analysis shows that *idrA* genes are enriched at sites with elevated nitrate and phosphate and low oxygen describe a likely niche of DIRM above oxygen minimum zones globally. I then build on our initial observation by observing the distribution of putative DIRM in the GEM database among numerous coastal and non-coastal environments. Data from the GEM database show that DIRM are most common in marine environments where the total iodine concentrations are higher than in terrestrial environments. I identify non-coastal regions of interest and describe how DIRM may contribute to iodine cycling in some of these ecosystems. Together these data broaden the potential habitats for DIRM and serves as a starting point from which to study iodine cycling and DIRM in multiple environments globally.

4.1 Introduction

Given the paucity of cultured DIRM it remains challenging to predict how representative the habitat of either *Denitromonas* sp. IR-12 or *Pseudomonas* sp. SCT are of dissimilatory iodate reducing microorganisms (DIRM) more broadly. Results from targeted gene deletions in the model DIRM, *Denitromonas,* and associated microbial physiology data provided strong evidence that Idr functions distinctly as an iodate reductase[115]. These observations enabled the development of a profile hidden Markov model (HMM) to find other IdrA proteins in curated genome databases such as the NCBI database. Phylogenetic analyses, comparative genomics, and neighborhood analyses of genomes presumed to have IdrA further refined predictions of DIRM from organisms possessing IdrA-like proteins. Our approach in Chapter two ultimately identified several axenic cultures in the phylum *Proteobacteria* as putative DIRM, and accompanying taxonomic descriptions described every isolate's association with marine life or coastal ecosystems (Table 2.3)[163]. However, culture-dependent methods miss bacteria that do not grow under specific culturing conditions or culturing conditions that have never been defined[184]. Additionally, the taxonomic descriptions typically provide high-level descriptions of the isolate's natural environment, often providing location and seldomly its geochemistry (Table 2.3). Thus, parsing databases with predominantly cultured taxa risks misrepresenting and potentially obfuscating the true diversity of DIRM niches. Since the ecological role of DIRM remains undefined, limiting searches for IdrA to cultured representatives may portray an incomplete portrait of the taxonomic and environmental diversity of these microorganisms.

Metagenomics, specifically shotgun metagenomics[185], proffers several benefits to the search for DIRM not afforded by examining only cultured microorganisms. Many publicly available metagenomes, particularly those from large public repositories, come associated with rich metadata sets from which to derive associations[185-187]. Shotgun metagenomic surveys also minimize culturing biases by sequencing all DNA within a given sample, making the entire process culture independent. Given enough sequencing depth, researchers can assemble individual genomes and identify diverse taxa missed by culture-based methods[188]. These culture-independent approaches capture the microbial diversity of an environment in its natural state and enable researchers to derive information about community constituents, their abundance, and the genomic potential of a given microbial consortium[189,190]. Crucially, many of these microbial community members may represent either unidentified or uncultured organisms. However, the costs of collecting, shipping, and sequencing samples often become prohibitively expensive for any single lab to design its own comprehensive global metagenomic database. To address the issue of cost, organizations like the Joint Genome Institute or the Tara Foundation have become repositories for global metagenomes and associated metadata[186,191]. Metagenomes from these sources are openly available and enable researchers to test microbial ecology hypotheses at a global scale.

Data presented herein search both un-binned open reading frames and binned metagenome-assembled genomes (MAGs) from the Tara Oceans metagenomes and the Genomes of Earth's Metagenomes (GEM) to identify locations containing DIRM. I employ a similar approach to search for IdrA in global metagenomes as used to identify DIRM in the NCBI database. Where binned MAGs are provided, I also assign taxonomic ranks to genomes containing *idrA* and expand the known host range of putative DIRM. I leverage the rich metadata provided by the Tara Oceans

metagenomic dataset to parse out key variables associated with DIRM presence in the open ocean and present a model for a previously unknown DIRM niche above oxygen minimum zones. Furthermore, using the GEM database, I identify multiple locations beyond marine environments as plausible DIRM habitats. Probing these public metagenome repositories provides insight into the distribution of DIRM globally and the iodine geochemistry of disparate DIRM niches.

4.2 Methods

4.2.1 Profile hidden Markov model (pHMM) development

Profile HMM development used the techniques described in chapter two. A summary of the techniques is provided below. A profile-HMM was constructed using HMMER 3.0 following a multiple sequence alignment using MUSCLE 3.8 on the molybdopterin oxidoreductase (Pfam_00384) seed set and *Denitromonas* sp. IR-12 /*P. stutzeri* SCT IdrA protein to identify additional iodate reductase proteins in public databases[124,125]. A separate arsenite oxidase (AioA) profile-HMM was created using analogous methods. Genomes from high probability BLAST hits for IdrA and AioA (E value = 0) and from the AioA and AioA-like protein clades identified in Saunders *et al.*[126] were downloaded from NCBI using the NCBI-genome-download tool (https://github.com/kblin/ncbi-genome-download). A neighborhood frequency analysis was performed, and ten genes upstream and downstream from the *aioA* or *idrA* locus were extracted from the associated GenBank files for each genome, and MMseqs2 was used to cluster homologous proteins as follows[123]: An all-vs.-all search using MMseqs2 was performed using e-value: 0.001, sensitivity: 7.5, and cover: 0.5. A sequence similarity network was built based on the pairwise similarities, and the greedy set cover algorithm from MMseqs2 was performed to define protein subclusters as described in detail by Méheust *et al.*[129]. The resulting subclusters were defined as subfamilies. The cutoff for the IdrA HMM was ultimately determined by iteratively setting the score to a value that excludes genomes that lack the $IdrP_1$/$IdrP_2$ homologs adjacent to IdrAB and set to a threshold of 640.

4.2.2 Distribution of iodate reductase in ocean metagenomes

The profile-HMM for iodate reductase (described above) was used to search all 40 million non-redundant open reading frames from the 243-sample Tara oceans dataset. Open reading frames were downloaded (available from https://www.ebi.ac.uk/ena/data/view/PRJEB7988) and translated to amino acid sequences using custom BioPython code[192,186,193]. The amino acid sequences translated from DNA extracted in the 0.22-micron and 0.45-micron range were then searched for hits using the IdrA profile-HMM set at a threshold score of 640. Hits were then grouped by the station for further analysis. Reads were mapped to scaffolds with Bowtie2[194] using the paired-end read mapper at default settings, and reads were counted using SAMtools[195]. Read abundance mapping to these unique IdrA hits were quantified by using the transcripts per million (TPM) method for read quantification as described in Ribicic *et al*[190,196]. Ten variables in the metadata associated with the chemical environment at each sampling location were analyzed using the principal component analysis module on scikit-learn 0.23.1[197]. All sites, regardless of *idrA*

presence, were included in the analysis. Missing metadata values were imputed using the Multivariate Imputation by Chained Equations method (MICE)[198]. Variables included in the analysis were 'Sampling depth (m)', 'Mean_Temperature (deg C)', 'Mean_Salinity (PSU)','Mean_Oxygen (umol/kg)', 'Mean_Nitrates(umol/L)', 'NO2 (umol/L)', 'PO4 (umol/L)', 'SI (umol/L)','NO2NO3 (umol/L)', and irradiance 'AMODIS:PAR8d,Einsteins/m-2/d-1'. Components were built using "pca.fit_transform()" and confidence ellipses at one standard deviation were set for each group. Component coefficients were extracted from principal components by using "pca.components_" and displayed as a loadings plot. Explained variance was also extracted from "pca.components_" to display on PCA axes. The map of *idrA* abundance was created using Cartopy 0.17.

4.2.3 Distribution of iodate reductase in global metagenomes

The profile HMM for iodate reductase was used to search the Genomes of Earth's Metagenomes (GEM) database provided by Nayfach *et al.* (2021)[191]. The catalog includes a total of 52,515 metagenome-assembled genomes (MAGs) representing 12,556 novel candidate species-level operational taxonomic units across 135 disparate phyla[191]. The protein sequence files (.faa) were retrieved from the GEM database (https://portal.nersc.gov/GEM/genomes) as the file faa.tar and unpacked as individual faa files, each representing an individual MAG. A custom bash script was written to iterate the hmmsearch function over the directory containing all MAGs using the options –noali and –tblout set, and a threshold of 640 was used as before. Hits were written to a separate file, and genome IDs were extracted from the file. Metadata was retrieved by downloading the genome_metadata.tsv file from the same directory. Genome IDs were then matched to the associated metadata using a separate custom bash script, and results were compiled for downstream analysis. Data management and graphing were performed using Python 3.7 with pandas and matplotlib.

4.2.4 Concatenated RpS/RpL tree

Phylogeny of genomes with *idrA* in the GEM database was determined using a modified version of the "Phylogenomics workflow" described in Graham *et al.* [199]. Briefly, a set of HMMs based on the RpS/RpL HMMs in Hug *et al*. [200] were used to search for 16 RpS/RpL proteins in the *idrA* positive genomes[201]. The workflow was automated using the identifyHMM script provided in the Phylogenomics workflow repo (https://github.com/edgraham/PhylogenomicsWorkflow) to search the annotated .faa files without the *–performProdigal* flag. Identified RpS or RpL proteins are then aligned using MUSCLE v 3.8 with the *-maxiters 16* flag included, trimmed using trimAl[202] with the *-automated 1* flag included, and concatenated using the *concat* script provided with BinSanity with the minimum number of sequences to be concatenated set at 8. The aligned file is then drawn as a phylogenetic tree using FastTree at standard settings with the *-gamma* and *-lg* flags and displayed using the interactive Tree of Life (https://itol.embl.de/) visual interface.

4.3 Results and discussion

4.3.1 Distribution of DIR populations in global oceans

Many organisms with genes for DIR were identified in diverse marine habitats where IO_3^- reduction is suspected to occur (Table 2.3). For example, *Litorimicrobium taeanense* is an aerobic, non-motile, *Alphaproteobacterium* isolated from a sandy beach in Taean, South Korea[203]. Other organisms such as *Endozoicomonas* sp. OPT23 and *Litoreibacter ascidiaceicola* were isolated from marine animals such as the intertidal marine sponge (*Ophlitaspongia papilla*) and the sea squirt (*Halocynthia aurantium*), respectively[204,205]. Additionally, organisms known to accumulate iodine, such as algae[206], are associated with these bacteria, as is the case with the bacterium *Rhodophyticola porphyridii* and the red algae *Porphyridium marinum*[207]. To further investigate this marine prevalence, I used the *idrA* subunit as a marker gene to determine DIRM distribution across the Tara Oceans metagenome dataset. Our approach also identified the read abundance mapping to these unique IdrA hits at the different sites by using the transcripts per million (TPM) method for read quantification[190,196]. With this method, the number of unique IdrA hits was directly proportional to the number of reads mapped to the hits (Figure 4.1A and 4.2). In general, locations with few unique IdrA hits lacked reads mapping to IdrA (Figure 4.2). I observed that 77% (74/96) of the hits arose from the mesopelagic zone at an average depth of about 461 meters (range 270m-800m) across identified stations (Figure 4.3). The remaining hits arose predominantly in epipelagic zones, such as the deep chlorophyll maximum in 21% of cases (20/96), and far fewer hits were observed in the mixed layer (1/96) or the surface water layer (1/96).

Although *idrA* presence exhibited some variability in depth, a geochemical feature common to all these hits was low oxygen concentrations. Most hits mapped to well-documented oxygen minimal zones in the Arabian Sea[208,209] and the Eastern Tropical Pacific[210-212]. Similarly, the North Pacific Subtropical and Polar Front (MRGID:21484) and the North Pacific Equatorial Countercurrent provinces (MRGID:21488) are two Longhurst provinces with OMZs that stand out in the Western hemisphere. At each location, the median dissolved oxygen concentration at *idrA* positive locations was consistently lower than the dissolved oxygen concentrations at *idrA* absent locations (65.24 µmol/kg versus 190.41 µmol/kg; Figure 4.1C). Among locations containing more than one *idrA* hit, the average oxygen concentration was about six times lower (11.03 µmol/kg); however, this average was skewed upward due to one outlier condition with 18 *idrA* hits (Cumulative TPM of 89.30; Figure 4.3) occurring at a dissolved oxygen concentration of 95.4 µmol/kg (TARA_137_DCM_0.22-3). Environments meeting these conditions were the most common in mesopelagic zones broadly. One notable exception were the multiple hits at the deep chlorophyll maximum (DCM) at station 137. However, further inspection of this DCM revealed that the sample matched the high nitrate and phosphate concentrations and low dissolved oxygen of other *idrA* positive mesopelagic environments more closely than the comparatively more oxygenated surface waters or deep chlorophyll maxima. Research from Farrenkopf *et al.* indicated that bacteria are responsible for IO_3^- reduction in oxygen minimum zones[114,213]. Further, Saunders *et al.* showed a preferential expression of *aioA*-like genes in the Eastern Pacific oxygen minimum zones, which our evidence now suggests are IO_3^--reductases (IdrA)[126].

To test whether locations with *idrA* possessed a unique chemical signature, I ran a principal component analysis using the variables associated with sample environments. The first two

components of these geochemical variables explained 70.7% of the variance observed between *idrA* present and *idrA* absent samples. I determined that *idrA* presence was correlated most strongly with increased nitrate, phosphate, and silicate concentrations (Figure 4.1B-C; Figure 4.4). Additionally, *idrA* presence was negatively correlated with dissolved oxygen concentrations (Figure 4.1B-C; Figure 4.4). Such an observation is atypical for highly productive nitrate and phosphate-depleted OMZs[208,214,215]. A possible explanation for this observation is that DIRM inhabit a unique niche above OMZs where residual O_2 concentrations above 20 µmol/kg prevents *fnr*-dependent expression of nitrate reductase[177,216]. Given the wide range of dissolved O_2 concentrations with *idrA* genes present (0.70-237.22 µmol/kg; Figure 4.3), these organisms potentially use IO_3^- as an alternative electron acceptor in both dysoxic (20-90 µmol/kg) and suboxic zones (≤20 µmol/kg). Furthermore, recent observations from Hardisty *et al.* show that iodate reduction occurs at locations with average O_2 concentrations of 11 µmol/kg, providing further evidence of a possible niche above the OMZ core for organisms with *idrA*[217]. Our explanation corroborates results from Farrenkopf *et al.* that shows an I^- maximum occurring at the boundary of the OMZ[209], but further studies into the biochemistry of IO_3^- reduction under suboxic conditions and the contribution of DIRM to I^- formation at this transition zone are necessary to undeniably link the I^- maximum with the presence of *idrA* directly.

4.3.2 Geographic distribution of DIR populations

Selecting metagenome datasets that capture the diversity of global ecosystems is imperative for creating a holistic model of DIRM distribution. While the Tara Oceans dataset clearly described DIRM distribution in marine metagenomes, transect samples from the open ocean are overrepresented in this dataset. To broaden the search for new DIRM niches, I parsed MAGs in the GEM database for *idrA* presence. The GEM dataset provides one of the largest standalone environmental MAG repositories with searchable metadata, representing multiple distinct ecosystems. MAGs from aquatic ecosystems are still well represented in the catalog (36.75%), and MAGs from terrestrial (6.54%), host-associated (40.97%), and engineered (15.74%) are also present[191]. Despite the broad ecosystem coverage, some geographic and sample type bias is present. Most MAGs arise from North America, Europe, or East Asia, while sub-categories like human and soil microbiomes make up 76.40% and 77.25% of host-associated and terrestrial MAGs, respectively. Nonetheless, the GEM database expands the known phylogenetic diversity of bacteria and archaea by 44%, which expands the search for *idrA* into novel taxa.

Results from the search identified a total of 352 MAGs with *idrA*, accounting for 0.67% of all genomes in the GEM database. These MAGs are distributed globally, except in and around the African continent, where sampling was sparse (Figure 4.5A). IdrA hits from marine, or marine-associated metagenomes accounted for 95% of all hits. While this search identified several new locations with DIRM, multiple sites overlap with those identified in the Tara Oceans survey, likely due to a redundancy in the datasets[191]. Specific geochemical data is not provided for each new open ocean location with an IdrA positive MAG; however, observations from the Tara Oceans survey suggest a similar niche for these DIRM. The GEM database also identifies additional marine niches at hydrothermal vents and in deep subsurface metagenomes. Although Table 2.3 describes some isolates arising from tubeworms near these vents, 11 metagenomes with putative DIRM (15/352 or 4% of all hits) were isolated from areas at or around hydrothermal vents like the

vent plume, diffuse vent fluid, or associated microbial mats. This observation expands the potential DIRM niche at hydrothermal vents from primarily tubeworm symbionts to broadly distributed around the hydrothermal vent. Anoxic fluids from the hydrothermal vent mix with very oxygenated deep ocean waters, creating unique nutrient-rich habitats with a range of temperatures and oxygen concentrations, some of which may be suitable for DIRM[218]. The IdrA positive MAGs from deep subsurface metagenomes are more perplexing since these environments are often oxygen poor, and IO_3^- is converted to I^- beyond 40 cm in depth[48,219]. Future biogeochemical surveys of these ecosystems should consider the role of these microorganisms in potentiating the iodine biogeochemical cycle and assess the distribution more precisely.

Also included in the MAGs from marine environments are the hits from metagenomes at or around coastal regions in North America, Antarctica, Australia, and Europe (Figure 4.5A), corroborating observations constraining DIR to iodine-rich marine environments. These coastal regions are often areas with high biological productivity and have seasonally active iodine cycles[86,87,110]. Although DIRM presence here may indicate a role in potentiating the iodine biogeochemical cycle in coastal regions, further studies are needed to link DIRM presence to the iodine biogeochemical cycle directly. While the metadata did not generally distinguish coastal from open ocean locations, 2% of all hits (6/352) were identified as salt marshes. Salt marshes are particularly notable since iodocarbon emissions from these ecosystems have been linked to climatic impacts caused by tropospheric ozone destruction and cloud condensation nuclei formation[17,40,108]. While the exact role of DIRM in this ecosystem has yet to be described, studies from rice paddies, an analogous terrestrial ecosystem, suggest that halocarbon (e.g., CH_3I) emissions increase with halide (e.g., I^-) concentrations. One may posit that DIRM contribute to the available iodide pools in salt marsh ecosystems, thus enabling the production of iodocarbons[220]. Further research and sampling of these ecosystems are necessary to draw further conclusions, especially since salt marshes are heavily underrepresented in the GEM database, accounting for only two metagenomes and 1.05% of all MAGs in the database.

Although DIRM habitats have been identified predominantly among marine ecosystems, IdrA positive genomes are relatively uncommon, accounting for only 3.77% of marine MAGs (324/8,578). IdrA is less common, even non-existent, among MAGs from non-marine systems. For instance, human microbiomes account for 31.25% of MAGs in the GEM database, yet no IdrA hits are associated with these metagenomes. Likewise, MAGs from hosts like arthropods, fungi, or plants show no hits to IdrA despite collectively accounting for 4.02% of MAGs. However, IdrA is found in MAGs from freshwater and saline Antarctic environments, accounting for the remaining 5% of IdrA positive hits. These MAGs represent 1.10% and 0.47% of all MAGs in each ecosystem, respectively, providing additional insight into other potential DIRM niches and associated lifestyles. Freshwater MAGs account for most terrestrial hits, while groundwater MAGs account for the remainder, suggesting that the iodine cycle may be active in these areas, despite lower concentrations of total iodine compared to marine ecosystems[221]. IdrA was also identified in Antarctic ecosystems near the Ross Archipelago and Prydz Bay. Sea ice here has been shown to concentrate inorganic and organic iodine, suggesting that psychrophilic DIRM may be associated with enriched iodine levels and cycling in these habitats[87,222]. These observations are also consistent with evidence from taxonomic descriptions suggesting organisms like the sea ice-dwelling microorganism, *Marinobacter psychrophilus* are putative DIRM[223]. The existence of

organisms with IdrA in non-marine environments begs the question about the role of DIRM in such specific habitats. DIRM may be involved in iodine mobility in these environments, but deriving meaningful statistics about the global prevalence of IdrA in similar ecosystems is confounded by the low number of representative samples. Thus, further analyses exploring iodine biogeochemistry across non-marine environments is necessary to draw meaningful conclusions from IdrA presence in these ecosystems.

4.3.3 Taxonomic distribution of DIR populations in the GEM database

Data presented in Chapter two (Figure 2.4B) shows that most organisms harboring IdrA belong to the phylum *Proteobacteria*, with only a couple belonging to *Chloroflexota*, *Nitrospinota*, and the Candidate Phyla Radiation. While most IdrA positive MAGs in the GEM database belong to the phylum *Proteobacteria* (51%), I identify several diverse taxa that were not previously known to harbor IdrA. The phylum SAR324, which NCBI assigns to *Proteobacteria* but GTDB considers as a separate phylum, accounts for the second most common taxon with positive IdrA hits (22%). 16S rRNA libraries correlate SAR324 abundance to low oxygen zones broadly, and some studies show the taxon enriched around oxygen minimum zones[224,225]. While SAR324 is among the most abundant bacteria found in marine ecosystems, little is known about the organism's physiology[225]. Evidence suggests it is metabolically flexible since some isolates fix carbon and possess sulfur oxidation genes[226]. The third most common phylum with IdrA is *Actinobacteria*, accounting for 17% of hits, with 55/59 belonging to the family *MedAcidi-G1.* This marine *Actinobacterium* is a presumed photoheterotroph with the capacity to produce acidirhodopsins[227]. Its predicted heterotrophic lifestyle arises from genes coding for numerous transporters and key enzymes of glycolysis and the TCA[227]. *MedAcidi-G1* genomes have been detected at the deep chlorophyll maxima and bathypelagic ecosystems broadly[227]. The remaining 10% of bacteria contain additional phyla not identified in chapter two like *Methylomirabilota* and two phylogenetically distinct UBP (uncultured bacterial phyla) taxa (Figure 4.6)[228]. Bacteria belonging to Methylomirabilota are intriguing since the candidate species belonging to this phylum *Methylomirabilis oxyfera* is proposed to couple methane oxidation to nitrite reduction[229]. While the taxon identified in the GEM database was not *M. oxyfera*, such an organism may inhabit a similar niche. UBP17 from a salt marsh metagenome on Skidway Island near Savannah, Georgia, and UBP10 from a deep subsurface metagenome near Santorini, Greece, was also identified. Since the physiology of UBP remains undefined, little can be inferred about their ecological roles; however, IdrA presence in these MAGs provides evidence that these organisms may grow by dissimilatory iodate reduction. Future work should focus on performing neighborhood analyses on these newly identified taxa and verifying the presence of the IRI to provide more conclusive evidence of DIR in these novel taxa.

4.4 Concluding remarks

Results from the GEM database affirm our hypothesis that most phyla with IdrA are generally constrained to marine environments with some exceptions. The Tara Oceans metagenomic survey suggests that sub-oxic waters above oxygen minimum zones are a niche for

DIRM. Our search for IdrA in the GEM database expanded the potential ecosystems with DIRM to include other marine habitats like the deep subsurface or hydrothermal vents. Furthermore, hits from terrestrial environments expand potential habitats beyond ecosystems where DIRM may exist to freshwater, groundwater, salt marshes, and polar deserts. Combined with a literature review of taxonomic descriptions, one can use metagenomic data to reconstruct and connect the numerous global ecosystems with an active iodine cycle to DIRM presence. Ultimately, the identification of IdrA among global ecosystems provides future researchers with new habitats to explore and presents additional questions about the contribution of DIRM to iodine biogeochemistry.

One of the challenges of utilizing metagenomic approaches to understanding the distribution of specific microorganisms and associated metabolisms is the confidence one has in results. A common issue is an overreliance on annotation and protein similarity to determine function[126]. Similarly, metagenomic studies relying on independent observations of specific marker genes may infer incorrect conclusions about the genomic potential of a particular site[230]. Between the data presented in chapters two and four, I describe a method that uses microbial physiology, genetics, comparative genomics, and computational biology to generate a model that identifies iodate reductase-like proteins in global metagenomes. Improvements to this model can be made as additional DIRM are identified and cultured.

4.5 Data availability

Python code, shell scripts, and excel spreadsheets made during the analysis of both GEM and Tara Ocean databases will be available on https://github.com/vmreyes12

4.6 Figures

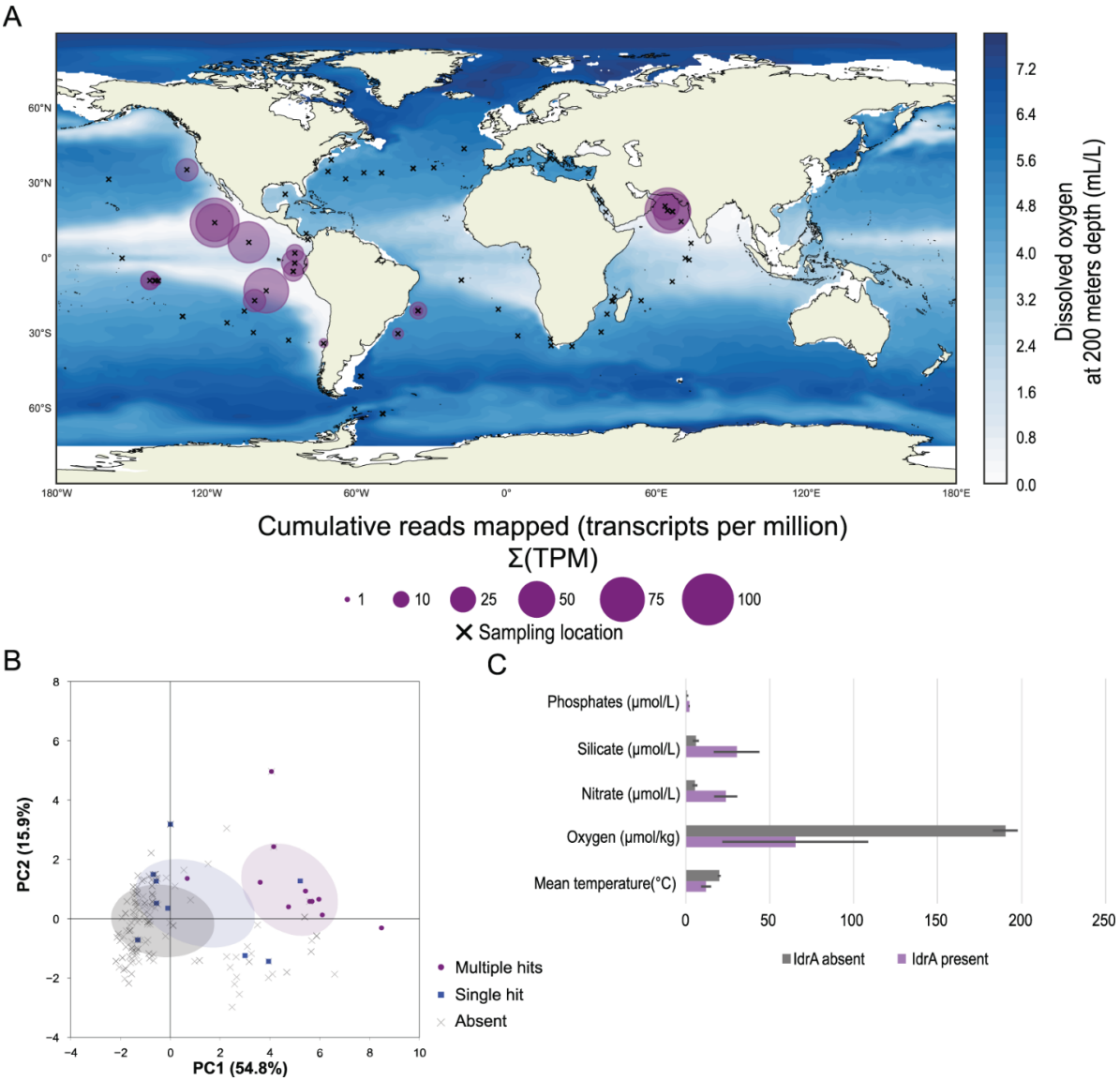

FIGURE 4.1: ANALYSIS OF TARA OCEANS DATASET IDENTIFIES POSSIBLE ECOLOGICAL NICHE ABOVE OXYGEN-MINIMUM ZONES. A) A map indicating sampled locations during the Tara expedition (x) alongside sampling locations with IdrA present (purple circles). Markers overlaid directly on top of each other demonstrate transect samples from different depths at a given location. The size of the purple circle shows the cumulative TPM at a particular site. **B**) A principal component analysis displaying the first two principal components. Locations are grouped by IdrA absent (x), presence of a single IdrA hit (■), or presence of multiple hits (●). Ellipses represent one standard deviation of the mean. The color of the ellipse corresponds to the variable grouping. **C**) The means of select environmental variables at IdrA present sites (purple) and IdrA absent sites (gray). Error bars indicate a 95% confidence interval. Units for each of the variables are located by the variable name.

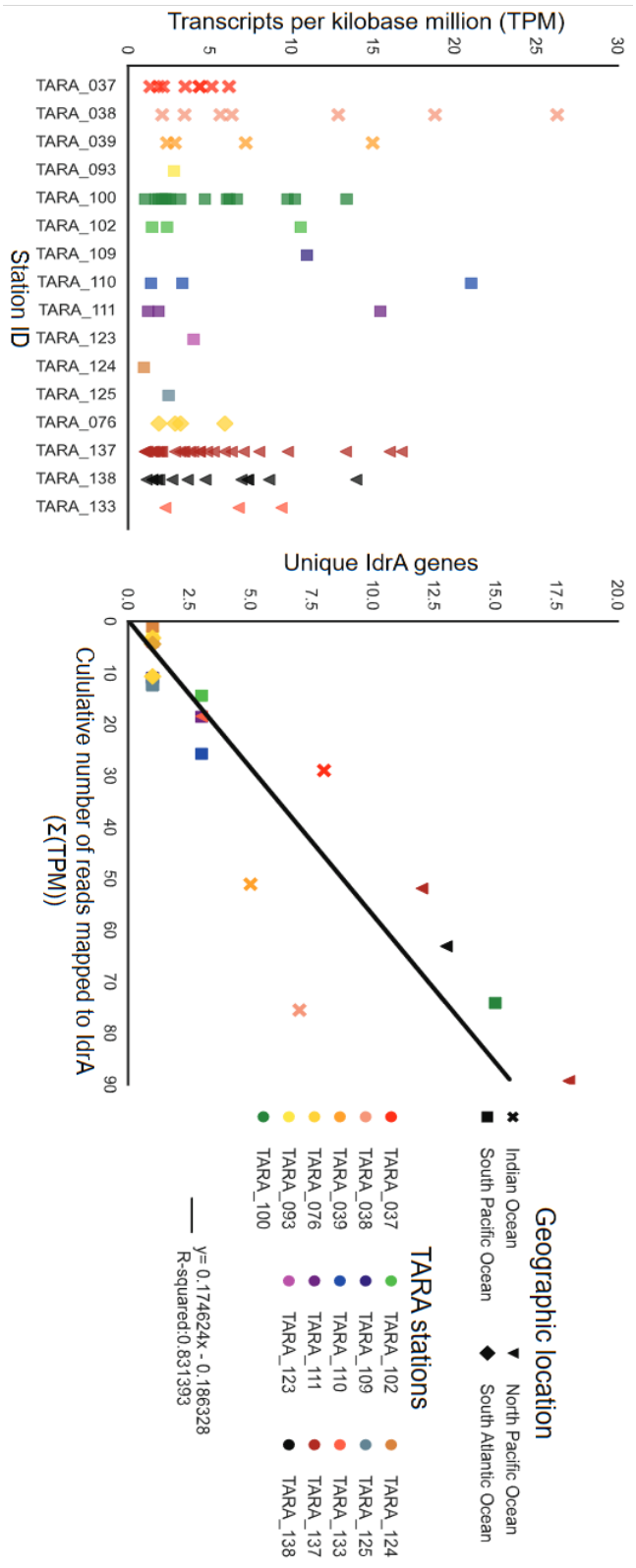
Transcripts per kilobase million (TPM)
0
5
10
15
20
25
30
Station ID
TARA_037
TARA_038
TARA_039
TARA_093
TARA_100
TARA_102
TARA_109
TARA_110
TARA_111
TARA_123
TARA_124
TARA_125
TARA_076
TARA_137
TARA_138
TARA_133
Unique IdrA genes
0.0
2.5
5.0
7.5
10.0
12.5
15.0
17.5
20.0
Cululative number of reads mapped to IdrA (Σ(TPM))
0
10
20
30
40
50
60
70
80
90
Geographic location
Indian Ocean
North Pacific Ocean
South Pacific Ocean
South Atlantic Ocean
TARA stations
TARA_037
TARA_102
TARA_124
TARA_038
TARA_109
TARA_125
TARA_039
TARA_110
TARA_133
TARA_076
TARA_111
TARA_137
TARA_093
TARA_123
TARA_138
TARA_100
y= 0.174624x - 0.186328
R-squared:0.831393

FIGURE 4.2: INDIVIDUAL TPM COUNTS AT TARA STATIONS AND CORRELATION TO UNIQUE IDRA GENES. The chart on the left shows the TPM of individual hits on a scaffold organized by Tara location identifier. Color represents the individual Tara station, while marker shape indicates general geographic location. The chart on the right correlates the number of unique IdrA hits at any given site to the cumulative TPM at an individual location. Tara station is denoted by color, and general geographic location is denoted by marker shape.

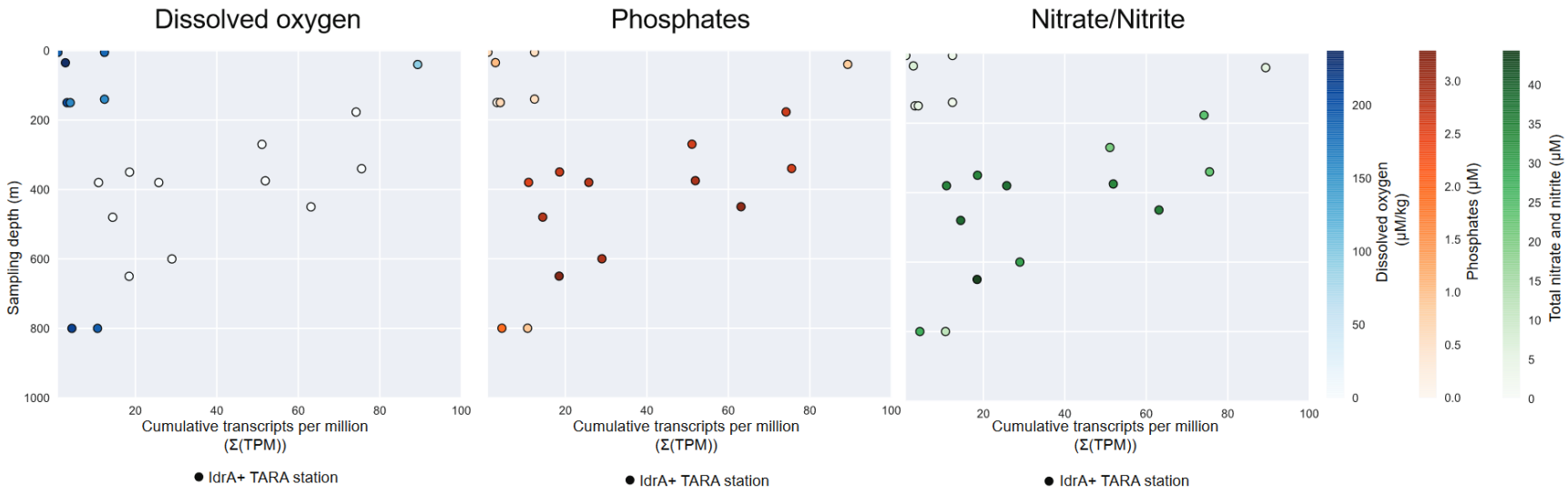
Dissolved oxygen
Phosphates
Nitrate/Nitrite
Sampling depth (m)
0
200
400
600
800
1000
20
40
60
80
100
Cumulative transcripts per million
(Σ(TPM))
IdrA+ TARA station
Dissolved oxygen
(µM/kg)
0
50
100
150
200
Phosphates (µM)
0.0
0.5
1.0
1.5
2.0
2.5
3.0
Total nitrate and nitrite (µM)
0
5
10
15
20
25
30
35
40

FIGURE 4.3: CUMULATIVE TPM PLOTTED BY THE DEPTH AND COLORED BY CONCENTRATION. All three charts demonstrate the cumulative TPM at an individual Tara station plotted against sampling depth. Stations with no IdrA hits are omitted. Color corresponds to the concentration of oxygen (blues), phosphates (oranges), or nitrates (greens). Darker colors represent higher concentrations. Color scales are normalized to the maximum concentration for each variable within the IdrA+ dataset.

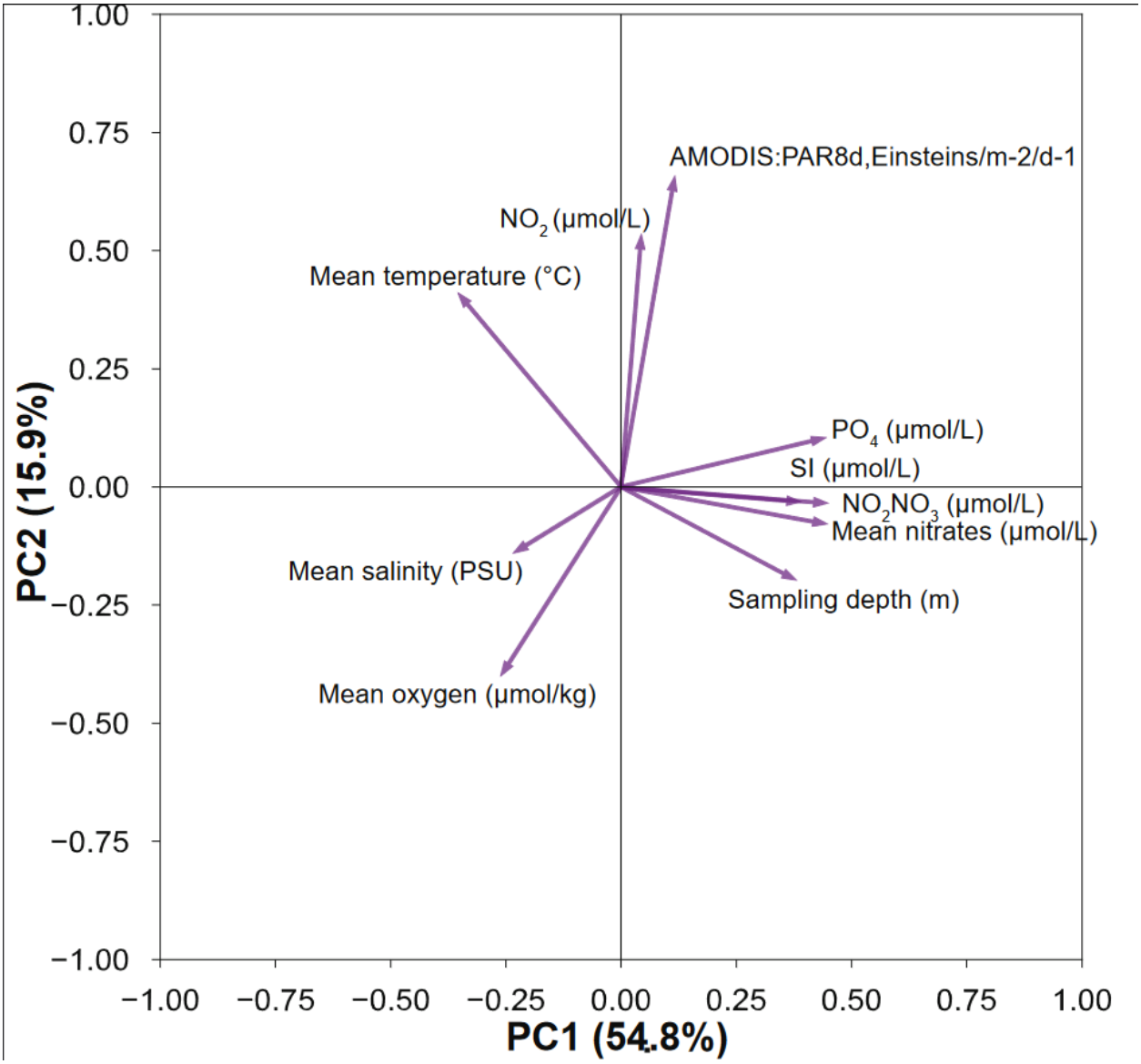

FIGURE 4.4: LOADING PLOT FOR PCA. A loading plot of the ten variables used in the first two principal components. Variables are identified at the end of each arrow.

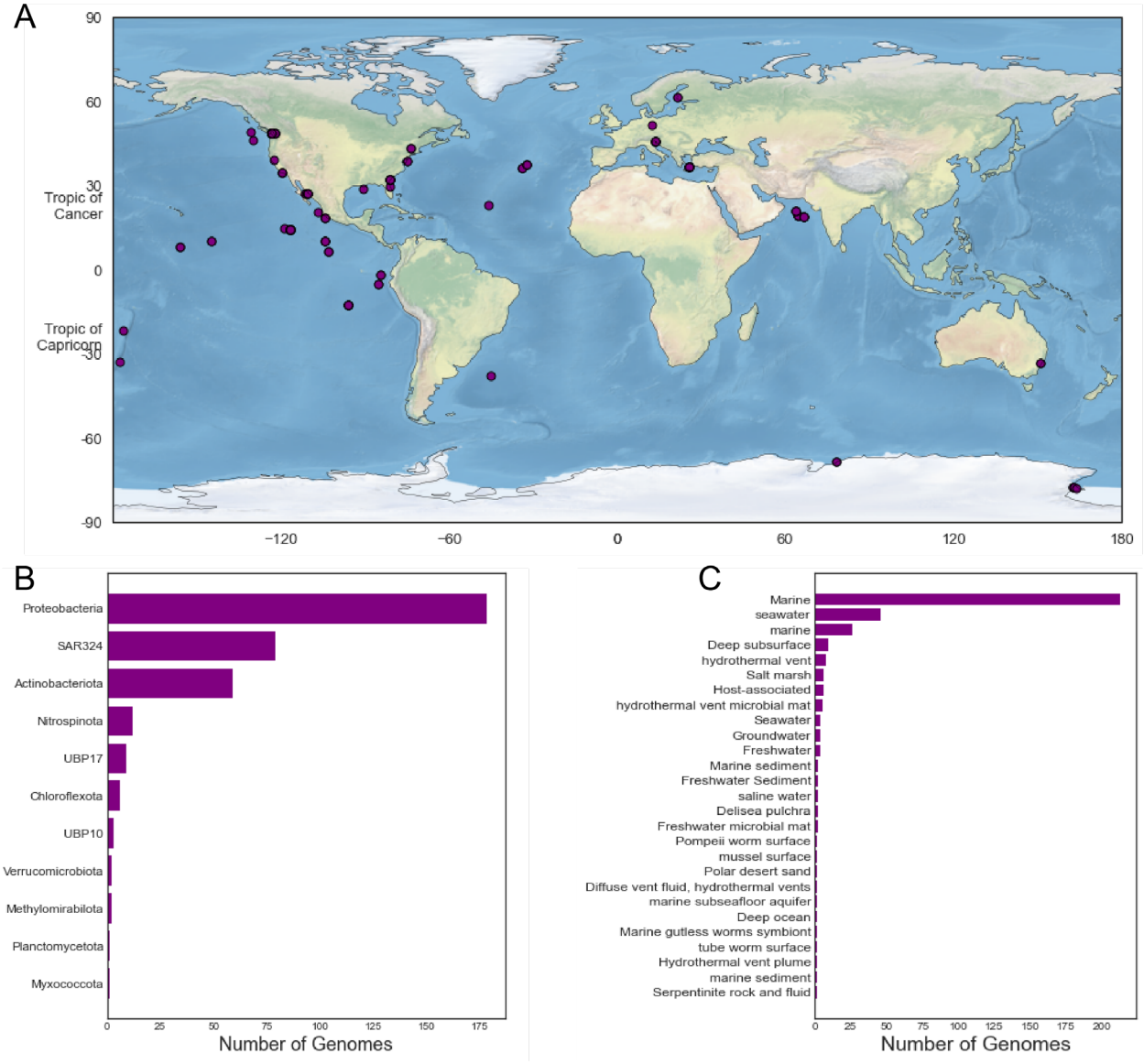

FIGURE 4.5: PHYLOGENETIC AND ECOLOGICAL DISTRIBUTION OF DIRM IN THE GEM DATABASE. A) A map showing all locations containing at least one IdrA hit in the GEM metagenome database. Purple circles represent hits. **B)** A bar plot showing the distribution of phyla with IdrA present in the genome. **C)** A bar plot showing the ecosystem distribution of phyla with IdrA.

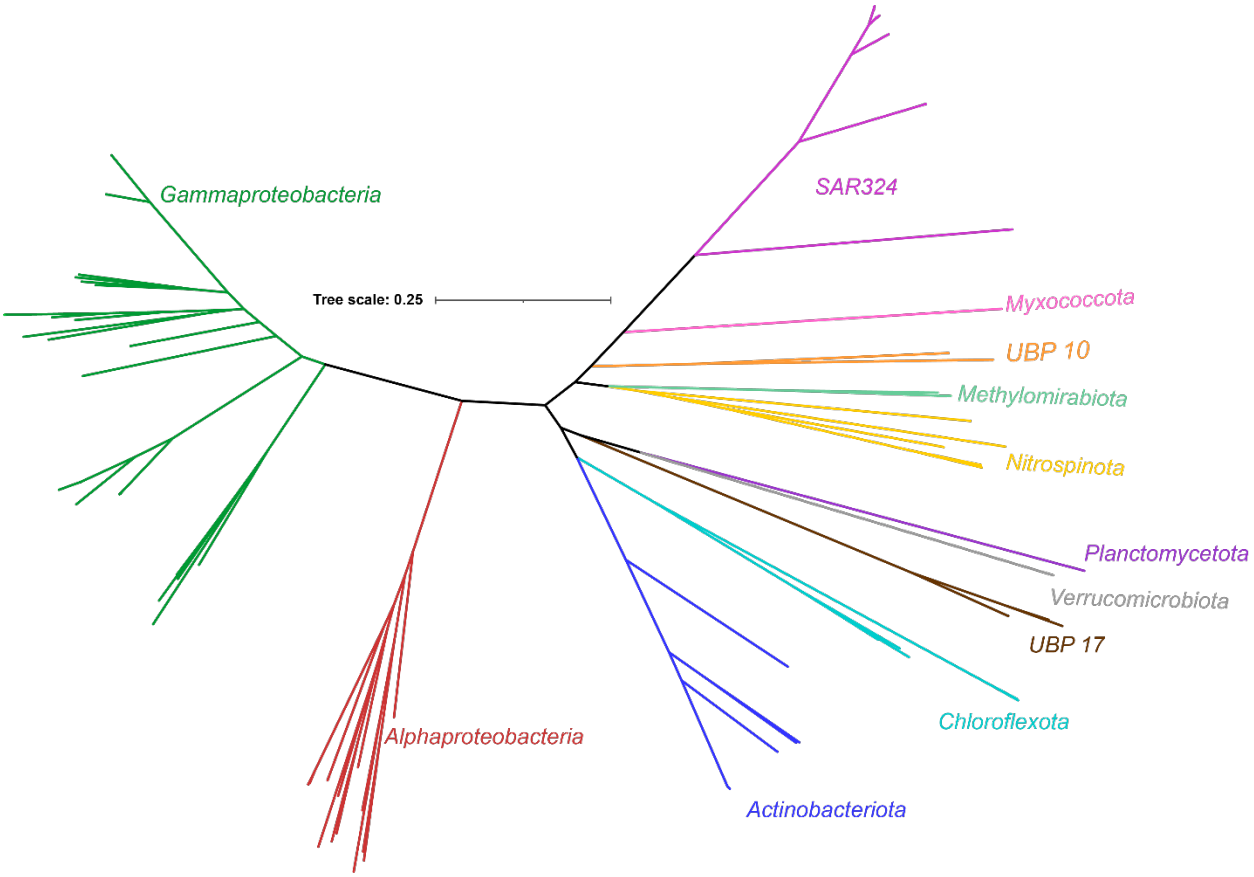

FIGURE 4.6: UNROOTED TREE DEMONSTRATING THE PHYLOGENY OF PUTATIVE DIRM IN THE GEM DATABASE. An unrooted tree showing using the concatenated RpS/RpL protein phylogeny for MAGs with IdrA. Names for each phylum are associated with the clade of the same color. GTDB phylogeny is used for all organisms.

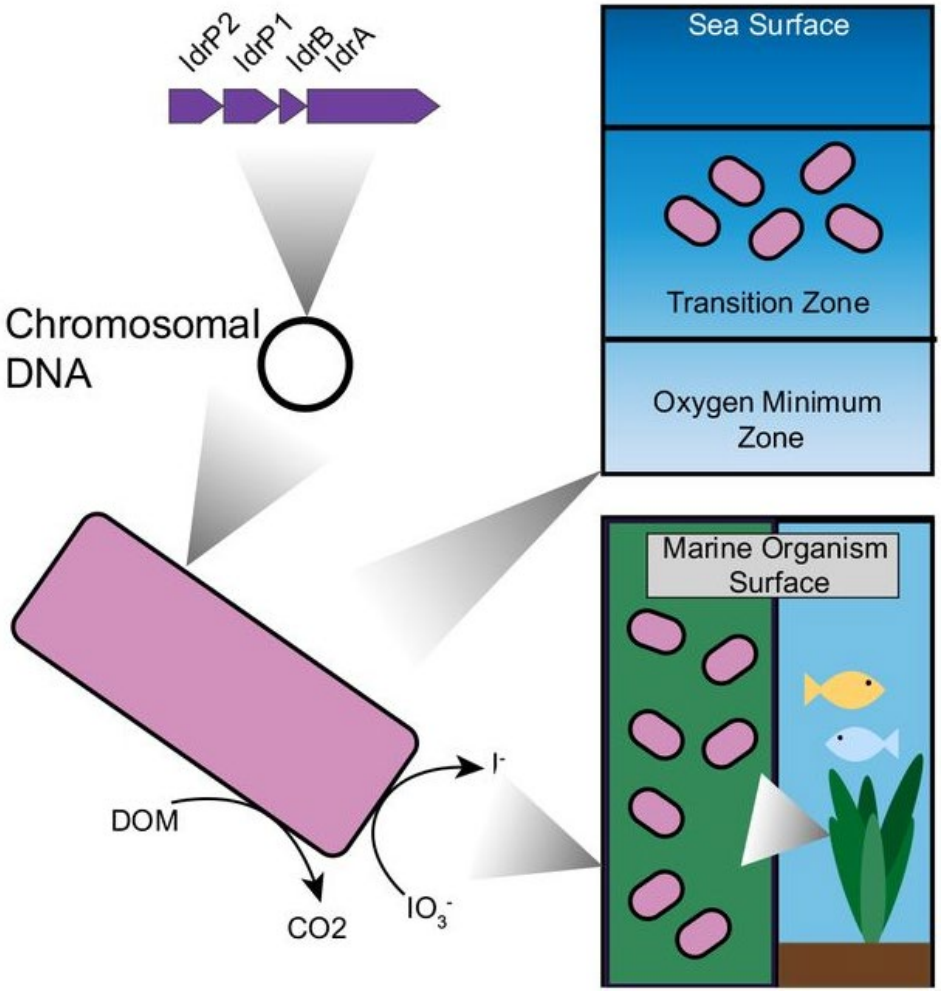

FIGURE 4.7: ECOLOGICAL MODEL OF IODATE REDUCING BACTERIA. Top right panel represents locations in the open ocean near oxygen minimum zones inhabited by DIRM. Bottom right panel represents host associated DIRM. DOM—dissolved organic matter.

Chapter Five: Isolation of a dissimilatory iodate-reducing *Aromatoleum sp.* from a freshwater creek in the San Francisco Bay Area

Abstract

Recent reports of dissimilatory iodate-reducing microorganisms (DIRM) have arisen from studies of bacteria in marine environments. These studies described the physiology and distribution of DIRM while also demonstrating their presence in iodine-rich marine environments. I demonstrated in chapter four that despite lower iodine concentrations, terrestrial and freshwater ecosystems may also harbor DIRM. I established numerous enrichments from coastal and freshwater environments that actively remove amended iodate. I describe the physiology and genome of a new DIRM isolate, *Aromatoleum toluclasticum* sp. TC-10, emerging from a freshwater creek microcosm. Like other DIRM, *A. toluclasticum* sp. TC-10 couples acetate oxidation to iodate reduction with a concomitant increase in the OD_{600}. Our results indicate that *A. toluclasticum* sp. TC-10 performs dissimilatory iodate reduction (DIR) using the recently described iodate reductase (Idr). I provide further evidence of horizontal gene transfer of the *idr* genes by demonstrating the lack of Idr in the closely related (99.93% 16S rDNA sequence identity) *A. toluclasticum* sp. MF63 and describe the heterogeneity of the accessory proteins associated with the iodate reduction island (IRI). These observations provide additional evidence that DIR is a horizontally acquired metabolism with broad environmental distribution beyond exclusively marine environments.

5.1 Introduction

Iodine (as ^{127}I) is an essential component of the mammalian diet for its role in thyroxine biosynthesis. The element is abundant in seawater, where it exists at several oxidation states averaging concentrations around 450 nM[107]. Kelp and algae bioconcentrate iodine as iodide (I^-) and produce iodocarbons that ultimately impact atmospheric chemistry and climate by catalyzing tropospheric ozone destruction[108,15]. In addition to a marine biogeochemical cycle, iodine also exhibits a terrestrial phase. Wet deposition of iodine in rainwater is a common way for iodine to enter terrestrial ecosystems, with rainwater concentrations ranging from 4 to 47 nM[231]. Dry deposition similarly relies upon iodine evolution from marine sources but is delivered through volatilized iodocarbons and iodine to littoral environments[232]. A higher iodine flux occurs by dry deposition (3.6-6.5 μmol m^{-2} yr^{-1}) than wet deposition (2.7 μmol m^{-2} yr^{-1})[233]. Ultimately, iodine deposition depends on distance from the ocean, with low soil iodine concentrations (<5 ppm) found at locations beyond 70 kilometers[231].

As the importance of the iodine biogeochemical cycle on both human health and global climate emerges, the biological mechanism behind the unexpected disequilibrium between iodate (IO_3^-) and I^-[107] remains an open question[42]. The physiochemical state of water suggests that iodine is most stable as IO_3^-, yet I^- predominates across many regions of high biological productivity globally[42,110]. Recent work has shown that a diverse group of dissimilatory iodate reducing microorganisms (DIRM) consisting mainly of marine *Proteobacteria* are likely responsible for this phenomenon in oceanic environments[163]. Metagenomic surveys suggest that DIRM are ubiquitous in the Earth's oceans and are associated with marine life or live above oxygen minimum zones[163]. DIRM are defined characteristically by the ability to reduce relatively high concentrations of iodate (IO_3^-) to iodide (I^-) and couple it to growth. Dissimilatory iodate respiration (DIR) is dependent on a dedicated iodate reduction genomic island (IRI) that is horizontally transferred between diverse taxa[163]. The IRI is composed of a heterodimeric iodate reductase (IdrAB), and two distinct putative cytochrome c peroxidases ($IdrP_1$ and $IdrP_2$). The IdrA is a highly conserved molybdenum-dependent member of the DMSO reductase protein superfamily closely related to dissimilatory nitrate reductases and perchlorate reductases[163].

Little is known about DIR in terrestrial or freshwater environments. However, the presence of iodine in many freshwater systems at variable oxidation states[231,233] suggests the existence of a microbially mediated terrestrial iodine redox cycle. Such an observation would be consistent with metabolisms like dissimilatory perchlorate and chlorate respiration that show broad distribution in environments with variable chlorate and perchlorate concentrations[234]. In this study, I collected sediment from numerous freshwater environments throughout the San Francisco Bay Area and cultured bacteria capable of reducing iodate to iodide. I describe the isolation of a new strain of *Aromatoleum toluclasticum* TC-10 from a freshwater environment, containing low chloride concentrations (~70mg/L Cl^-)[235] and no marine water input. Like TC-10, the *Aromatoleum* type strain, *A. toluclasticum* MF63, was also isolated from a freshwater environment[236]. The *Aromatoleum* genus is widely distributed in the environment and displays significant eco-physiological diversity potentiated by its large pangenome and numerous mobile elements[237,238]. Consistent with that, I show that TC-10 is a DIRM that possesses the *idrABP1P2* genes, enabling it to grow via dissimilatory iodate reduction, making it the first freshwater DIRM isolated. I

compare the genome of TC-10 to the type strain *Aromatoleum toluclasticum* sp. MF-63[236], and show the iodate reducing capability is specific to TC-10 and mobile in *Aromatoleum*. These results ultimately broaden the range to search for novel DIRM and provide a possible ecological role for free-living *Aromatoleum* species beyond their ability to degrade petroleum-based contaminants[239].

5.2 Methods

5.2.1 Media, chemicals, and culture conditions

Anoxic enrichment cultures from freshwater environments were grown at 30°C in a freshwater minimal medium (FMM) containing 0.25g NH4Cl, 0.40g NaH2PO4, 1.0g Na2HPO4, 0.1g KCl, and a vitamin and mineral mix described previously in Carlstrom *et al*.[118]. Enrichments cultures from marine environments used artificial pore medium (APM) previously described in Reyes-Umana *et al*.[163]. All media had a pH of 7.2, and oxygen was removed by boiling the media and cooling the media under an atmosphere of 100% N_2. Media was subsequently dispensed into bottles or tubes under an atmosphere of 100% N_2 and sealed with a butyl rubber stopper. Conditions containing iodate and acetate used the sodium salts of these compounds (Sigma Aldrich, USA). Cultures were grown aerobically on either FMM, R2A (HiMedia, USA), or R2A agar (BD Biosciences, USA). Growth of cultures was measured using a Thermo Scientific™ GENESYS™ 20 set at a wavelength of 600 nm. Growth cultures in Hungate tubes used a specially built adapter for measurement on the GENESYS™ 20. *Aromatoleum toluclasticum* MF63 was procured from ATCC (ATCC 700605), recovered on Tryptic Soy Broth (BD Biosciences, USA). *Aromatoleum toluclasticum* TC-10 is deposited with ATCC (Accession Pending). The 16S rRNA gene sequence and whole genome sequence are deposited in GenBank under accessions numbers OK665926 and PRJNA776029 respectively.

5.2.2 Isolation of *Aromatoleum toluclasticum* sp. TC-10

Sediment from multiple locations across the San Francisco Bay Area (California, USA) was collected. Sediment was added in triplicate in either anoxic APM or anoxic FMM when collected from marine or freshwater sources, respectively. After degassing under a 100% N_2 atmosphere, all enrichments were amended with 2mM iodate and 10mM acetate and grown for 14 days. Iodate and acetate consumption was monitored, and microcosms showing total removal of iodate were plated on R2A agar. Single colonies were isolated on R2A agar, re-streaked, and confirmed by colony morphology, microscopic evaluation, and sequencing of the 16S rRNA gene. The microcosms containing riverbank sediment at Tunitas Creek (37°35'67.4" N, -122°39'81.7" W) near San Gregorio, California contained the isolate *Aromatoleum toluclasticum* sp. TC-10.

5.2.3 Iodate, acetate, and iodide quantification

A Dionex™ IonPac™ AS25 Anion Exchange Column (Thermo Fischer, USA) was used to measure iodate, iodide, and acetate in triplicate. All samples were diluted at 1:25 in deionized water and loaded onto the autosampler for processing. A serial dilution starting at 1 mM of the standard molecule was used to generate the standard curve. Standards were linear over a range of

0.03mM to 1mM. Acetate peaks were consistently detected at 3.6 minutes, iodate peaks at 3.8 minutes, and iodide at 11.5 minutes at a flow rate of 1mL/min.

5.2.4 Genome sequencing, comparative genomics, and phylogenetic analysis

Genome sequencing and library preparation for both *A. toluclasticum* strains was performed by the Vincent J. Coates Genomics Sequencing Laboratory at UC Berkeley on an Illumina NovaSeq6000 using 150 paired-end reads. Reads passed FastQC quality controls, were trimmed using Sickle 1.33, and assembled using SPAdes 3.9[240]. Prokka version 1.14 using standard settings was used to generate genome annotations and the general feature format file (.gff), which was used to navigate and visualize the genome on the Artemis software (available from http://sanger-pathogens.github.io)[122]. The California regional map was drawn using Cartopy 0.19. The average nucleotide identity (ANI) was calculated using FastANI v1.32, and genome synteny and organization were evaluated using the nucmer function provided by Mummer 4.0 with default settings to produce a delta file and graphed using mummerplot with both the "layout" and "filter" tags present. Synteny and organization of contig 18 used similar methods but omitted the "layout" and "filter" tags to visualize inversions and rearrangements. Insertion site sequences were determined using the show-aligns function for contig 18 against the two neighboring contigs on the *A. toluclasticum* sp. MF63 reference genome using standard settings. The IslandViewer4 web interface and MGEfinder were used as orthologous methods to predict genomic islands from the draft genome[162,241]. Phylogeny and gene neighborhood analysis for IdrA was performed by redrawing the IdrA phylogenetic tree used in Reyes-Umana *et al.* with TC-10[163]. Briefly, NasA, NasC, and NapA were used as outgroups, all sequences were aligned using MUSCLE, and the tree was drawn using standard settings on FastTree with the -boot tag set at 10,000[124,242]. The phylogenetic tree was visualized using iToL. The visualization of bootstrap values and gene neighborhoods was displayed using Adobe Illustrator[243]. Protein subfamilies were assigned by submitting sequences for analysis on Pfam 34.0. Clades were collapsed using the triangle visualization where the two side lengths are proportional to the node's closest and farthest child leaves.

5.3 Results

5.3.1 Isolation of *Aromatoleum toluclasticum* sp. TC-10

Aquatic sediments from around the San Francisco Bay Area were collected as inoculum for ten sets of anoxic enrichment cultures, each amended with 10 mM acetate and 2 mM iodate. Complete iodate removal after 14 days was observed in six out of ten microcosm sets (Figure 5.1A). Active microcosms were passaged three times in anoxic basal media and subsequently grown on R2A agar plates aerobically. A single colony from the Tunitas creek microcosm (San Gregorio, California) yielded a non-fastidious culturable isolate. 16S rRNA gene sequencing indicated an axenic culture closely related (99.93% sequence identity) to *Aromatoleum toluclasticum* sp. MF63^T (ATCC 700605), in the family *Rhodocyclaceae* of the phylum *Proteobacteria*. *A. toluclasticum* sp. MF63 was initially isolated by Song *et al.* in Moffet Field,

California, about 34 miles east of San Gregorio, from shallow aquifer sediment in 1999[236]. To differentiate our isolate from MF63, I designated the latest strain as TC-10, referring to "Tunitas creek" and its microcosm bottle number. Like MF63, TC-10 forms short motile rods and is a non-fastidious facultative anaerobe. Anaerobically, TC-10 grows on acetate or lactate with nitrate or iodate as sole electron acceptors. The genus has recently been reclassified as *Aromatoleum* in response to emerging biological and comparative genomic data[237]. Interestingly, both *A. toluclasticum* sp. MF-63 and TC-10 possess nearly identical NarGHI proteins (>99% amino acid identity); however, in contrast to strain TC-10, strain MF-63 cannot utilize IO_3^-, supporting previous observations that the dissimilatory nitrate reductase does not enable iodate reduction in DIRM[104,163].

5.3.2 Dissimilatory iodate reduction in *Aromatoleum toluclasticum* sp. TC-10

Cells of *A. toluclasticum* sp. TC-10 grew on a minimal freshwater medium with acetate and IO_3^- as the sole electron donor and acceptor, respectively. The working IO_3^- concentration was reduced from 2 mM to 1 mM, shortening the lag phase in TC-10. Growth studies revealed that TC-10 accumulated cell mass as measured by an increase in optical density at 600 nm (OD_{600}) with concomitant reduction of IO_3^- to I^- (Figure 5.1B). No growth occurred for heat-killed cultures or under conditions lacking either acetate or iodate. Ion chromatography data showed that TC-10 consumed a total of 0.98 ± 0.05 mM IO_3^- (mean ± standard deviation, n=4) while oxidizing 1.31 ± 0.25 mM acetate (mean ± standard deviation, n=4), resulting in a final optical density increase of 0.076 (Figure 5.1B and 5.1C). These data suggest an average stoichiometry of 0.75 mol of IO_3^- consumed per mol of acetate. Optical density to dry weight relationships for rod-shaped bacteria of similar dimensions (*E. coli*) suggests that an OD_{600} increase of 1.0 is equivalent to 0.39 grams dry cell weight per liter[133]. Assuming a dry cell mass of 50% carbon, the corrected stoichiometry accounting for acetate incorporation into cells is 90% of the theoretical value according to:

$$3\ CH_3COOH + 4\ IO_3^- \rightarrow 6\ CO_2 + 4\ I^- + 6\ H_2O \quad (1)$$

The stoichiometry, energetics, and mechanism of iodate reduction are similar in both *A. toluclasticum* sp. TC-10 and *Denitromonas* sp. 1R-12[163]. In *A. toluclasticum,* 52% of the total carbon is assimilated into biomass, whereas *Denitromonas* sp. IR-12 assimilated 31% of total carbon into biomass. Moreover, the doubling time for TC-10 growing on iodate (T_D=7.7 h, μ=0.09) is on the same order of magnitude as *Denitromonas* sp. IR-12 (T_D=11.0 h, μ=0.06). These results are consistent with biomass accumulation patterns in organisms using highly oxidized electron acceptors like nitrate (NO_3^-/N_2, $E^{o\prime}$ = +0.713 V)[137] and perchlorate (ClO_4^-/Cl^-, $E^{o\prime}$ = +0.797 V)[116]. Furthermore, while iodate is a suitable terminal electron acceptor for either organism (IO_3^-/I^- $E^{o\prime}$ = +0.72 V), both *A. toluclasticum* sp. TC-10 and *Denitromonas* sp. 1R-12 grow faster on O_2 (T_D=1.23 h-1.64 h, μ = 0.42-0.56), which is consistent with oxygen's energetic favorability (O_2/H_2O, $E^{o\prime}$ = +0.820 V).

Prior examples of DIRM show that they possess a genomic island known as the IRI[163]. This island contains *idrABP1P2* genes that enable DIRM to respire IO_3^- as a terminal electron acceptor[163]. Like the DIRM *Denitromonas* sp. IR-12 and *Pseudomonas* sp. SCT, *A. toluclasticum* sp. TC-10 possesses the IRI, which is lacking in the closely related the non-iodate reducing *A.*

toluclasticum sp. MF-63 (Figure 5.2C). This observation is consistent with recent evidence demonstrating the necessity of *idrA* for iodate respiration in *Denitromonas* sp. 1R-12[163]. The genome of *A. toluclasticum* sp. TC-10 also provides additional evidence consistent with the proposed hybrid enzymatic-abiotic model proposed for DIR in *Denitromonas* sp. 1R-12[163]. In this model, iodate is initially reduced by IdrAB which accepts electrons from the quinone pool via a cytochrome c551 and performs a four-electron transfer with a resultant production of the chemically unstable intermediate hypoiodous acid (HIO). The HIO then undergoes abiotic disproportionation to yield I^- and IO_3^- in a 2:1 ratio. Both TC-10 and MF63 lack genes resembling chlorite dismutase (*cld*), further supporting that *cld* is not involved in DIR as was proposed for *Pseudomonas* sp. SCT [115]. Apart from *Pseudomonas* sp. SCT and a *Sedimenticola thiotaurini* from a marine metagenome, *idrA* and *cld* genes are mutually exclusive. The lack of *cld* in TC-10 is consistent with the observed mutual exclusivity of organisms with *cld* and *idr*[163]. Together, these observations support the parsimonious DIR model involving a specialized iodate reductase that performs a four-electron transfer to an unstable hypoiodous acid intermediate that disproportionates to IO_3^- and I^-[163].

5.3.3 Evolutionary history of the IRI in *Aromatoleum toluclasticum* sp. TC-10

Both strains of *Aromatoleum toluclasticum* share a close evolutionary history given the high degree of similarity between both organisms, presenting a unique opportunity to study the IRI. 16S rRNA gene sequencing shows 99.93% nucleotide identity for both *Aromatoleum toluclasticum* strains between positions 27 and 1492. Whole-genome sequencing of TC-10 shows an average nucleotide identity of 98.20% to the type strain *Aromatoleum toluclasticum* sp. MF63, affirming the 16S phylogeny of TC-10. Since DIR is a distinguishing feature of TC-10, I generated a synteny plot to show the conserved regions, rearrangement, and insertion between both strains (Figure 5.2A). The synteny plot identified an 89 kb contig in strain TC-10 with numerous inconsistent gaps mapping to the MF63 genome (Figure 5.2B). In TC-10, the *idr* genes are located on a 12.7 kb region directly upstream from a stretch of identical sequence near the *ueh* operon. The island is flanked further by a short segment mapping to an arsenosugar biosynthesis gene *fbiD* (TIGR04282) in the MF63 genome (Figure 5.2C). The discontinuity occurs at an intergenic region at the 3' end and within the *fbiD* gene at the 5' end. The TC-10 genome assembly shows the IRI in the middle of a long contig; however, the flanking regions map to two separate contigs on the MF63 genome, suggesting genome rearrangement has occurred. The same region in MF63 lacks *idr* genes but has an IS3-like transposase and associated hypothetical proteins. While the same IS3-like transposase is present in TC-10, the IS element is not associated with the IRI in its genome.

Traditional markers of horizontal gene transfer such as GC skew or inverted repeats were absent at the site of IRI integration in TC-10. GC content at the IRI is similar to the genome at large (64.75% GC island vs. 66.08% GC genome), and tools such as Tandem Repeats Finder[244] identified no tandem repeats indicative of transposase mediated insertion. Further investigation warranted the use of tools with more robust predictive capacity, such as IslandViewer4[162] and MGEfinder[241]. The latter method identified numerous mobile genetic elements using both its standard and sensitive modes but did not identify regions surrounding the IRI as a mobile genetic element. Similarly, IslandViewer4 did not identify the IRI as a mobile genetic element; however,

a 4.6 kb island containing the molybdopterin biosynthesis gene *moaA* and the arsenosugar biosynthesis gene *fbiD* was predicted as mobile by codon usage bias with an HMM (SIGI-HMM)[162](Figure 5.2D). Since the IRI starts at *fbiD* in TC-10, it is possible that mechanisms mobilizing these genes also mobilize *idr*, and similar codon usage bias in known DIRM at the *idr* locus obfuscates its provenance. The evolutionary history of the *idr* gene neighborhood in TC-10 provides further evidence for horizontal transfer. To date, all experimentally confirmed DIRM belong to a small clade with ten genomes with diverse amino acid primary sequences—the amino acid identity (AAI) between TC-10 and *Denitromonas* sp. IR-12 IdrA is 76%, and 84% between TC-10 and *Pseudomonas* sp. SCT. There is also significant conservation of synteny between *idrABP$_1$P$_2$*, consistent with the previous observations[163]. The gene product for *idrAB,* a prerequisite for DIR, forms a phylogenetically similar molybdopterin oxidoreductase to arsenite oxidase (Aio)[115,163]. The *idrAB* is always preceded by two putative cytochrome c peroxidases *idrP$_1$P$_2$,* whose products share only 37% AAI, suggesting that both play separate roles in detoxification reactions[163]. Taken together, synteny and predicted gene function suggest that *idrABP$_1$P$_2$* have similar roles in both *A. toluclasticum* and other DIRM.

Outside of the *idr* genes, several putative DIRM genomes that clade with known DIRM are missing accessory genes sometimes associated with IRI. Out of the ten genomes, two are missing the two-component system, five are missing a c551-like cytochrome c, and five are missing the *moaA* gene (Figure 5.3). The two-component system likely plays a role in sensing IO_3^- in the environment, as Idr expression has been demonstrated to be inducible upon exposure to IO_3^- [104,115]. The cytochrome c551 is a soluble electron transfer protein that presumably plays a role in transferring electrons from the quinone pool via *bc1*[163]. However, given its prevalence, organisms without cyt c_{551} in the IRI likely use a cyt c_{551} encoded elsewhere in the genome. Similarly, *moaA*, which is involved in molybdopterin synthesis, a prerequisite for DMSO reductases, is found broadly among diverse taxa, and DIRM lacking and IRI associated *moaA* likely use molybdopterin synthesis genes elsewhere in the genome[245]. Lastly, many of the markers of horizontal transfer in *Denitromonas* sp. IR-12 also exists in *A. toluclasticum* sp. TC-10 including the *mer* and *cus* genes (8.5 kb and 15.2 kb upstream, respectively)[157,160,161]. Thus, the presence of the IRI exclusively in TC-10, the variability of genes directly surrounding *idr*ABP$_1$P$_2$, and markers of horizontal transfer surrounding the IRI provide further evidence that DIR is a horizontally acquired metabolism.

5.4 Discussion

This study cultured iodate reducing microorganisms from multiple freshwater and saltwater sources across the San Francisco Bay Area. Our survey yielded a new dissimilatory iodate reducing microorganism, *Aromatoleum toluclasticum* sp. TC-10, from freshwater creek sediment. This organism represents the third known DIRM in pure culture and the first isolated from a low-salinity environment[235]. I demonstrated that *A. toluclasticum* sp. TC-10 couples IO_3^- reduction to acetate oxidation to conserve energy for growth. TC-10 also possesses many of the same genomic and physiological features of the known DIRM *Denitromonas* sp. IR-12. Crucially, the lack of *cld* homologs in both *Denitromonas* sp. IR-12 and *A. toluclasticum* sp. TC-10 challenges previously proposed models suggesting a role for *cld* in DIR[115]. The paucity of *cld*

among both validated and predicted DIRM further suggests that *cld* in the *Pseudomonas* sp. SCT genome is aleatory[163]. These observations are indicative of a parsimonious DIR model independent from *cld* and suggest that *Pseudomonas* sp. SCT reduces iodate like other DIRM. The *cld* in *Pseudomonas* sp. SCT is possibly a remnant of the composite transposon mobilizing the chlorate reduction island found in some *Pseudomonas* spp. previously[246]. Future experiments exploring the protein biochemistry of the iodate reductase are needed to shed light on the intermediates of DIR.

This study also provides further evidence that the iodate reductase belongs to a phylogenetically distinct clade of molybdopterin oxidoreductases and represents a component part of a composite genomic island containing the iodate respiratory genes that is horizontally transferred. I incidentally demonstrate the limitations of 16S rRNA gene sequencing in understanding the biology and ecology of environmental microorganisms[247,248]. Although 16S rRNA gene sequencing serves as a powerful tool for quickly identifying and classifying microorganisms, studies have long since noted that bacteria with identical 16S sequences can exhibit different gene content and nucleotide identity[249]. The similarity between both *Aromatoleum* isolates and modern sequencing technologies enabled a thorough comparison of the horizontally transferred IRI and its surrounding gene neighborhood. The iodate reductase A subunit (IdrA) clades with known DIRM, providing evidence that predicted DIRM in this group likely grow by DIR. I further validate the conserved synteny of the iodate reduction genes and show the limited conservation of genes surrounding the IRI. Genes involved in electron transfer (i.e., cyt C_{551}) are missing in the TC-10 IRI, while molybdopterin cofactor synthesis genes are missing in the IR-12 IRI. Our observation suggests that DIRM lacking individual auxiliary components of the IRI likely use genomically encoded homologs. These results also affirm previous observations suggesting that genomes with conserved synteny at *idrABP$_1$P$_2$* are likely DIRM[163]. The diversity of genes surrounding the iodate respiration genes also suggests different evolutionary histories for the IRI. While no specific transfer mechanism was proposed due to a lack of clear evidence, I provide a detailed description of the IRI insertion site for future comparisons.

Ultimately, understanding the distribution, physiology, and diversity of DIRM depends on isolating and characterizing the physiology and genetics of new strains. Although I cannot rule out the possibility of marine origin from nearby sea spray, all *Aromatoleum* species to date have been isolated exclusively from pristine and contaminated freshwater sources[237]. Thus, our study expands the known distribution of the metabolism to coastal freshwater environments. Iodine deposited in these zones may be abundant enough for microorganisms to use it as a terminal electron acceptor. Therefore, future work surveying iodate removal should consider terrestrial sites in littoral zones with microbially mediated iodine biogeochemical cycling.

5.5 Figures

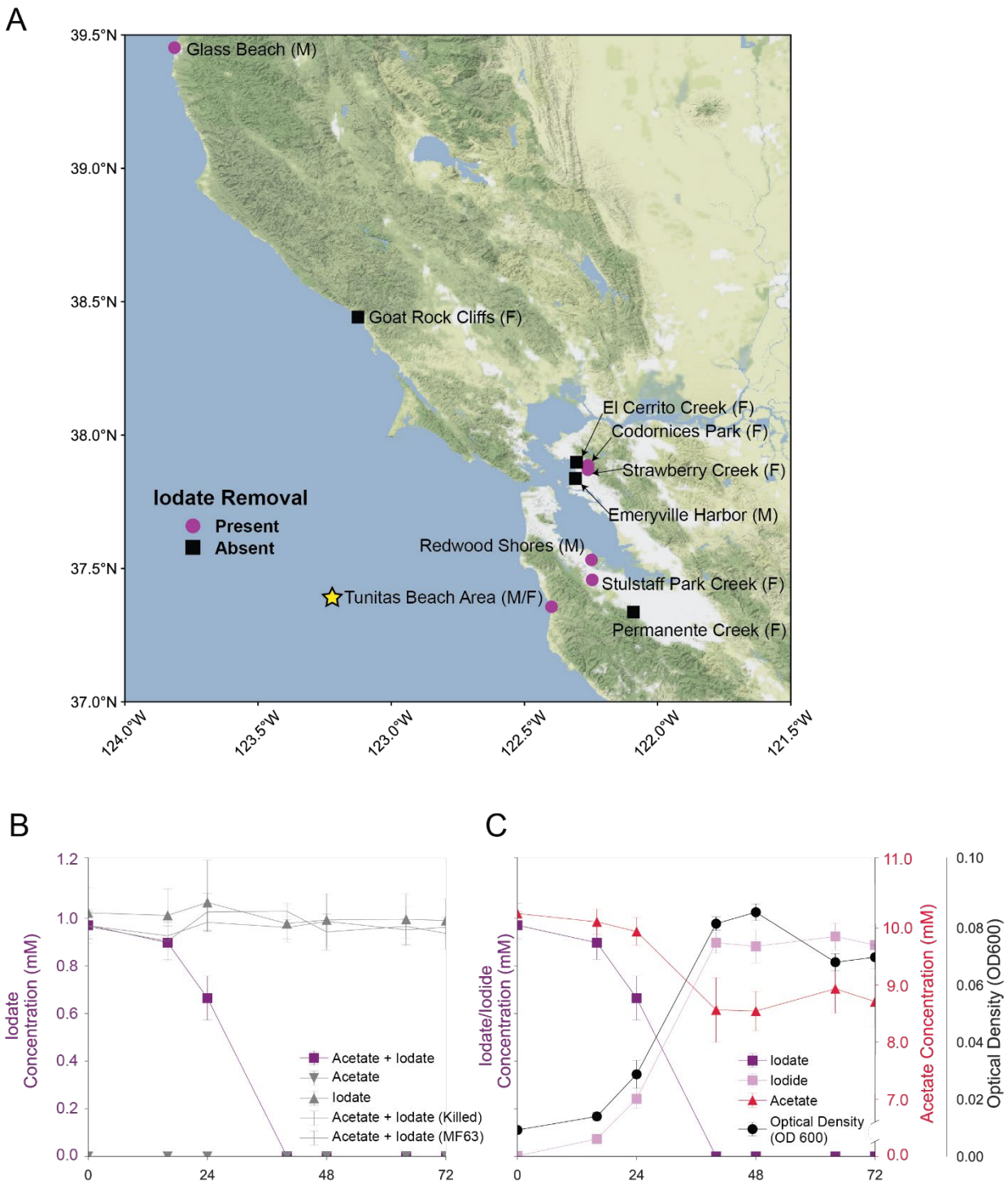

FIGURE 5.1: DISSIMILATORY IODATE REDUCTION IN FRESHWATER ENVIRONMENTS. A) A map of the San Francisco Bay Area showing all sampled locations. Locations sampled for marine enrichments denoted by (M) and locations sampled for freshwater enrichments denoted by (F) Samples from locations showing removal of 2mM iodate denoted by purple circles (●). The location where *Aromatoleum toluclasticum* sp. A yellow star denotes TC-10. Samples from

locations without iodate removal are denoted by black boxes (■). B) A time course showing removal of iodate in the acetate + iodate condition and no removal of iodate in alternative conditions. C) A time course showing the removal of acetate and iodate coupled to an increase in the optical density of the cell culture.

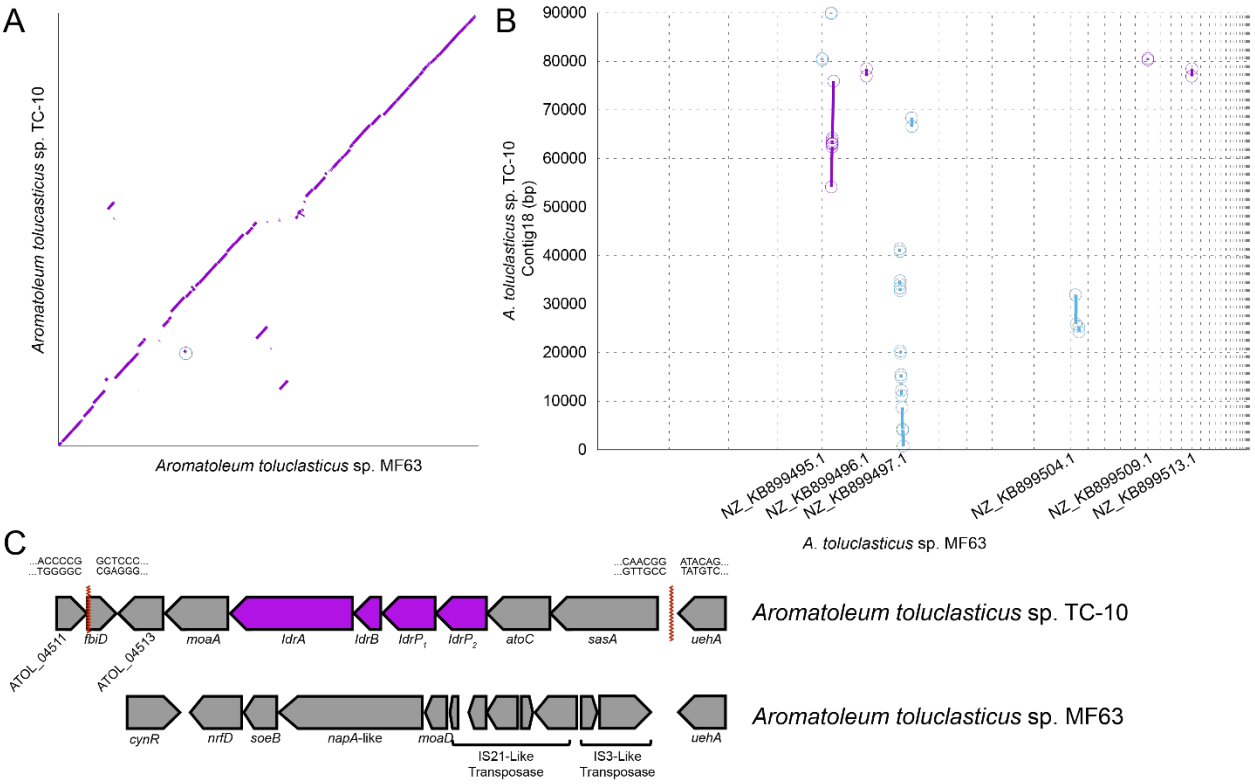

FIGURE 5.2: A GENOMIC ANALYSIS OF AROMATOLEUM TOLUCLASTICUM. A) A synteny plot showing regions of major synteny, weak synteny, and gaps between *Aromatoleum toluclasticum* MF63 and TC-10. B) A synteny plot showing the regions of conservation along with node 18 in TC-10, which contains the IRI. The gap between 41,363 and 54,119 bp signifies the region containing the IRI. C) The IRI in TC-10 with catalytic *idr* genes is denoted by the purple color. Red serrated lines denote borders of the IRI. Sequences flanking serrated lines represent the nucleotide sequence at either side of the IRI border. MF63 is provided below as a comparison to demonstrate the lack of the IRI near *uehA*.

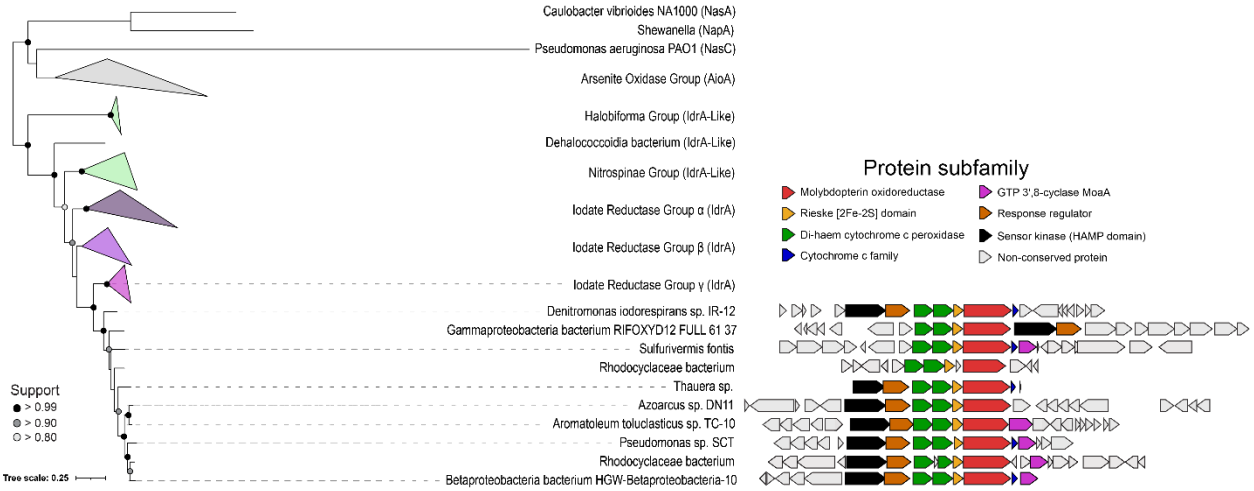

FIGURE 5.3: A PHYLOGENETIC TREE REPRESENTING THE MAJOR GROUPS OF IDRA. Collapsed clades are represented as triangles to show the interclade distance. IdrA clade containing all cultured representatives of DIRM is expanded. Gene neighborhoods show +/- 10 genes from IdrA when present. Genes are colored based on Pfam annotation if the protein family shows up in more than 50% of the clade's genomes.

Chapter Six: Concluding Remarks

The overarching motivation behind this project was to examine whether the presumed promiscuity of the type II DMSO reductase towards IO_3^- was responsible for iodate reduction broadly. Given ample evidence that bacteria can turn over IO_3^- via nitrate or perchlorate reductases, our initial approach was to test microorganisms that perform denitrification or dissimilatory perchlorate reduction. Upon learning that none of the organisms in our lab collection expected to reduce IO_3^- did so, I searched the environment for representative organisms. My isolation attempts were eventually fruitful, and I identified the current publicly available model DIRM, *Denitromonas* sp. IR-12. I demonstrate that like *Pseudomonas* sp. SCT, *Denitromonas* sp. IR-12 couples the oxidation of acetate to the reduction of iodate and concomitant growth. I show the molybdenum dependence of this phenotype, demonstrate the energetics of dissimilatory iodate reduction, and establish that cells can conserve energy via this pathway.

Denitromonas sp. IR-12 revealed several things not previously known about dissimilatory iodate-reducing microorganisms. I identified that the DMSO reductase in *Denitromonas* was very similar to the arsenite oxidase Aio; however, unlike the arsenite oxidase, subtle changes in the amino acid sequence and an association with two different cytochrome c peroxidase-like proteins enabled the organism to use IO_3^- as a substrate. Further work identified the breadth of DIRM among cultured bacterial taxa and taxonomically classified the majority of DIRM in the phylum *Proteobacteria*. Upon identifying the genes unique to DIRM, a systematic approach of single-gene mutants determined the essentiality of each gene predicted to form the iodate reductase. I show that despite possessing a related DMSO reductase (i.e., nitrate reductase), nitrate reductase subunits cannot rescue the function of the iodate reductase. Preliminary overexpression analyses of the $IdrP_1$ in $\Delta idrP_2$ also show that $IdrP_2$ likely performs a separate function than $IdrP_1$. My work on understanding the genetics of DIR ultimately establishes a system upon which others can study the biochemistry of DIR. Future work should explore the cross-complementarity of phylogenetically similar $IdrP_1$ proteins and obtain a foundational understanding of iodate reductase kinetics.

The accessibility of large metagenomic databases and high-power computing tools has also enabled us to learn about the distribution of DIRM broadly. This dissertation applied both metagenomic, and machine learning approaches to learning about DIRM and their environment. Metagenomic datasets with curated geochemical metadata helped identify a niche for DIRM near multiple oxygen minimum zones globally. These data showed that DIRM are present in environments with elevated nitrate and phosphate and reduced oxygen. More broad databases with less rich metadata revealed that DIRM are broadly among numerous phyla and are associated with marine and terrestrial environments. While further research is needed to confirm the cross-phylum distribution of the IRI, such an observation would present a unique instance of a mobile genomic island conferring a dissimilatory metabolism.

Subsequent attempts to isolate DIRM resulted in the identification of the freshwater DIRM *Aromatoleum toluclasticum* sp. TC-10. The isolation of TC-10 affirmed the prior observation of *idrA* like genes among terrestrial environments. An assessment of the iodate reduction phenotype in *Aromatoleum* concluded that it too conserves energy from DIR. Fortuitously, strain TC-10 was a non-type strain of *Aromatoleum toluclasticum*, and a rigorous

comparative genomics analysis ultimately determined the boundaries of the IRI and delineated the difference between core and accessory IRI genes. Beyond confirming many of the observations from our *Denitromonas* study, *Aromatoleum toluclasticum* sp. TC-10 expanded the potential ecosystems wherein researchers can isolate DIRM.

This dissertation ultimately contributed to identifying a gene producing a protein with a unique and novel function. It identified a class of microorganisms only casually described in the literature and showed its broad distribution among several global ecosystems. The genetic system in *Denitromonas* leaves a collection of single mutant strains from which future researchers can examine the biochemistry of DIR and refine the proposed parsimonious DIR model. The relative ease with which one grows *Denitromonas* also enables future researchers to study the protein biochemistry of the iodate reductase and assess the function of its components. Such analyses have the potential to explain how subtle changes in amino acid primary sequences can result in very different behaviors, as is the case with Aio and Idr. Furthermore, identifying new DIRM and their habitats can expand our collective knowledge of microbial lifestyles associated with DIR. Organisms such as the chemolithotrophic sulfur oxidizer *Sulfurivermis fontis* or the psychrophilic microorganism *Marinobacter psychrophilus* arise from drastically different environments than either *Denitromonas* or *Aromatoleum*.

The proposed diversity of DIRM and its distribution among specific environments suggest that the iodine biogeochemical cycle may be active in areas beyond our world's oceans. Researchers can explore how microorganisms with presumably different lifestyles to cultured DIRM contribute to iodine cycling and how they interact with other members of the local microbial community. These endeavors will ultimately reveal to what extent DIRM contribute to biogeochemical phenomena such as the IO_3^-:I^- disequilibrium and subsequent I^- enrichment in areas with high biological productivity. They may also reveal the evolutionary pressure for microorganisms to adopt the IRI and explain the benefit of maintaining this genomic island. Future research in this field will hopefully refine many of the ecological proposals outlined in this dissertation. Nevertheless, this work serves as a testament to the diversity of microbial metabolism and empowers researchers seeking to parameterize the iodine cycle.

Addendum: A description of the genus *Denitromonas gen. nov.*

Abstract

The genus *Denitromonas* is currently a non-validated taxon that has been identified in several recent publications as members of microbial communities arising from marine environments. Very little is known about the biology of *Denitromonas* spp. and no pure cultures are presently found in any culture collections. The current epitaph of *Denitromonas* was given to the organism under the assumption that all members of this genus are denitrifying bacteria. This study performs phenotypic and genomic analyses on three new *Denitromonas* species isolated from tidal mudflats in the San Francisco Bay. I demonstrate that *Denitromonas* species are indeed all facultative denitrifying bacteria and utilize a variety of carbon sources. In addition, individual strains also use the esoteric electron acceptors perchlorate, chlorate, and iodate. Both 16S and Rps/Rpl phylogenetic analyses place *Denitromonas* as a deep branching clade in the family *Rhodocyclaceae,* separate from either *Azoarcus* or *Aromatoleum*. Genome sequencing reveals a G+C content ranging from 63% to 68%, and genome sizes range between 4.2-5.2 Mb. Genes for salt tolerance and denitrification are distinguishing features that separate *Denitromonas* species from the related *Azoarcus* and *Aromatoleum* genera.

A.1 Introduction

The family *Zoogloeaceae* includes an ecologically and metabolically diverse group of organisms involved in nitrogen cycling and consists of numerous diazotrophs and denitrifiers with different ecological niches[250]. Among the several genera in the family, there exists a poorly defined boundary between the broadly inclusive genus *Azoarcus*[251], the recently proposed genus *Aromatoleum*[237], and the proposed genus *Denitromonas*. *Azoarcus* commonly possess denitrification genes and persist in the environment as either endophytes or free-living microorganisms. Endophytic *Azoarcus* species such as strain BH72 exhibit exclusively endophytic lifestyles and have only been observed as part of rhizosphere[252]. These *Azoarcus* are commonly studied to understand endophytic nitrogen fixation and the evolution and regulation of their nitrogenase genes[253,254]. Free-living *Azoarcus* species are often found in BTEX (benzene, toluene, ethylbenzene, and xylene) contaminated water systems where they can degrade these toxic hydrocarbons anaerobically under denitrifying conditions[255,256]. The combination of different lifestyles, genome identity, and ecological niches has led some researchers to propose that some free-living *Azoarcus* be reclassified as *Aromatoleum*[237].

Unlike *Azoarcus* or *Aromatoleum*, *Denitromonas* has only been described as constituents of marine-derived microbial communities. All characterized *Denitromonas* species are free living microorganisms isolated from saline environments, making salt tolerance yet another distinguishing feature between *Aromatoleum*, some *Azoarcus*, and *Denitromonas*. However, various descriptions of *Denitromonas* are limited to a 16S rRNA gene on NCBI. The lack of complete genomes and publicly available isolates makes distinguishing the ecological and phylogenetic patterns between *Azoarcus*, *Aromatoleum*, and *Denitromonas* challenging. S. Orla-Jensen first proposed the genus in 1909 because denitrification was a unique characteristic limited to this genus at the time[257,258]. A review of the literature since Jensen's proposal identifies three separate studies characterizing five distinct *Denitromonas* isolates that focus primarily on their respiratory metabolisms. Yip and Gu characterize the halophilic isolate *Denitromonas indolicum* MPKc and its ability to degrade 2-methylindole; however, the strain is not deposited in any culture collections and information about its genome is missing[132]. Of the four *Denitromonas spp.* with sequenced genomes, Carlstrom *et al.* briefly describe three isolates of *Denitromonas halophilus* from an anaerobic marine microbial community that reduces perchlorate to chloride and couples its reduction to growth[118]. Barnum *et al.* further describe a parasitic symbiosis between several chlorate respiring bacteria and *Denitromonas sp.* SFB-1, based on the competitive utilization of the chlorate intermediate formed during anaerobic perchlorate reduction by SFB-1 for growth[259]. Similarly, Reyes-Umana *et al.* describe an isolate of *Denitromonas* capable of using iodate as a terminal electron acceptor and coupling its reduction to growth[163].

While several studies have identified organisms belonging to the genus *Denitromonas*, the genus itself has not validly been characterized, and thus has no nomenclature standing on the List of Prokaryotic names with Standing in Nomenclature (LSPN)[260,261]. This study seeks to validly publish the taxon *Denitromonas gen. nov.* and holistically demonstrate a clear distinction between the four sequenced *Denitromonas* isolates and the *Azoarcus,* and *Aromatoleum* species through 16S ribosomal gene phylogeny, ribosomal protein phylogeny, average nucleotide identity, and biochemical assays. Additionally, while Orla-Jensen raised issues with the epitaph *Denitromonas*

due to the ubiquity of denitrification among bacteria, I chose to maintain the original epitaph for consistency and historical recognition[257]. I also demonstrate that *Denitromonas* species are free living, metabolically versatile, and possess genes associated with salt tolerance. These defining features of the genus likely explain why isolates arise from marine environments, and suggest that *Denitromonas* forms a new, possibly under-sampled, genus belonging to the family *Zoogloeaceae* that inhabits a distinct niche from *Aromatoleum* and *Azoarcus*.

A.2 Methods

A.2.1 Media, chemicals, and culture conditions

Denitromonas species were isolated from San Francisco Bay intertidal flat sediment as previously described[118]. All isolates were confirmed by single colony selection on agar plates with subsequent sequencing of the 16S ribosomal gene (16S rRNA gene: see below). Isolates were grown routinely both aerobically or anaerobically at 30°C using either a defined marine media, or Reasoner's 2A (R2A) agar or medium (HiMedia, USA). The defined marine media contains the following per liter: 30.8g NaCl, 1.0g NH_4Cl, 0.77g KCl, 0.1g KH_2PO_4, 0.20g $MgSO_4 \cdot 7H_2O$, 0.02g $CaCl_2 \cdot 2\ H_2O$, 7.16g HEPES, along with vitamin and mineral mixes as described in Carlstrom *et al.* [118]. The anaerobic medium was boiled and dispensed under an atmosphere of 100% N_2 and sealed with a butyl rubber stopper. After autoclaving, each liter of media was aseptically amended with 34.24mL 0.4M $CaCl_2$ and 26.07mL 2M $MgCl_2 \cdot 6H_2O$ from sterile stock solutions. All chemicals used in this study used sodium salts and were purchased through Sigma Aldrich (Sigma Aldrich, USA). Thermo Scientific™ GENESYS™ 20 spectrophotometer was used to measure growth via optical density at 600 nm (OD_{600}). The Analytical Profile Index (API) 20 NE system was used to determine enzymatic activities following the manufacturer's instructions (BioMérieux, France). Carbon utilization profiles, pH and salinity optima were determined by monitoring OD_{600} increase using the TECAN Sunrise™ 96-well microplate reader. Temperature range was determined by growth of isolates on R2A agar plates at 4°C, 14°C, 20°C, 25°C, 30°C, and 37°C.

A.2.2 Taxonomic assessment

Taxonomy assignments were made using (i) 16S rRNA gene sequence; (ii) alignment of the ribosomal marker proteins (Rps and Rpl)[262]; (iii) multigene alignments using the Genome Taxonomy Database (GTDB)[263]; and (iv) alignment fraction analysis of average nucleotide identity (ANI) [264]. Primers 27F and 1492R were used to amplify the 16S rRNA gene in all isolates by PCR. Resulting products were sequenced by Sanger sequencing. 16S rRNA gene sequences belonging to the genera *Azoarcus*, *Aromatoleum,* and *Denitromonas* were downloaded from NCBI in the FASTA (.fna) file format and aligned using MUSCLE 3.8[124]. An approximately maximum-likelihood phylogenetic tree was generated using FastTree, specifying 10,000 resamples and using the standard settings for all other options[242]. The resultant tree was visualized in a ladderized format using the *ete3* toolkit[128]. *Aromatoleum* species still listed under their original genus designation of *Azoarcus* on NCBI were renamed to reflect current proposed taxonomic classification.

Whole genomes belonging to the genera *Azoarcus*, *Aromatoleum*, and *Denitromonas* were downloaded from NCBI as protein FASTA files (.faa) and were run using the following select modules from the phylogenomics workflow described by Graham *et al.*[199] (https://github.com/edgraham/PhylogenomicsWorkflow). All .faa files were concatenated into a single FASTA file, and the script *identifyHMM* was used at standard settings without the --*performProdigal* flag to identify the set of Ribosomal proteins (Rps) and Ribosomal Protein Large subunit (Rpl) markers from Hug *et al.*[200]. The *identifyHMM* script produced individual lists of hits for each Rps or Rpl marker, and hits for each marker were then aligned using MUSCLE 3.8 with the *-maxiters 16* flag included. Alignments were trimmed using trimAl[202] with the *-automated 1* flag included, and the *concat* script that comes packaged with BinSanity was run with the minimum number of sequences to be concatenated set at 8. The phylogenetic tree was built using FastTree at standard settings while also including the *-gamma* and *-lg* flags. The tree was visualized using the *ete3* toolkit. In parallel, the Genome Taxonomy Database (GTDB) (version 202) web browser was also used to search for the taxonomy of *Denitromonas*.

A.2.3 Average nucleotide identity (ANI) and alignment fraction (AF) analysis

Whole genomes belonging to the genera *Azoarcus*, *Aromatoleum*, and *Denitromonas* were downloaded from NCBI as nucleotide FASTA files (.fna) and analyzed with FastANI using the *"many to many"* option[265] (https://github.com/ParBLiSS/FastANI). The output file was then transformed into a pivot table using pandas 1.2, and setting the index, columns, and values to the query, reference, and ANI, respectively. The index and column were sorted using the tree order from the RpS/RpL phylogenetic analysis and displayed as a heatmap using the seaborn 0.11 package. Alignment fractions were calculated from the output by dividing the count of bidirectional mappings by the total number of mappings for any one pair. Genus boundaries were determined using the methods outlined by Barco *et al.,* which uses alignment frequency and average nucleotide identity[264]. Briefly, a non-parametric Wilcoxon test was used to determine the boundaries for the *Denitromonas* genus ($p \leq 0.05$) by comparing type species belonging to *Denitromonas* (N=4) against non-type species belonging to *Azoarcus* (N=18). *Denitromonas iodorespirans* was used as the reference strain, and strains exceeding the boundary were classified as *Denitromonas*.

A.2.4 Protein subfamily and Denitromonas core genome analysis

Protein subfamilies were identified using the *subfamilies.py* script from Méheust *et al.*[266] on the concatenated protein FASTA file (.faa) for all 38 *Aromatoleum*, *Azoarcus*, and *Denitromonas* species. This script uses MMSeqs2 to perform an *all vs. all* search using parameters set at an e-value: 0.001, sensitivity: 7.5, and cover: 0.5. A sequence similarity network was built based on the pairwise similarities, and the *greedy set-cover* algorithm from MMseqs2 was performed to define protein subclusters. The resultant clusters were exported as a tab-separated file listing all identified proteins and their associated subfamilies. Feature tables belonging to the genera *Azoarcus*, *Aromatoleum*, and *Denitromonas* were downloaded from NCBI as feature_table.txt files to associate locus tag, genome ID, and gene product information with the MMseqs2 output using *pandas*. The resultant dataframe was converted to a presence and absence

matrix with values of either 1 (present) or 0 (absent) using the *groupby* function, transposed, and genomes were then sorted using the phylogenetic tree order from the RpS/RpL analysis. Clusters were subsequently ordered by the presence frequency in descending order, starting with conserved protein subfamilies found in all genomes on the left. A global *all vs all* Jaccard similarity score was calculated for each genome in the dataset using the *jaccard_score* function on scikitlearn 0.24 and setting the method to "micro". Results of the presence/absence matrix and the Jaccard similarity index were displayed using seaborn 0.11. Protein subfamilies unique to all *Denitromonas* were identified by taking the inverse intersection of *Aromatoleum* and *Azoarcus* subfamily dataframe and *Denitromonas* subfamily dataframe. A similar analysis of the "shell" proteins (defined as present in all but one *Denitromonas* species) used a similar method. The Kyoto Encyclopedia of Genes and Genomes (KEGG) was used to annotate the *Denitromonas* genomes using the *BlastKOALA* tool, and denitrification genes were identified by inputting the resulting K-numbers table into the KEGG Mapper *Reconstruct* tool.

A.2.5 Microscopy

A Meiji MT4200L compound microscope (Meiji Techno Co., Japan) set with a 10x ocular lens was used to determine cell size under the 100x objective. Ocular lens was set with a scale bar and was calibrated to a 45μM nylon fiber to determine size of bars in the eyepiece. Individual cells were measured, and size was reported as range for vegetative cells. Motility was determined by observing twitching or movement under the 100x objective.

A.3 Results and Discussion

A.3.1 Cultured *Denitromonas spp.* forms a phylogenetically distinct clade

A representative 16S rRNA gene phylogenetic analysis of *Zoogloeaceae* (Figure A.1A) inconsistently classifies *Denitromonas* and *Azoarcus*. *Denitromonas* is missing from the clade containing the recently reclassified *Aromatoleum* species, supporting the hypothesis that *Aromatoleum* forms a phylogenetically distinct monophyletic clade[237]. *Thauera* forms a separate clade containing some *Denitromonas* species. However, these partial 16S rRNA gene sequences arise from uncultured clones in bioreactor systems[267,268], and were classified with older taxonomic databases that assigned taxonomy using only the 16S rRNA gene[269-271]. These *Denitromonas* 16S rRNA gene sequences should be reassigned to *Thauera* to align with the more recently described taxonomic differences between *Azoarcus* and *Thauera*[250]. The branch of *Denitromonas* containing *D. halophilus*, *D. ohloneium*, and *D. iodorespirans* clade with other *Denitromonas* species exclusively. There is good bootstrap support (≥99%) separating *Denitromonas* from its closest relative *Azoarcus* (Figure A.1A), suggesting that the *Denitromonas* clade containing the four isolates form a distinct monophyletic group.

While 16S rRNA gene phylogeny provides an overview of the diversity of *Zoogloeaceae*, current standards of prokaryotic classification recommend using the entire genome to determine reliable taxonomic assignment[272]. Currently, 38 whole genomes are provided on NCBI for the closely related *Zoogloeaceae* family: *Azoarcus*, *Aromatoleum*, and *Denitromonas*. Figure 1B

shows the concatenated ribosomal protein phylogeny of the different species within these genera. Using the *Rhodocyclaceae* bacterium *Azospira oryzae* as an outgroup, *Denitromonas spp.* form a distinct, monophyletic, deep branching clade that is separate from either *Azoarcus* or *Aromatoleum*. There is good bootstrap support (≥99%) for the distinction between *Denitromonas* and *Azoarcus* consistent with distinct evolutionary histories for these two genera. Additionally, all *Zoogloeaceae* show less than 80% average nucleotide identity (ANI) to *Denitromonas* (Figure A.2A). While these observations suggest that *Denitromonas* forms a separate genus, the determination of a genus is fluid and varies among different bacterial families and orders. Recently, Barco *et al.* proposed a statistical test to discern the differences in the alignment fraction (AF) and average nucleotide identity between type and non-type strains of a genus to estimate a cutoff for a genus[264]. Using this method, I estimated the genus cutoff for *Denitromonas* to be at an ANI of 82.70 (p=0.011) and an AF of 0.51 (p=0.011). All fully sequenced *Denitromonas* currently fall above this threshold, suggesting that all belong to the same genus (Figure A.3). Within this group, *D. ohloneium* SFB-1 and *D. ohloneium* SFB-2 show 99.99% ANI, suggesting that these are different strains of the same species. *D. halophilus* shows 94% ANI with either *D. ohloneium* isolates, suggesting that *D. halophilus* is a different species. *D. iodorespirans* shows the lowest ANI (85%) to other *Denitromonas* species, further suggesting that the species diversity of the genus is likely under-sampled. Although the family *Zoogloeaceae* is a validly published taxon[273], a recent proposal to reduce polyphyly reclassifies the class *Betaproteobacteria* as an order of *Gammaproteobacteria* thus changing the higher taxonomic ranks of *Denitromonas*, *Azoarcus*, and *Aromatoleum*[274]. The taxonomic ranks proposed by the Genome Taxonomy Database version 202 (http://gtdb.ecogenomic.org/) classifies the family *Zoogloeaceae* into the family *Rhodocyclaceae*, which belongs to the order *Burkholderiales* in the class *Gammaproteobacteria*. Within the family *Rhodocyclaceae*, *Denitromonas* is proposed as a distinct genus, further supporting our observations. Together, these data suggest that *Denitromonas* forms a distinct genus with a different evolutionary history from other members of the same family.

A.3.2 *Denitromonas spp.* possess protein subfamilies suited for marine environments

To further delineate possible functional differences between *Denitromonas spp.* and other *Zoogloeaceae*, an analysis of the proteome of all 38 sequenced *Zoogloeaceae* was performed. Proteins were clustered into 7465 different subfamilies using MMSeqs2 and displayed as a presence-absence matrix (Figure A.4). The matrix was then scored by calculating the Jaccard similarity index on pairwise comparisons for each genome (Figure A.2B). Figure A.2B demonstrates that *Aromatoleum* species possess a similar set of core proteins compared to other genera. I observe a difference in protein subfamily similarity between species related to *A. diolicum* and those in either the CIB or toluclasticum groups, indicating a possible difference in lifestyle as previously reported[237]. Likewise, *Denitromonas* species shows a different set of proteins that are internally similar within the genus but distinct from other genera. *Denitromonas* clearly forms a core cluster with similarity scores of 0.85 or above between all members of the genus (Figure A.2B). Similarity scores greater than 0.85 are in line with the similarity score between other genera in *Zoogloeaceae*, which all form similar clusters that track closely with taxonomy and ANI (Figure A.1B, Figure A.2A). *Azoarcus halotolerans* and *Azoarcus* sp. HKL-1 show relatively close Jaccard scores of greater than 0.75 to *Denitromonas* species, which is in line with the ribosomal protein

phylogeny described earlier (Figure A.1B). To understand the functional differences between *Denitromonas* and other *Zoogloeaceae*, I analyzed the panproteome of the family *Zoogloeaceae* for protein subfamilies (i) present only in *Denitromonas*; (ii) present only in *Azoarcus* and *Denitromonas*; and (iii) missing from *Denitromonas*. Out of the 7465 protein subfamilies, there are 145 subfamilies unique to *Denitromonas* and absent from all other *Zoogloeaceae*, which accounts for 2% of the *Zoogloeaceae* panproteome. Of these 145 protein subfamilies, 82/145 subfamilies (57%) are annotated as hypothetical proteins, and 45/145 subfamilies (31%) are present in all *Denitromonas* species.

Denitromonas species possess several protein subfamilies involved in metal homeostasis that are not found in either *Azoarcus* or *Aromatoleum*. Subfamilies found in all *Denitromonas* species involved in metal transport include a FeoA ferrous iron transporter-associated protein, a metal ABC transporter permease, and a calcium/proton antiporter. FeoA proteins are cytoplasmically expressed and are essential in ferrous iron transport broadly; however, their exact function in iron transport in *Denitromonas* remains unknown[275] but may be related to an excess ferrous iron detoxification mechanism for nitrate reducing species as previously outlined by Carlson *et al*[276]. Similarly, not much is known about the metal ABC transporter permeases found in all *Denitromonas* species. Proteins belonging to this cluster are inconsistently annotated as *znuB* on NCBI, suggesting that this protein may be involved in zinc, manganese, or divalent metal metabolism. ZnuB homologs in other bacteria have been noted for their involvement in copper resistance or iron transport[277]. Calcium proton antiporters have been characterized in *E. coli* and *Azotobacter vinelandii*, where they have been shown to regulate calcium transport into and out of the cell and generate a proton motive force[278,279]. While the function of calcium in bacteria remains enigmatic, $Ca^{2+}/2H^{+}$ antiporters have been found in numerous bacteria from saline and alkaline environments, where they have been associated with salt tolerance[280,281]. Since *Azoarcus* and *Aromatoleum* are not exclusively found in marine environments, proteins belonging to these clusters likely demonstrate that *Denitromonas* species have adapted to mildly alkaline marine environments where they compete for the paucity of divalent metals[282,283].

Organisms reclassified as *Aromatoleum* have been exclusively identified in freshwater systems[236], whereas *Denitromonas* and deep branching *Azoarcus* species in the BH72 group (e.g., *A. indigens* and *A. olearius* BH72) are consistently identified in marine environments or material sourced from marine environments (see table A.1). Several genes are present in *Denitromonas* and *Azoarcus* but absent in *Aromatoleum* include the *nqr* operon (*nqrACFM*), the LEA type 2 proteins, and class GN sortases. The *nqr* operon is involved in maintaining a sodium motive force in numerous marine microorganisms and enables respiration in high salinity/high pH ecosystems[284,285]. *Denitromonas* spp. and *Azoarcus halotolerans* have LEA type 2 proteins which play an essential role in abiotic stress caused by drought, cold, or salinity. The LEA type 2 proteins specifically contain a domain known as the water stress and hypersensitive response (WHy) domain which protects against dehydration[286]. Lastly, both *Denitromonas* and *Azoarcus* possess the poorly described class GN sortase enzymes. Sortase enzymes are widespread in gram-positive bacteria and enable cell wall protein sorting; however, their role in gram-negative organisms remains unknown, and their distribution is limited to halotolerant proteobacteria[287].

Denitromonas and *Azoarcus* are phylogenetically closely related diverging during an early evolutionary event. Both genera have origins in saline or brackish environments, whereas

Aromatoleum arise from a relatively new clade of organisms found in fresh contaminated water. *Azoarcus* forms a more diverse clade of organisms that have adapted to survive in both saline and freshwater systems, while *Denitromonas* forms a clade of organisms that are predominantly found in brackish or saline environments. Intertidal mudflats in estuarine environments like the San Francisco Bay are exposed to consistent changes in salinity and oxygen[288]. The presence of genes associated with salt tolerance and metal transport, along with the ability to use numerous terminal electron acceptors, suggests that *Denitromonas* species have adapted to an environment with transient changes in salinity and nutrients. The metabolic diversity of *Denitromonas*, along with the dynamic environment they inhabit, suggests that this genus adopts a generalist, free-living lifestyle in brackish marine environments.

A.4 Description of *Denitromonas* gen. nov.

Denitromonas gen. nov. (De.ni.tro.mo'na.s) L. abl. *De* from; Chem. n. *nitro* nitrogen; L. nom. *monas* meaning unit; NL abl. *Denitromonas* unit descending from nitrogen, which refers to the ability of all members from the genus to obtain energy through dissimilatory nitrate reduction to N_2 gas.

Cells are rod-shaped, motile, mesophilic, and heterotrophic. All *Denitromonas* species are facultatively anaerobic chemoorganotrophs between 1.5-2.0 μM long by 0.6-0.7 μM wide. Cells grow in a wide range of salinity from 0%-5% but optimally in brackish or saline water between 1% and 3%. Cells grow over a pH range of 6.8 to 8.2 with a growth optimum at pH 7.2. *Denitromonas* grows over a temperature range of 14°C-30°C. The G+C content ranges from 63% to 68%, and genome sizes range between 4.2-5.2 Mb. *Denitromonas* are metabolically versatile and utilize a variety of carbon sources including acetate, lactate, succinate, butyrate, fumarate, pyruvate, and propionate. Members of *Denitromonas* do not ferment glucose, are urease positive, and hydrolyze esculin. All *Denitromonas* are denitrifying bacteria that utilize nitrate as a terminal electron acceptor producing N_2. A summary of the metabolic profile for each species is found in table A.2.

A.4.1 Description of *Denitromonas iodorespirans* IR-12 sp. nov.

Denitromonas iodorespirans (i.o.do.resp'ir.ans) Chem. n. *iodo* iodine; L. pres. part. *respirans* breathing; NL pres. part. *iodorespirans* iodine-breathing, referencing the ability to use iodate as a terminal electron acceptor for growth.

Denitromonas iodorespirans is a facultatively aerobic organoheterotroph isolated from an intertidal mudflat in the San Francisco Bay near Berkeley, CA. It grows by oxidizing lactate or acetate with concomitant reduction of oxygen (O_2), nitrate (NO_3^-), or iodate (IO_3^-) in a defined marine medium at 3% salinity at a pH of 7.2. Alternatively, *D. iodorespirans* can grow on R2A in either liquid or solid agar plates and can use a variety of carbon sources aerobically (Table A.2). On solid R2A agar, it forms small smooth reddish white colonies with a minute portion of crimson red and ash grey that deepen in color to a peach blossom red after 48-72 hours. Growth occurs between 14-37°C but is consistently grown at 30°C. An analysis of the genome shows all the genes

involved in denitrification and assimilatory nitrate reduction (NarGHI, NapAB, NirK, NorBC, and NosZ), and nitrogen fixation (nifDHK).

The genome of *D. iodorespirans* is 5,181,847 bp (average coverage 64.2x) with 4697 CDS, a G+C content of 66.54%, 57 tRNAs, one tmRNA, and one CRISPR array with associated Cas2-3, Cas 5d, and a Cas4-Cas1 fusion. It has a single plasmid 81,584 bp long whose function remains unclear. The complete genome has been deposited in GenBank (GCA_018524365.1), currently consisting of 202 contigs. The type strain *Denitromonas iodorespirans* IR-12^T has been deposited in the American Type Culture Collection (TSD-242).

A.4.2 Description of *Denitromonas halophilus* sp. nov.

Denitromonas halophilus (ha.lo. phi'l.us) Gr. gen. *halos* salt; Gr. part. adj. *philos* loving; N.Gr. pres. part. *halophilus* salt-loving, referring to the organism's ability to grow in saline environments.

The description of *Denitromonas halophilus* SFB-3 expands on observations from Carlstrom *et al.* and was amended to include details regarding its genome. *D. halophilus* is a facultatively aerobic organoheterotroph isolated from an intertidal mudflat in the San Francisco Bay near Berkeley, CA[118]. It grows by completely oxidizing lactate or acetate with concomitant reduction of oxygen (O_2), nitrate (NO_3^-), perchlorate (ClO_4^-), or chlorate (ClO_3^-) in a defined marine medium at 3% salinity and a pH of 7.2. It forms small, round, rough, white colonies. Colony colors deepen to an orange-colored white colonies with a very small portion of tile red, king's yellow, and ash grey on R2A agar after 48-72 hours. It can utilize a variety of carbon sources as outlined on table A.2. *D. halophilus* possesses all the genes necessary for assimilatory nitrate reduction and denitrification (NarGHI, NapAB, NirK, NorBC, and NosZ).

The genome of *D. halophilus* is 4,393,467 bp (average coverage 151.3x) has 4154 CDS, with 4,105 coding for proteins, 49 tRNAs, and no CRISPR array or plasmid. Its G+C content is 63.72%. The complete genome has been deposited in GenBank (accession number: GCA_007625155.1), consisting of 34 contigs. The type strain *Denitromonas halophilus* SFB-3^T has been deposited in the American Type Culture Collection (TSD-270).

A.4.3 Description of *Denitromonas ohloneium* nom. nov.

Denitromonas ohloneium (oh.lo.nei'.um) N. *ohlone* as it pertains to the occupied Ohlone land in modern-day Berkeley, California; L. nom. *ium* belonging to; NL nom. *ohloneium* belonging to the Ohlone land.

The description of *Denitromonas ohloneium* expands from Barnum *et al*. and was amended to include details regarding its genome and the newly proposed nomenclature[259]. The proposed species epitaph pays homage to the multiple Ohlone tribes of central coastal California, who are the original inhabitants of the present day San Francisco Bay Area[289]. *Denitromonas ohloneium* SFB-1 was originally provided the epitaph of *Denitromonas halophilus* SFB-1 but the ANI between both species falls below the cutoff of 95%[290], resulting in homonymy. *Denitromonas ohloneium* SFB-1 is a facultatively aerobic organoheterotroph isolated from an intertidal mudflat in the San Francisco Bay near Berkeley, CA. It grows by oxidizing lactate or acetate with

concomitant reduction of oxygen (O_2), nitrate (NO_3^-), or perchlorate (ClO_4^-) in a defined marine medium at 3% salinity at a pH of 7.2. Alternatively, it grows in a defined marine medium at a salinity of 1% NaCl, pH of 7.2, and temperature of 30°C. On R2A it forms small smooth white colonies after 48-72 hours. *D. ohloneium* possesses all the genes necessary for denitrification and assimilatory nitrate reduction to ammonia (NarGHI, NapAB, NirK, NorBC, and NosZ).

The genome of *D. ohloneium* is 4,416,963 bp (average coverage of 129.6x) with 4,121 CDS with 4,111 coding for proteins. Its G+C content is 64.05% and has no CRISPR array or plasmid DNA. The complete genome has been deposited in GenBank (accession number: GCA_007625205.1), consisting of 40 contigs. The species has two strains, the type strain *Denitromonas ohloneium* SFB-1^T and SFB-2. The type strain has been deposited in the American Type Culture Collection (TSD-271).

A.5 Figures and Tables

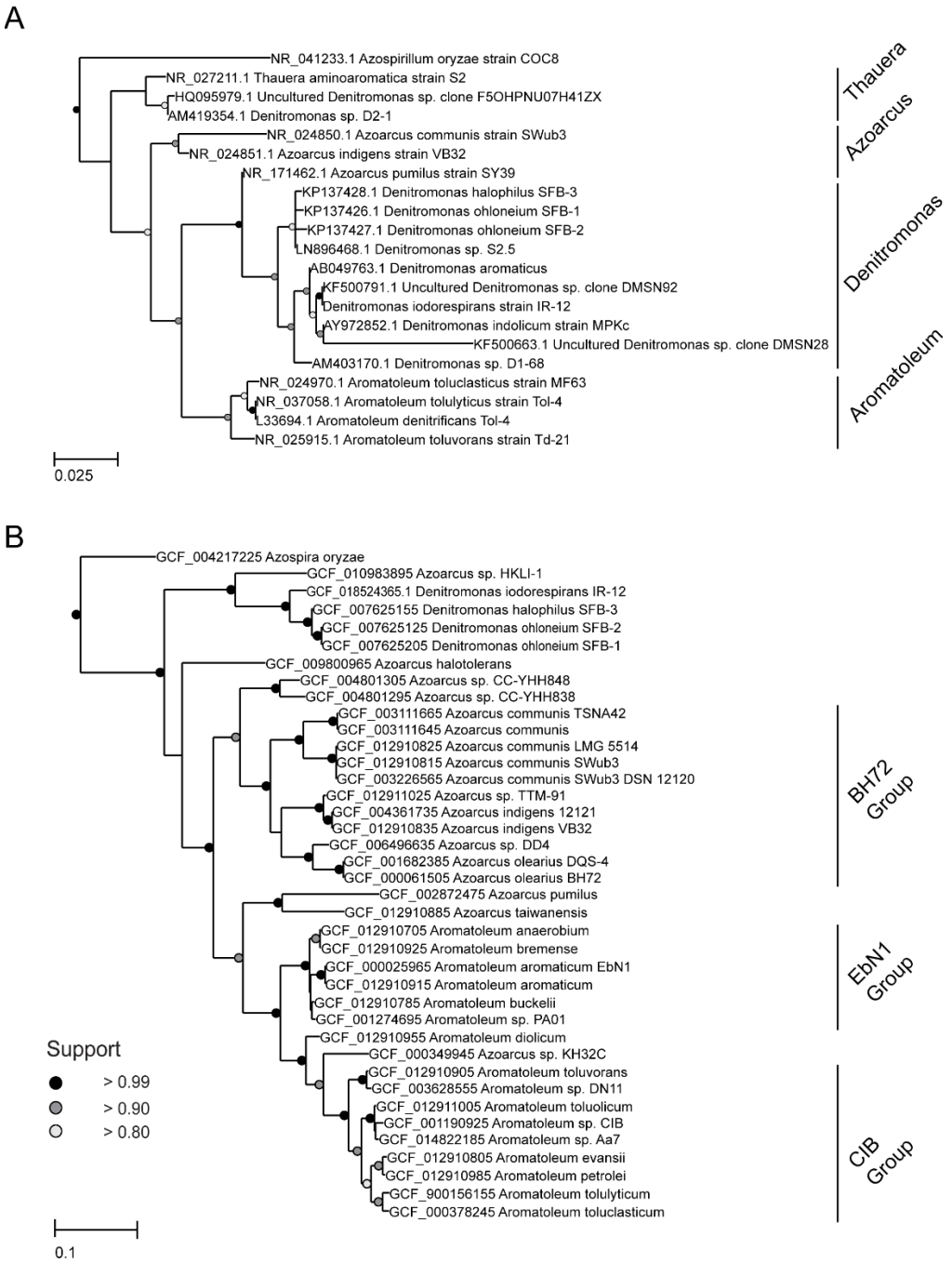

FIGURE A.1: 16S AND RIBOSOMAL PROTEIN PHYLOGENY. The 16S phylogeny (A) and RpS/RpL phylogeny (B) of several *Zoogloeaceae* are summarized. *Denitromonas* forms a monophyletic clade in the poorly defined paraphyletic *Azoarcus* group. Support values are signified by the color at each bifurcation.

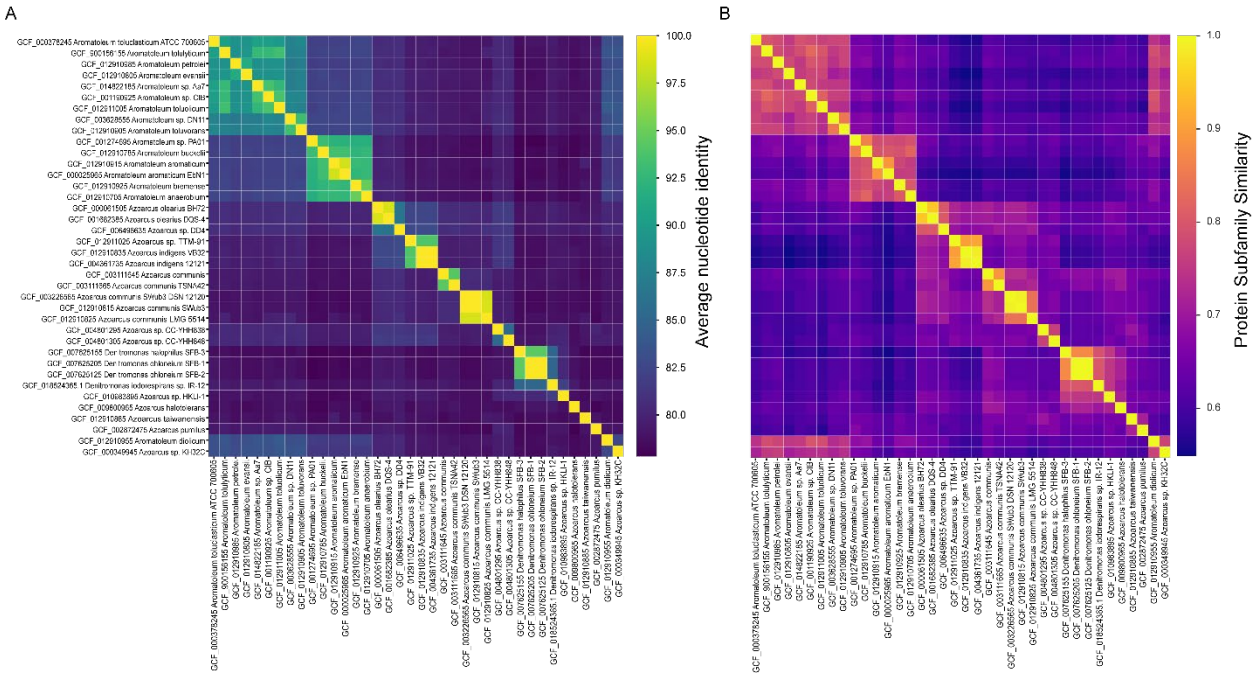

FIGURE A.2: AVERAGE NUCLEOTIDE IDENTITY AND PROTEIN SUBFAMILIY SIMILARITY. A) The pairwise average nucleotide identity for each organism in the family *Zoogloeaceae* ordered by pairwise similarity. Average nucleotide identity represented as a percentage. B) Protein clusters for each genome were represented as a presence and absence matrix (Figure A.4) and a pairwise comparison of each genome was performed using the Jaccard similarity index. Scores of 1.0 represents an identical set of protein subfamilies between any two given genomes.

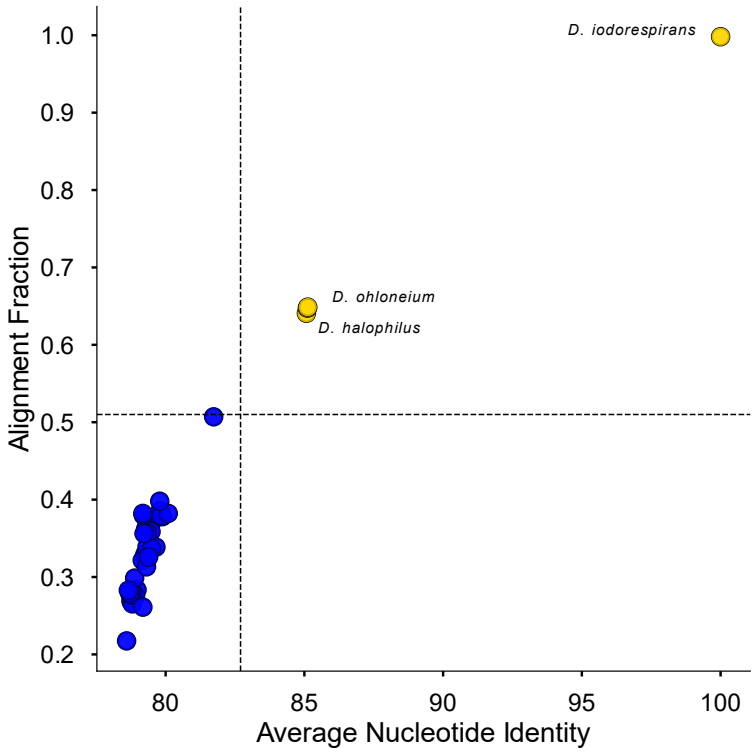

FIGURE A.3: ALIGNMENT FRACTION VS. AVERAGE NUCLEOTIDE IDENTITY. The alignment fraction plotted against the average nucleotide identity is shown above. *Denitromonas iodorespirans* is used as the reference strain. Yellow data points demonstrate the isolates that are confidently (Wilcoxon $p \leq 0.05$) classified as *Denitromonas* whereas points in blue demonstrate related organisms that are significantly different from the type species. Significance is demonstrated by the dotted black lines where only strains in the top right quadrant are considered to belong the same genus. Distinction between *D. ohloneium* SFB-1 and SFB-2 not visible due to high similarity between genomes.

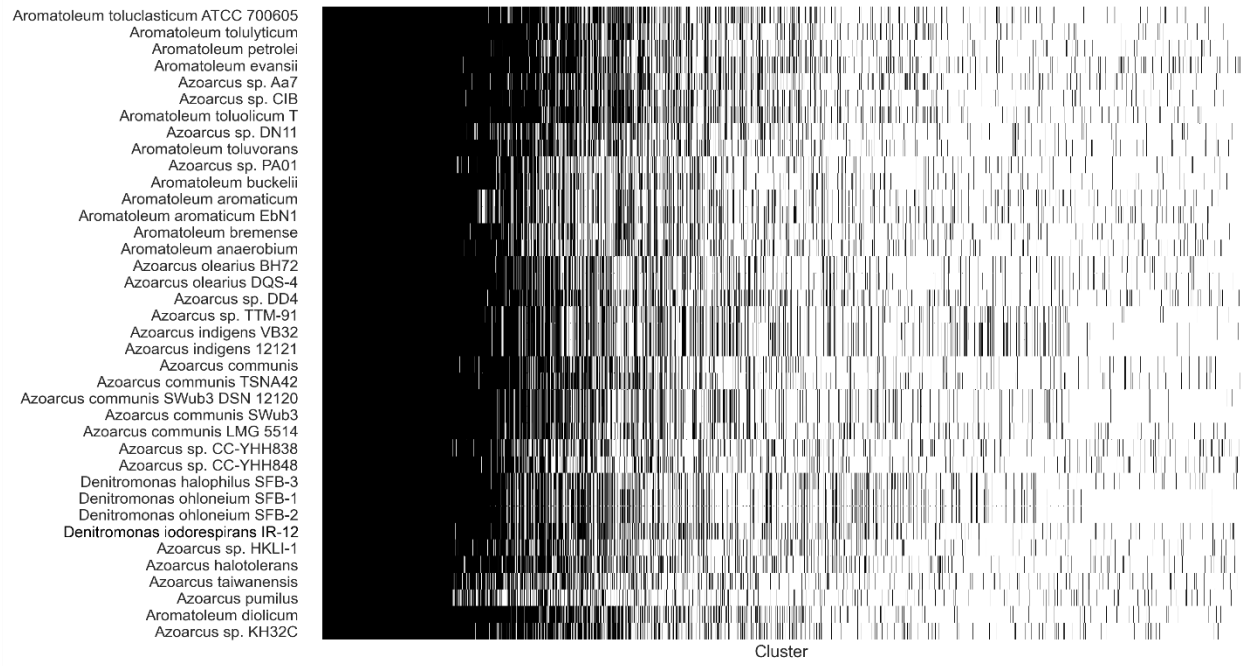

FIGURE A.4: PRESENCE AND ABSENCE OF CONSERVED PROTEINS. Proteins from all genomes were clustered using the MMSeqs2 algorithm and displayed as a presence and absence matrix.

TABLE A.1: 16S SEQUENCES OF DENITROMONAS ISOLATES FROM NCBI.

Name	Location	Associated Metabolism	Accession
Denitromonas sp. S2.5	Kalo Vig (sediment)	Nitrate-reducing Fe (II)oxidizer	LN896468.1
Denitromonas sp. D2-1	marine aquaculture	Nitrate-reducing	AM403171.1
Denitromonas sp. D12-45.1	marine aquaculture	Nitrate-reducing	AM403240.1
Denitromonas sp. XBIO-NKHA1	oil brine	n.d.	MT441915.1
Denitromonas sp. D1-68	marine aquaculture	Nitrate-reducing	AM403170.1
Denitromonas sp. 37	Wastewater treatment	n.d	DQ104209.1
Denitromonas indolicum strain MPKc 16S	Inner Deep Bay (Hong Kong, Sediment)	2-methylindole oxidation[132]	AY972852.1
Denitromonas aromaticus	Activated sludge	n.d.	AB049763.1
Uncultured Denitromonas sp. clone strain ARF21	Air Cathode Microbial Fuel Cell Reactor (saline)[12]	n.d.	MN880253.1
Uncultured Denitromonas sp. isolate endo43	Date palm endophyte	n.d.	KU579242.1
Uncultured Denitromonas sp. clone SA13	Sludge	n.d.	KJ572425.1
Uncultured Denitromonas sp. clone SA58	Sludge	n.d.	KJ572454.1
Uncultured Denitromonas sp. clone SA62	Sludge	n.d.	KJ572459.1
Uncultured Denitromonas sp. clone SA70	Sludge	n.d.	KJ572466.1
Uncultured Denitromonas sp.	Microbial Fuel Cell Having Carbon Nanotube Anodes[13]	n.d.	KJ411935.1
Uncultured Denitromonas sp. clone SPU:DMJS40	activated sludge	n.d.	KF500624
Uncultured Denitromonas sp. clone SPU:DMJS62	activated sludge	n.d.	KF500643.1
Uncultured Denitromonas sp. clone SPU:DMJS65	activated sludge	n.d.	KF500645.1

Uncultured Denitromonas sp. clone DMSN28	activated sludge	n.d.	KF500663.1
Uncultured Denitromonas sp. clone SPU:DMSN194	activated sludge	n.d.	KF500887.1
Uncultured Denitromonas sp. clone F5OHPNU07HZJ1B	Gypsum-Treated Oil Sands Tailings Pond	n.d.	HQ067056.1
Uncultured Denitromonas sp. clone F5OHPNU07IF648	Gypsum-Treated Oil Sands Tailings Pond	n.d.	HQ095246.1
Uncultured Denitromonas sp. clone F5OHPNU07H41ZX	Gypsum-Treated Oil Sands Tailings Pond	n.d.	HQ095979.1
Uncultured Denitromonas sp. isolate DGGE gel band 3alfa	Fish canning effluent	n.d.	HQ184392.1
Uncultured Denitromonas sp. isolate DGGE gel band 3beta 16S	Fish canning effluent	n.d.	HQ184393.1

TABLE A.2: METABOLIC PROFILES OF DENITROMONAS SPECIES. + dictates ability to utilize substrate, - dictates an inability to utilize substrate.

	Denitromonas iodorespirans IR-12	*Denitromonas ohlonieum SFB-1*	*Denitromonas halophilus SFB-3*
Physical Characteristics			
Temperature (Range)	14°C - 37°C	14°C - 30°C	14°C - 30°C
pH (Range)	6.8-8.2	6.8-8.2	6.8-8.2
pH (Optimum)	7.2	7.2	7.2
Salinity (Range)	0-5%	0-3%	0-5%
Salinity Optimum	1-3%	1-3%	1-3%
Length (μM)	1.5-2.0	1.0-1.5	1.5-2.0
Width (μM)	0.5-1.0	0.5-1.0	0.5-1.0
Motile	+	+	+
Enzymatic Activity (72 Hours)			
Glucose Fermentation	-	-	-
Indole Production	-	-	-
Arginine Dihydrolase	+	-	+
Urease	+	+	+
Esculin hydrolysis	+	+	+
Gelatin Hydrolysis	-	-	-
beta-galactosidase activity	-	-	-
Carbon Assimilation (48 Hours)			
Acetate (10 mM)	+	+	+
Lactate (10 mM)	+	+	+
Glucose (5 mM)	-	-	-
Succinate (10 mM)	+	+	+
Butyrate (5 mM)	+	+	+
Malate (10 mM)	-	-	-
Glycerol (10 mM)	-	-	-
Formate (10 mM)	-	-	-
Fumarate (10 mM)	+	+	+
Yeast Extract (1%)	+	+	-
Pyruvate (10 mM)	+	+	+
Propionate (10 mM)	+	+	+
Terminal Electron Acceptor Usage			
Oxygen	+	+	+
Nitrate	+	+	+
Perchlorate	-	+	+
Chlorate	-	+	+
Iodate	+	-	-

References

1 Carpenter, L. J. in *Encyclopedia of Atmospheric Sciences* 205-219 (Elsevier, 2015).

2 Chemburkar, S. R., Deming, K. C. & Reddy, R. E. Chemistry of thyroxine: an historical perspective and recent progress on its synthesis. *Tetrahedron* **66**, 1955-1962, doi:10.1016/J.TET.2009.12.044 (2010).

3 Schweizer, U. & Steegborn, C. Thyroid hormones—from crystal packing to activity to reactivity. *Angewandte Chemie International Edition* **54**, 12856-12858, doi:10.1002/anie.201506919 (2015).

4 Rosenfeld, L. Discovery and Early Uses of Iodine. *Journal of Chemical Education* **77**, 984, doi:10.1021/ed077p984 (2000).

5 Swain, P. A. Bernard Courtois (1777-1838) famed for discovering iodine (1811) and his life in Paris from 1798. *Bull. Hist. Chem* **30**, 103 (2005).

6 Kelly, F. C. (SAGE Publications, 1961).

7 Loriaux, D. 100-104 (2016).

8 Organization, W. H. Goitre as a determinant of the prevalence and severity of iodine deficiency disorders in populations. (World Health Organization, 2014).

9 I-131 Exposure, I. o. M. C. o. T. S. R. t. & Tests, N. R. C. C. o. E. o. t. A. P. t. I. f. t. N. A. B. *Health Risks of I-131 Exposure*. (National Academies Press (US), 1999).

10 Zhang, S. *et al.* Iodine-129 and Iodine-127 speciation in groundwater at the Hanford site, US: iodate incorporation into calcite. *Environmental science & technology* **47**, 9635-9642 (2013).

11 Hu, Q., Zhao, P., Moran, J. E. & Seaman, J. C. Sorption and transport of iodine species in sediments from the Savannah River and Hanford Sites. *Journal of Contaminant Hydrology* **78**, 185-205 (2005).

12 Lebel, L. S., Dickson, R. S. & Glowa, G. A. Radioiodine in the atmosphere after the Fukushima Dai-ichi nuclear accident. *Journal of Environmental Radioactivity* **151**, 82-93, doi:10.1016/j.jenvrad.2015.06.001 (2016).

13 O'Dowd, C. D. *et al.* Marine aerosol formation from biogenic iodine emissions. *Nature* **417**, 632-636, doi:10.1038/nature00775 (2002).

14 Burkholder, J., Curtius, J., Ravishankara, A. & Lovejoy, E. Laboratory studies of the homogeneous nucleation of iodine oxides. (2004).

15 Cuevas, C. A. *et al.* Rapid increase in atmospheric iodine levels in the North Atlantic since the mid-20th century. *Nature Communications* **9**, 1452, doi:10.1038/s41467-018-03756-1 (2018).

16 Wang, S. *et al.* Active and widespread halogen chemistry in the tropical and subtropical free troposphere. *Proceedings of the National Academy of Sciences of the United States of America* **112**, 9281-9286, doi:10.1073/pnas.1505142112 (2015).

17 Stevenson, D. S. *et al.* Evolution of tropospheric ozone radiative forcing. *Geophysical Research Letters* **25**, 3819-3822, doi:10.1029/1998GL900037 (1998).

18 Li, D., Kaplan, D. I., Knox, A. S., Crapse, K. P. & Diprete, D. P. Aqueous 99Tc, 129I and 137Cs removal from contaminated groundwater and sediments using highly effective low-cost sorbents. *Journal of Environmental Radioactivity* **136**, 56-63, doi:10.1016/j.jenvrad.2014.05.010 (2014).

19 Yu. Khazov, I. M., A. Rodionov. Decay Radiation Results (I131). *Nuclear Data Sheets* **107**, 2715 (2006).

20 Baverstock, K., Blomqvist, L., Klein, G., Paile, W., Repacholi, M., Helmer, R. (ed Protection of the Human Environment) (1999).

21 Timar, J., Elekes, Z., Singh, B. Decay Radiation Results (I129). *Nuclear Data Sheets* **121**, 143 (2014).

22 Rao, U. & Fehn, U. Sources and reservoirs of anthropogenic iodine-129 in western New York. *Geochimica et Cosmochimica Acta* **63**, 1927-1938, doi:10.1016/S0016-7037(99)00133-7 (1999).

23 Köhler, F. *et al.* Sorption of iodine in soils: insight from selective sequential extractions and X-ray absorption spectroscopy. *Environ Sci Pollut Res* **26**, 23850-23860, doi:10.1007/s11356-019-05623-y (2019).

24 Tsunogai, S. & Sase, T. Formation of iodide-iodine in the ocean. *Deep Sea Research and Oceanographic Abstracts* **16**, 489-496, doi:10.1016/0011-7471(69)90037-0 (1969).
25 Kupper, F. C. *et al.* Iodide accumulation provides kelp with an inorganic antioxidant impacting atmospheric chemistry. *Proceedings of the National Academy of Sciences* **105**, 6954-6958, doi:10.1073/pnas.0709959105 (2008).
26 Johnson, C. C. a. F., F.M. (ed British Geological Survey) (2003).
27 Blanchard, D. & Woodcock, A. Bubble formation and modification in the sea and its meteorological significance. *Tellus* **9**, 145-158 (1957).
28 Woodcock, A. H. Salt nuclei in marine air as a function of altitude and wind force. *J. Meteor.* **10**, 362-371, doi:10.1175/1520-0469(1953)010<0366:SNIMAA>2.0.CO;2 (1953).
29 Miyake, Y. & Tsunogai, S. Evaporation of iodine from the ocean. *Journal of Geophysical Research (1896-1977)*, 3989-3993, doi:10.1029/JZ068i013p03989@10.1002/(ISSN)2156-2202.TGNARA1 (2012).
30 Komabayasi, M. Enrichment of Inorganic Ions with Increasing Atomic Weight in Aerosol, Rainwater and Snow in Comparison with Sea Water. *Journal of the Meteorological Society of Japan. Ser. II* **40**, 25-38, doi:10.2151/jmsj1923.40.1_25 (1962).
31 Moyers, J. L. & Duce, R. A. Gaseous and particulate iodine in the marine atmosphere. *Journal of Geophysical Research (1896-1977)* **77**, 5229-5238, doi:10.1029/JC077i027p05229 (1972).
32 Read, K. A. *et al.* Extensive halogen-mediated ozone destruction over the tropical Atlantic Ocean. *Nature* **453**, 1232-1235, doi:10.1038/nature07035 (2008).
33 MacDonald, S. M. *et al.* A laboratory characterisation of inorganic iodine emissions from the sea surface: dependence on oceanic variables and parameterisation for global modelling. *Atmos. Chem. Phys.* **14**, 5841-5852, doi:10.5194/acp-14-5841-2014 (2014).
34 Lovelock, J. E. Natural halocarbons in the air and in the sea. *Nature* **256**, 193-194, doi:10.1038/256193a0 (1975).
35 Manley, S. L. & Dastoor, M. N. Methyl iodide (CH3I) production by kelp and associated microbes. *Marine Biology* **98**, 477-482, doi:10.1007/BF00391538 (1988).
36 Winter, J. M. & Moore, B. S. Exploring the chemistry and biology of vanadium-dependent haloperoxidases. *The Journal of biological chemistry* **284**, 18577-18581, doi:10.1074/jbc.R109.001602 (2009).
37 Carpenter, L. J., Malin, G., Liss, P. S. & Küpper, F. C. Novel biogenic iodine-containing trihalomethanes and other short-lived halocarbons in the coastal east Atlantic. *Global Biogeochemical Cycles* **14**, 1191-1204, doi:10.1029/2000GB001257 (2000).
38 Gonzales, J., Tymon, T., Küpper, F. C., Edwards, M. S. & Carrano, C. J. The potential role of kelp forests on iodine speciation in coastal seawater. *PLOS ONE* **12**, e0180755, doi:10.1371/journal.pone.0180755 (2017).
39 Pillar, E. A., Guzman, M. I., Rodriguez, J. M., Pillar, E. A. & Guzman, M. I. Conversion of Iodide to Hypoiodous Acid and Iodine in Aqueous Microdroplets Exposed to Ozone Repository Citation Conversion of Iodide to Hypoiodous Acid and Iodine in Aqueous Microdroplets Exposed to Ozone Notes/Citation Information Conversion of Iodide to Hypoiodous Acid and Iodine in Aqueous Microdroplets Exposed to Ozone. *Part of the Analytical Chemistry Commons Environmental Chemistry Commons Environmental Sciences Commons Inorganic Chemistry Commons, and the Physical Chemistry Commons Published in Environmental Science & Technology* **47**, 10971-10979 (2013).
40 Wang, S. *et al.* Active and widespread halogen chemistry in the tropical and subtropical free troposphere. *Proceedings of the National Academy of Sciences of the United States of America* **112**, 9281-9286, doi:10.1073/pnas.1505142112 (2015).
41 Cuevas, C. A. *et al.* Rapid increase in atmospheric iodine levels in the North Atlantic since the mid-20th century. *Nature Communications* **9**, 1452, doi:10.1038/s41467-018-03756-1 (2018).

42 Luther, G. W., Wu, J. & Cullen, J. B. Redox Chemistry of Iodine in Seawater Frontier Molecular Orbital Theory Considerations. *Aquatic Chemistry Advances in Chemistry*, doi:10.1021/ba-1995-0244.ch006 (1995).
43 Tsunogai, S. & Henmi, T. Iodine in the surface water of the ocean. *Journal of the Oceanographical Society of Japan* **27**, 67-72, doi:10.1007/BF02109332 (1971).
44 Campos, M. L. A. M., Farrenkopf, A. M., Jickells, T. D. & Luther, G. W. A comparison of dissolved iodine cycling at the Bermuda Atlantic Time-series Station and Hawaii Ocean Time-series Station. *Deep Sea Research Part II: Topical Studies in Oceanography* **43**, 455-466, doi:10.1016/0967-0645(95)00100-X (1996).
45 Elderfield, H. & Truesdale, V. W. On the biophilic nature of iodine in seawater. *Earth and Planetary Science Letters* **50**, 105-114, doi:10.1016/0012-821X(80)90122-3 (1980).
46 Jickells, T. D., Boyd, S. S. & Knap, A. H. Iodine Cycling in the Sargasso Sea and the Bermuda Inshore Waters. *Marine Chemistry Elsevier Science Publishers B.V* **24**, 61-82 (1988).
47 Nakayama, E., Kimoto, T., Isshiki, K., Sohrin, Y. & Okazaki, S. Determination and distribution of iodide- and total-iodine in the North Pacific Ocean - by using a new automated electrochemical method. *Marine Chemistry* **27**, 105-116, doi:10.1016/0304-4203(89)90030-3 (1989).
48 Kennedy, H. A. & Elderfield, H. Iodine diagenesis in pelagic deep-sea sediments. *Geochimica et Cosmochimica Acta* **51**, 2489-2504, doi:10.1016/0016-7037(87)90300-0 (1987).
49 Truesdale, V. W. The biogeochemical effect of seaweeds upon close-to natural concentrations of dissolved iodate and iodide in seawater – Preliminary study with Laminaria digitata and Fucus serratus. *Estuarine, Coastal and Shelf Science* **78**, 155-165, doi:10.1016/J.ECSS.2007.11.022 (2008).
50 Lage, O. M. & Graça, A. P. in *Algae - Organisms for Imminent Biotechnology* (InTech, 2016).
51 Wong, G. T. The marine geochemistry of iodine. *Rev. Aquat. Sci.* **4**, 45-73 (1991).
52 Tian, R. *et al.* Iodine speciation: a potential indicator to evaluate new production versus regenerated production. *Deep Sea Research Part I: Oceanographic Research Papers* **43**, 723-738 (1996).
53 Tian, R. & Nicolas, E. Iodine speciation in the northwestern Mediterranean Sea, method and vertical profile. *Marine Chemistry* **48**, 151-156 (1995).
54 Farrenkopf, A. M., Luther, G. W., Truesdale, V. W. & Van Der Weijden, C. H. Sub-surface iodide maxima: evidence for biologically catalyzed redox cycling in Arabian Sea OMZ during the SW intermonsoon. *Deep Sea Research Part II: Topical Studies in Oceanography* **44**, 1391-1409, doi:https://doi.org/10.1016/S0967-0645(97)00013-1 (1997).
55 Farrenkopf Ay, A. M. *et al.* Reduction of iodate in seawater during Arabian Sea incubations and in laboratory cultures of the marine Shewanella putrefaciens strain MR-4 shipboard bacterium. *Marine Chemistry* **57**, 347-354 (1997).
56 Councell, T. B., Landa, E. R. & Lovley, D. R. MICROBIAL REDUCTION OF IODATE.
57 Chance, R., Malin, G., Jickells, T. & Baker, A. R. Reduction of iodate to iodide by cold water diatom cultures. *Marine Chemistry* **105**, 169-180, doi:10.1016/j.marchem.2006.06.008 (2007).
58 Waite, T. J. & Truesdale, V. W. Iodate reduction by Isochrysis galbana is relatively insensitive to de-activation of nitrate reductase activity—are phytoplankton really responsible for iodate reduction in seawater? *Marine Chemistry* **81**, 137-148, doi:10.1016/S0304-4203(03)00013-6 (2003).
59 Wong, G. T., Piumsomboon, A. U. & Dunstan, W. M. The transformation of iodate to iodide in marine phytoplankton cultures. *Marine Ecology Progress Series* **237**, 27-39 (2002).
60 Youngblut, M. D. *et al.* Perchlorate Reductase Is Distinguished by Active Site Aromatic Gate Residues. *The Journal of biological chemistry* **291**, 9190-9202, doi:10.1074/jbc.M116.714618 (2016).
61 Küpper, F. *et al.* Iodine uptake in Laminariales involves extracellular, haloperoxidase-mediated oxidation of iodide. *Planta* **207**, 163-171 (1998).

62 de laCuesta, J. L. & Manley, S. L. Iodine assimilation by marine diatoms and other phytoplankton in nitrate-replete conditions. *Limnology and oceanography* **54**, 1653-1664 (2009).
63 Gozlan, R. & Margalith, P. Iodide oxidation by a marine bacterium. *Journal of Applied Bacteriology* **36**, 407-417 (1973).
64 Suzuki, M. *et al.* Iodide oxidation by a novel multicopper oxidase from the alphaproteobacterium strain Q-1. *Applied and environmental microbiology* **78**, 3941-3949 (2012).
65 Amachi, S. *et al.* Isolation of iodide-oxidizing bacteria from iodide-rich natural gas brines and seawaters. *Microbial ecology* **49**, 547-557 (2005).
66 Morrison, M. & Bayse, G. S. Catalysis of iodination by lactoperoxidase. *Biochemistry* **9**, 2995-3000 (1970).
67 Taurog, A. in *Proceedings of the 1969 Laurentian Hormone Conference* Vol. 26 (ed E. B. Astwood) 189-247 (Academic Press, 1970).
68 Chasteen, N. D. Vanadium in biological systems. *Physiology and Biochemistry*, 225 (1990).
69 Vilter, H., Glombitza, K.-W. & Grawe, A. Peroxidases from Phaeophyceae. I: Extraction and detection of the peroxidases. *Botanica Marina* **26**, 331-340 (1983).
70 Vilter, H. Peroxidases from phaeophyceae: A vanadium(V)-dependent peroxidase from Ascophyllum nodosum. *Phytochemistry* **23**, 1387-1390, doi:https://doi.org/10.1016/S0031-9422(00)80471-9 (1984).
71 Kimblin, C., Bu, X. & Butler, A. Modeling the Catalytic Site of Vanadium Bromoperoxidase: Synthesis and Structural Characterization of Intramolecularly H-bonded Vanadium(V) Oxoperoxo Complexes, [VO(O2)(NH2pyg2)]K and [VO(O2)(BrNH2pyg2)]K. *Inorganic Chemistry* **41**, 161-163, doi:10.1021/ic010892j (2002).
72 de Boer, E., van Kooyk, Y., Tromp, M. G. M., Plat, H. & Wever, R. Bromoperoxidase from Ascophyllum nodosum: a novel class of enzymes containing vanadium as a prosthetic group? *Biochimica et Biophysica Acta (BBA) - Protein Structure and Molecular Enzymology* **869**, 48-53, doi:https://doi.org/10.1016/0167-4838(86)90308-0 (1986).
73 Ohshiro, T., Nakano, S., Takahashi, Y., Suzuki, M. & Izumi, Y. Occurrence of bromoperoxidase in the marine green macro-alga, ulvella lens, and emission of volatile brominated methane by the enzyme. *Phytochemistry* **52**, 1211-1215, doi:https://doi.org/10.1016/S0031-9422(99)00404-5 (1999).
74 Krenn, B. E., Plat, H. & Wever, R. The bromoperoxidase from the red alga Ceramium rubrum also contains vanadium as a prosthetic group. *Biochimica et Biophysica Acta (BBA) - Protein Structure and Molecular Enzymology* **912**, 287-291, doi:https://doi.org/10.1016/0167-4838(87)90100-2 (1987).
75 Plat, H., Krenn, B. E. & Wever, R. The bromoperoxidase from the lichen Xanthoria parietina is a novel vanadium enzyme. *Biochemical Journal* **248**, 277-279, doi:10.1042/bj2480277 (1987).
76 Butler, A. Vanadium haloperoxidases. *Current Opinion in Chemical Biology* **2**, 279-285, doi:https://doi.org/10.1016/S1367-5931(98)80070-7 (1998).
77 Tschirret-Guth, R. A. & Butler, A. Evidence for organic substrate binding to vanadium bromoperoxidase. *Journal of the American Chemical Society* **116**, 411-412 (1994).
78 Gozlan, R. & Margalith, P. Iodide oxidation by Pseudomonas iodooxidans. *Journal of Applied Bacteriology* **37**, 493-499 (1974).
79 Yuliana, T., Ebihara, K., Suzuki, M., Shimonaka, C. & Amachi, S. A novel enzyme-based antimicrobial system comprising iodide and a multicopper oxidase isolated from Alphaproteobacterium strain Q-1. *Applied Microbiology and Biotechnology* **99**, 10011-10018, doi:10.1007/s00253-015-6862-0 (2015).
80 Shiroyama, K., Kawasaki, Y., Unno, Y. & Amachi, S. A putative multicopper oxidase, IoxA, is involved in iodide oxidation by Roseovarius sp. strain A-2. *Bioscience, Biotechnology, and Biochemistry* **79**, 1898-1905, doi:10.1080/09168451.2015.1052767 (2015).
81 Li, H.-P. *et al.* Bacterial production of organic acids enhances H2O2-dependent iodide oxidation. *Environmental Science & Technology* **46**, 4837-4844, doi:10.1021/es203683v (2012).

82 Hughes, C. *et al.* Oxidation of iodide to iodate by cultures of marine ammonia-oxidising bacteria. *Marine Chemistry* **234**, 104000, doi:https://doi.org/10.1016/j.marchem.2021.104000 (2021).
83 Truesdale, V. W. Iodine in inshore and off-shore marine waters. *Marine Chemistry* **6**, 1-13, doi:https://doi.org/10.1016/0304-4203(78)90002-6 (1978).
84 George, T. F. W., Ajcharaporn, U. P. & William, M. D. The transformation of iodate to iodide in marine phytoplankton cultures. *Marine Ecology Progress Series* **237**, 27-39 (2002).
85 Hepach, H., Hughes, C., Hogg, K., Collings, S. & Chance, R. Senescence as the main driver of iodide release from a diverse range of marine phytoplankton. *Biogeosciences* **17** (2020).
86 Bluhm, K., Croot, P., Wuttig, K. & Lochte, K. Transformation of iodate to iodide in marine phytoplankton driven by cell senescence. *Aquatic Biology* **11**, 1-15 (2010).
87 Chance, R. *et al.* Seasonal and interannual variation of dissolved iodine speciation at a coastal Antarctic site. *Marine Chemistry* **118**, 171-181, doi:https://doi.org/10.1016/j.marchem.2009.11.009 (2010).
88 Jia-Zhong, Z. & Whitfield, M. Kinetics of inorganic redox reactions in seawater: I. The reduction of iodate by bisulphide. *Marine Chemistry* **19**, 121-137 (1986).
89 Mackin, J. E., Aller, R. C. & Ullman, W. J. The effects of iron reduction and nonsteady-state diagenesis on iodine, ammonium, and boron distributions in sediments from the Amazon continental shelf. *Continental Shelf Research* **8**, 363-386, doi:https://doi.org/10.1016/0278-4343(88)90009-X (1988).
90 Coleman, M. L., Hedrick, D. B., Lovley, D. R., White, D. C. & Pye, K. Reduction of Fe (III) in sediments by sulphate-reducing bacteria. *Nature* **361**, 436-438 (1993).
91 Mok, J. K. *et al.* Iodate Reduction by Shewanella oneidensis Does Not Involve Nitrate Reductase. *Geomicrobiology Journal*, 1-10, doi:10.1080/01490451.2018.1430189 (2018).
92 Toporek, Y. J. *et al.* Metal Reduction and Protein Secretion Genes Required for Iodate Reduction by Shewanella oneidensis. *Appl Environ Microbiol* **85**, doi:10.1128/aem.02115-18 (2019).
93 Schuetz, B., Schicklberger, M., Kuermann, J., Spormann, A. M. & Gescher, J. Periplasmic electron transfer via the c-type cytochromes MtrA and FccA of Shewanella oneidensis MR-1. *Applied and environmental microbiology* **75**, 7789-7796, doi:10.1128/AEM.01834-09 (2009).
94 McEwan, A. G., Ridge, J. P., McDevitt, C. A. & Hugenholtz, P. The DMSO Reductase Family of Microbial Molybdenum Enzymes; Molecular Properties and Role in the Dissimilatory Reduction of Toxic Elements. *Geomicrobiology Journal* **19**, 3-21, doi:10.1080/014904502317246138 (2002).
95 Youngblut, M. D. *et al.* Perchlorate Reductase Is Distinguished by Active Site Aromatic Gate Residues. *The Journal of biological chemistry* **291**, 9190-9202, doi:10.1074/jbc.M116.714618 (2016).
96 Tsunogai, S. & Sase, T. Formation of iodide-iodine in the ocean. *Deep Sea Research and Oceanographic Abstracts* **16**, 489-496, doi:10.1016/0011-7471(69)90037-0 (1969).
97 Zehr, J. P. & Ward, B. B. Nitrogen Cycling in the Ocean: New Perspectives on Processes and Paradigms. *Applied and Environmental Microbiology* **68**, 1015-1024, doi:10.1128/aem.68.3.1015-1024.2002 (2002).
98 Lee, B. D. *et al.* Iodate and nitrate transformation by Agrobacterium/Rhizobium related strain DVZ35 isolated from contaminated Hanford groundwater. *Journal of Hazardous Materials* **350**, 19-26, doi:https://doi.org/10.1016/j.jhazmat.2018.02.006 (2018).
99 Morpeth, F. F. & Boxer, D. H. Kinetic analysis of respiratory nitrate reductase from Escherichia coli K12. *Biochemistry* **24**, 40-46, doi:10.1021/bi00322a007 (1985).
100 Kengen, S. W. M., Rikken, G. B., Hagen, W. R., van Ginkel, C. G. & Stams, A. J. M. Purification and Characterization of (Per)Chlorate Reductase from the Chlorate-Respiring Strain GR-1. *Journal of Bacteriology* **181**, 6706-6711, doi:10.1128/jb.181.21.6706-6711.1999 (1999).
101 Tan, Z. & Reinhold-Hurek, B. Dechlorosoma suillum Achenbach et al. 2001 is a later subjective synonym of Azospira oryzae Reinhold-Hurek and Hurek 2000. *Int J Syst Evol Microbiol* **53**, 1139-1142, doi:10.1099/ijs.0.02606-0 (2003).

102 Wang, O. *et al.* Functional redundancy in perchlorate and nitrate electron transport chains and rewiring respiratory pathways to alter terminal electron acceptor preference. *Frontiers in microbiology* **9**, 376 (2018).
103 Amachi, S. *et al.* Dissimilatory iodate reduction by marine Pseudomonas sp. strain SCT. *Applied and environmental microbiology* **73**, 5725-5730, doi:10.1128/AEM.00241-07 (2007).
104 Amachi, S. *et al.* Dissimilatory iodate reduction by marine Pseudomonas sp. strain SCT. *Applied and environmental microbiology* **73**, 5725-5730, doi:10.1128/AEM.00241-07 (2007).
105 Carpenter, L. J. in *Encyclopedia of Atmospheric Sciences* 205-219 (Elsevier, 2015).
106 Chemburkar, S. R., Deming, K. C. & Reddy, R. E. Chemistry of thyroxine: an historical perspective and recent progress on its synthesis. *Tetrahedron* **66**, 1955-1962, doi:10.1016/J.TET.2009.12.044 (2010).
107 Küpper, F. C. *et al.* Commemorating two centuries of iodine research: an interdisciplinary overview of current research. *Angewandte Chemie International Edition* **50**, 11598-11620, doi:10.1002/anie.201100028 (2011).
108 Manley, S. L. & Dastoor, M. N. Methyl iodide (CH3I) production by kelp and associated microbes. *Marine Biology* **98**, 477-482, doi:10.1007/BF00391538 (1988).
109 Luther, G. W., Wu, J. & Cullen, J. B. in *Aquatic Chemistry* Vol. 244 *Advances in Chemistry* Ch. 6, 135-155 (American Chemical Society, 1995).
110 Gonzales, J., Tymon, T., Küpper, F. C., Edwards, M. S. & Carrano, C. J. The potential role of kelp forests on iodine speciation in coastal seawater. *PLoS One* **12**, e0180755, doi:10.1371/journal.pone.0180755 (2017).
111 Vedamati, J., Goepfert, T. & Moffett, J. W. Iron speciation in the eastern tropical South Pacific oxygen minimum zone off Peru. *Limnology and Oceanography* **59**, 1945-1957, doi:https://doi.org/10.4319/lo.2014.59.6.1945 (2014).
112 Councell, T. B., Landa, E. R. & Lovley, D. R. Microbial reduction of iodate. *Water, Air, and Soil Pollution* **100**, 99-106 (1997).
113 Youngblut, M. D. *et al.* Perchlorate reductase is distinguished by active site aromatic gate residues. *Journal of Biological Chemistry* **291**, 9190-9202, doi:10.1074/jbc.M116.714618 (2016).
114 Farrenkopf, A. M., Dollhopf, M. E., Chadhain, S. N., Luther, G. W. & Nealson, K. H. Reduction of iodate in seawater during Arabian Sea incubations and in laboratory cultures of the marine Shewanella putrefaciens strain MR-4 shipboard bacterium. *Marine Chemistry* **57**, 347-354 (1997).
115 Yamazaki, C. *et al.* A novel dimethylsulfoxide reductase family of molybdenum enzyme, Idr, is involved in iodate respiration by Pseudomonas sp. SCT. *Environmental Microbiology* **22**, 2196-2212, doi:10.1111/1462-2920.14988 (2020).
116 Youngblut, M. D., Wang, O., Barnum, T. P. & Coates, J. D. (Per)chlorate in biology on earth and beyond. *Annual Review of Microbiology* **70**, 435-457, doi:10.1146/annurev-micro-102215-095406 (2016).
117 Toporek, Y. J. *et al.* Metal reduction and protein secretion genes required for iodate reduction by Shewanella oneidensis. *Applied Environmental Microbiology* **85**, doi:10.1128/aem.02115-18 (2019).
118 Carlström, C. I. *et al.* Characterization of an anaerobic marine microbial community exposed to combined fluxes of perchlorate and salinity. *Applied Microbiology and Biotechnology* **100**, 9719-9732, doi:10.1007/s00253-016-7780-5 (2016).
119 Brinkmann, T., Specht, C. H. & Frimmel, F. H. Non-linear calibration functions in ion chromatography with suppressed conductivity detection using hydroxide eluents. *Journal of Chromatography A* **957**, 99-109 (2002).
120 Bankevich, A. *et al.* SPAdes: a new genome assembly algorithm and its applications to single-cell sequencing. *J Comput Biol* **19**, 455-477, doi:10.1089/cmb.2012.0021 (2012).
121 Wick, R. R., Schultz, M. B., Zobel, J. & Holt, K. E. Bandage: interactive visualization of de novo genome assemblies. *Bioinformatics* **31**, 3350-3352, doi:10.1093/bioinformatics/btv383 (2015).

122 Seemann, T. Prokka: Rapid prokaryotic genome annotation. *Bioinformatics* **30**, 2068-2069, doi:10.1093/bioinformatics/btu153 (2014).
123 Steinegger, M. & Söding, J. MMseqs2 enables sensitive protein sequence searching for the analysis of massive data sets. *Nature Biotechnology* **35**, 1026-1028, doi:10.1038/nbt.3988 (2017).
124 Edgar, R. C. MUSCLE: Multiple sequence alignment with high accuracy and high throughput. *Nucleic acids research* **32**, 1792-1797, doi:10.1093/nar/gkh340 (2004).
125 Finn, R. D., Clements, J. & Eddy, S. R. HMMER web server: Interactive sequence similarity searching. *Nucleic Acids Res.* **39**, W29-W37, doi:10.1093/nar/gkr367 (2011).
126 Saunders, J. K., Fuchsman, C. A., McKay, C. & Rocap, G. Complete arsenic-based respiratory cycle in the marine microbial communities of pelagic oxygen-deficient zones. *Proceedings of the National Academy of Sciences, USA* **116**, 9925-9930, doi:10.1073/pnas.1818349116 (2019).
127 Price, M. N., Dehal, P. S. & Arkin, A. P. FastTree 2--approximately maximum-likelihood trees for large alignments. *PLoS One* **5**, e9490, doi:10.1371/journal.pone.0009490 (2010).
128 Huerta-Cepas, J., Serra, F. & Bork, P. ETE 3: Reconstruction, analysis, and visualization of phylogenomic data. *Molecular biology and evolution* **33**, 1635-1638 (2016).
129 Méheust, R., Burstein, D., Castelle, C. J. & Banfield, J. F. The distinction of CPR bacteria from other bacteria based on protein family content. *Nature Communications* **10**, 4173, doi:10.1038/s41467-019-12171-z (2019).
130 Barnum, T. P. *et al.* Genome-resolved metagenomics identifies genetic mobility, metabolic interactions, and unexpected diversity in perchlorate-reducing communities. *ISME J* **12**, 1568-1581, doi:10.1038/s41396-018-0081-5 (2018).
131 Scornavacca, C., Zickmann, F. & Huson, D. H. Tanglegrams for rooted phylogenetic trees and networks. *Bioinformatics* **27**, i248-i256, doi:10.1093/bioinformatics/btr210 (2011).
132 Yip, K. C.-W. & Gu, J.-D. A novel bacterium involved in the degradation of 2-methylindole isolated from sediment of Inner Deep Bay of Hong Kong. *Applied Environmental Biotechnology* **1**, 52-63 (2015).
133 Glazyrina, J. *et al.* High cell density cultivation and recombinant protein production with Escherichia coli in a rocking-motion-type bioreactor. *Microbial Cell Factories* **9**, 1-11, doi:10.1186/1475-2859-9-42 (2010).
134 Loferer-Krössbacher, M., Klima, J. & Psenner, R. Determination of bacterial cell dry mass by transmission electron microscopy and densitometric image analysis. *Applied Environmental Microbiology* **64**, 688-694, doi:10.1128/aem.64.2.688-694.1998 (1998).
135 McInerney, M. J. & Beaty, P. S. Anaerobic community structure from a nonequilibrium thermodynamic perspective. *Canadian Journal of Microbiology* **34**, 487-493, doi:10.1139/m88-083 (1988).
136 Stern, J. H. & Passchier, A. A. The heats of formation of triiodide and iodate ions. *Journal of Physical Chemistry* **66**, 752-753, doi:10.1021/j100810a041 (1962).
137 Weber, K. A., Achenbach, L. A. & Coates, J. D. Microorganisms pumping iron: anaerobic microbial iron oxidation and reduction. *Nature Reviews Microbiology* **4**, 752-764, doi:10.1038/nrmicro1490 (2006).
138 Leimkühler, S. & Iobbi-Nivol, C. Bacterial molybdoenzymes: Old enzymes for new purposes. *FEMS Microbiol Rev* **40**, 1-18, doi:10.1093/femsre/fuv043 (2016).
139 McEwan, A. G., Ridge, J. P., McDevitt, C. A. & Hugenholtz, P. The DMSO reductase family of microbial molybdenum enzymes: Molecular properties and role in the dissimilatory reduction of toxic elements. *Geomicrobiology Journal* **19**, 3-21, doi:10.1080/01490450231724613 8 (2002).
140 Chaudhuri, S. K., O'Connor, S. M., Gustavson, R. L., Achenbach, L. A. & Coates, J. D. Environmental factors that control microbial perchlorate reduction. *Applied and environmental microbiology* **68**, 4425-4430, doi:10.1128/aem.68.9.4425-4430.2002 (2002).
141 Snel, B., Bork, P. & Huynen, M. A. Genomes in flux: the evolution of archaeal and proteobacterial gene content. *Genome research* **12**, 17-25 (2002).

142 Dabir, D. V. *et al.* A role for cytochrome c and cytochrome c peroxidase in electron shuttling from Erv1. *EMBO journal* **26**, 4801-4811 (2007).
143 Martins, D., Kathiresan, M. & English, A. M. Cytochrome c peroxidase is a mitochondrial heme-based H2O2 sensor that modulates antioxidant defense. *Free Radical Biology and Medicine* **65**, 541-551 (2013).
144 Almagro Armenteros, J. J. *et al.* SignalP 5.0 improves signal peptide predictions using deep neural networks. *Nature Biotechnology* **37**, 420-423, doi:10.1038/s41587-019-0036-z (2019).
145 Berks, B. C. The Twin-Arginine Protein Translocation Pathway. *Annual Review of Biochemistry* **84**, 843-864, doi:10.1146/annurev-biochem-060614-034251 (2015).
146 Toporek, M., Michałowska-Kaczmarczyk, A. M. & Michałowski, T. Disproportionation reactions of HIO and NaIO in static and dynamic systems. *American Journal of Analytical Chemistry* **5**, 1046 (2014).
147 Ellis, K. V. & Van Vree, H. B. R. J. Iodine used as a water-disinfectant in turbid waters. *Water Research* **23**, 671-676, doi:https://doi.org/10.1016/0043-1354(89)90198-X (1989).
148 Alternative drinking-water disinfectants: Bromine, iodine, and silver. 52-55 (World Health Organization, 2018).
149 Liebensteiner, M. G., Pinkse, M. W. H., Schaap, P. J., Stams, A. J. M. & Lomans, B. P. Archaeal (per) chlorate reduction at high temperature: An interplay of biotic and abiotic reactions. *Science* **340**, 85-87 (2013).
150 Dudley, M., Salamone, A. & Nerenberg, R. Kinetics of a chlorate-accumulating, perchlorate-reducing bacterium. *Water Research* **42**, 2403-2410, doi:https://doi.org/10.1016/j.watres.2008.01.009 (2008).
151 Melnyk, R. A. *et al.* Novel mechanism for scavenging of hypochlorite involving a periplasmic methionine-rich peptide and methionine sulfoxide reductase. *MBio* **6** (2015).
152 Ordoñez, O. F., Rasuk, M. C., Soria, M. N., Contreras, M. & Farías, M. E. Haloarchaea from the Andean Puna: Biological role in the energy metabolism of arsenic. *Microbial Ecology* **76**, 695-705, doi:10.1007/s00248-018-1159-3 (2018).
153 Anantharaman, K. *et al.* Thousands of microbial genomes shed light on interconnected biogeochemical processes in an aquifer system. *Nature Communications* **7**, 1-11, doi:10.1038/ncomms13219 (2016).
154 Becraft, E. D. *et al.* Rokubacteria: Genomic Giants among the Uncultured Bacterial Phyla. *Frontiers in Microbiology* **8**, doi:10.3389/fmicb.2017.02264 (2017).
155 He, Z. *et al.* A novel denitrifying methanotroph of the NC10 phylum and its microcolony. *Scientific Reports* **6**, 1-10, doi:10.1038/srep32241 (2016).
156 Melnyk, R. A. *et al.* Identification of a perchlorate reduction genomic island with novel regulatory and metabolic genes. *Applied and environmental microbiology* **77**, 7401-7404, doi:10.1128/AEM.05758-11 (2011).
157 Juhas, M. *et al.* Genomic islands: tools of bacterial horizontal gene transfer and evolution. *FEMS Microbiology Reviews* **33**, 376-393, doi:10.1111/j.1574-6976.2008.00136.x (2009).
158 Reiter, W. D., Palm, P. & Yeats, S. Transfer RNA genes frequently serve as integration sites for prokaryotic genetic elements. *Nucleic acids research* **17**, 1907-1914, doi:10.1093/nar/17.5.1907 (1989).
159 Larbig, K. D. *et al.* Gene islands integrated into tRNAGly genes confer genome diversity on a Pseudomonas aeruginosa clone. *Journal of Bacteriology* **184**, 6665-6680, doi:10.1128/JB.184.23.6665-6680.2002 (2002).
160 Boyd, E. & Barkay, T. The mercury resistance operon: from an origin in a geothermal environment to an efficient detoxification machine. *Frontiers in microbiology* **3**, 349 (2012).
161 Besaury, L. *et al.* Abundance and diversity of copper resistance genes cusA and copA in microbial communities in relation to the impact of copper on Chilean marine sediments. *Marine Pollution Bulletin* **67**, 16-25, doi:https://doi.org/10.1016/j.marpolbul.2012.12.007 (2013).

162 Bertelli, C. *et al.* IslandViewer 4: expanded prediction of genomic islands for larger-scale datasets. *Nucleic acids research* **45**, W30-W35, doi:10.1093/nar/gkx343 (2017).
163 Reyes-Umana, V., Henning, Z., Lee, K., Barnum, T. P. & Coates, J. D. Genetic and phylogenetic analysis of dissimilatory iodate-reducing bacteria identifies potential niches across the world's oceans. *The ISME Journal*, doi:10.1038/s41396-021-01034-5 (2021).
164 Palleroni, N. J. in *Bergey's Manual of Systematics of Archaea and Bacteria* 1-1.
165 de Geus, D. C. *et al.* Crystal Structure of Chlorite Dismutase, a Detoxifying Enzyme Producing Molecular Oxygen. *Journal of Molecular Biology* **387**, 192-206, doi:10.1016/j.jmb.2009.01.036 (2009).
166 Boulineau, S. *et al.* Single-cell dynamics reveals sustained growth during diauxic shifts. *PLoS One* **8**, e61686 (2013).
167 Solopova, A. *et al.* Bet-hedging during bacterial diauxic shift. *Proceedings of the National Academy of Sciences* **111**, 7427-7432, doi:10.1073/pnas.1320063111 (2014).
168 Khademian, M. & Imlay, J. A. Escherichia coli cytochrome c peroxidase is a respiratory oxidase that enables the use of hydrogen peroxide as a terminal electron acceptor. *Proceedings of the National Academy of Sciences* **114**, E6922-E6931, doi:10.1073/pnas.1701587114 (2017).
169 Rizzolo, K. *et al.* A widely distributed diheme enzyme from Burkholderia that displays an atypically stable bis-Fe(IV) state. *Nature Communications* **10**, 1101, doi:10.1038/s41467-019-09020-4 (2019).
170 Duval, S., Santini, J. M., Nitschke, W., Hille, R. & Schoepp-Cothenet, B. The small subunit AroB of arsenite oxidase: lessons on the [2Fe-2S] Rieske protein superfamily. *Journal of Biological Chemistry* **285**, 20442-20451 (2010).
171 Schneider, D. & Schmidt, C. L. Multiple Rieske proteins in prokaryotes: Where and why? *Biochimica et Biophysica Acta (BBA) - Bioenergetics* **1710**, 1-12, doi:https://doi.org/10.1016/j.bbabio.2005.09.003 (2005).
172 Ellis, P. J., Conrads, T., Hille, R. & Kuhn, P. Crystal Structure of the 100 kDa Arsenite Oxidase from Alcaligenes faecalis in Two Crystal Forms at 1.64 Å and 2.03 Å. *Structure* **9**, 125-132, doi:https://doi.org/10.1016/S0969-2126(01)00566-4 (2001).
173 Denke, E. *et al.* Alteration of the midpoint potential and catalytic activity of the Rieske iron-sulfur protein by changes of amino acids forming hydrogen bonds to the iron-sulfur cluster. *Journal of Biological Chemistry* **273**, 9085-9093 (1998).
174 Melnyk, R. A., Clark, I. C., Liao, A. & Coates, J. D. Transposon and deletion mutagenesis of genes involved in perchlorate reduction in Azospira suillum PS. *mBio* **5**, e00769-00713, doi:10.1128/mBio.00769-13 (2013).
175 Jackson, W. A. *et al.* Global patterns and environmental controls of perchlorate and nitrate co-occurrence in arid and semi-arid environments. *Geochimica et Cosmochimica Acta* **164**, 502-522, doi:https://doi.org/10.1016/j.gca.2015.05.016 (2015).
176 Lybrand, R. A. *et al.* Nitrate, perchlorate, and iodate co-occur in coastal and inland deserts on Earth. doi:10.1016/j.chemgeo.2016.05.023 (2016).
177 Shalel Levanon, S., San, K.-Y. & Bennett, G. N. Effect of oxygen on the Escherichia coli ArcA and FNR regulation systems and metabolic responses. *Biotechnology and Bioengineering* **89**, 556-564, doi:10.1002/bit.20381 (2005).
178 Fülöp, V., Ridout, C. J., Greenwood, C. & Hajdu, J. Crystal structure of the di-haem cytochrome c peroxidase from Pseudomonas aeruginosa. *Structure* **3**, 1225-1233, doi:https://doi.org/10.1016/S0969-2126(01)00258-1 (1995).
179 Atack, J. M. & Kelly, D. J. in *Advances in Microbial Physiology* Vol. 52 (ed Robert K. Poole) 73-106 (Academic Press, 2006).
180 Turner, S., Reid, E., Smith, H. & Cole, J. A novel cytochrome c peroxidase from Neisseria gonorrhoeae: a lipoprotein from a Gram-negative bacterium. *Biochemical Journal* **373**, 865-873 (2003).

181 Wang, Y. *et al.* MauG, a Novel Diheme Protein Required for Tryptophan Tryptophylquinone Biogenesis. *Biochemistry* **42**, 7318-7325, doi:10.1021/bi034243q (2003).
182 Herren, C. D., Rocha, E. R. & Smith, C. J. Genetic analysis of an important oxidative stress locus in the anaerobe Bacteroides fragilis. *Gene* **316**, 167-175 (2003).
183 Bingham-Ramos, L. K. & Hendrixson, D. R. Characterization of two putative cytochrome c peroxidases of Campylobacter jejuni involved in promoting commensal colonization of poultry. *Infection and immunity* **76**, 1105-1114 (2008).
184 Amann, R. I., Ludwig, W. & Schleifer, K.-H. Phylogenetic identification and in situ detection of individual microbial cells without cultivation. *Microbiological reviews* **59**, 143-169 (1995).
185 Quince, C., Walker, A. W., Simpson, J. T., Loman, N. J. & Segata, N. Shotgun metagenomics, from sampling to analysis. *Nature Biotechnology* **35**, 833-844, doi:10.1038/nbt.3935 (2017).
186 Karsenti, E. The making of Tara Oceans: Funding blue skies research for our Blue Planet. *Molecular Systems Biology* **11**, 811, doi:10.15252/msb.20156271 (2015).
187 Chen, I.-M. A. *et al.* The IMG/M data management and analysis system v. 6.0: new tools and advanced capabilities. *Nucleic acids research* **49**, D751-D763 (2021).
188 Wilkins, L. G. E., Ettinger, C. L., Jospin, G. & Eisen, J. A. Metagenome-assembled genomes provide new insight into the microbial diversity of two thermal pools in Kamchatka, Russia. *Scientific Reports* **9**, 3059, doi:10.1038/s41598-019-39576-6 (2019).
189 Pérez-Cobas, A. E., Gomez-Valero, L. & Buchrieser, C. Metagenomic approaches in microbial ecology: an update on whole-genome and marker gene sequencing analyses. *Microb Genom* **6**, mgen000409, doi:10.1099/mgen.0.000409 (2020).
190 Ribicic, D. *et al.* Microbial community and metagenome dynamics during biodegradation of dispersed oil reveals potential key-players in cold Norwegian seawater. *Marine Pollution Bulletin* **129**, 370-378, doi:https://doi.org/10.1016/j.marpolbul.2018.02.034 (2018).
191 Nayfach, S. *et al.* A genomic catalog of Earth's microbiomes. *Nature Biotechnology*, doi:10.1038/s41587-020-0718-6 (2020).
192 Cock, P. J. *et al.* Biopython: Freely available Python tools for computational molecular biology and bioinformatics. *Bioinformatics* **25**, 1422-1423 (2009).
193 Pesant, S. *et al.* Open science resources for the discovery and analysis of Tara Oceans data. *Scientific Data* **2**, 1-16, doi:10.1038/sdata.2015.23 (2015).
194 Langmead, B. & Salzberg, S. L. Fast gapped-read alignment with Bowtie 2. *Nature methods* **9**, 357 (2012).
195 Li, H. *et al.* The sequence alignment/map format and SAMtools. *Bioinformatics* **25**, 2078-2079 (2009).
196 Wagner, G. P., Kin, K. & Lynch, V. J. Measurement of mRNA abundance using RNA-seq data: RPKM measure is inconsistent among samples. *Theory in Biosciences* **131**, 281-285, doi:10.1007/s12064-012-0162-3 (2012).
197 Pedregosa, F. *et al.* Scikit-learn: Machine learning in Python. *Journal of Machine Learning Research* **12**, 2825-2830 (2011).
198 Azur, M. J., Stuart, E. A., Frangakis, C. & Leaf, P. J. Multiple imputation by chained equations: what is it and how does it work? *Int J Methods Psychiatr Res* **20**, 40-49, doi:10.1002/mpr.329 (2011).
199 Graham, E., Heidelberg, J. & Tully, B. Potential for primary productivity in a globally-distributed bacterial phototroph. *The ISME journal* **12**, 1861-1866 (2018).
200 Hug, L. A. *et al.* A new view of the tree of life. *Nature Microbiology* **1**, doi:10.1038/nmicrobiol.2016.48 (2016).
201 Hug, L. A. *et al.* A new view of the tree of life. *Nature Microbiology* **1**, doi:10.1038/nmicrobiol.2016.48 (2016).
202 Capella-Gutiérrez, S., Silla-Martínez, J. M. & Gabaldón, T. trimAl: a tool for automated alignment trimming in large-scale phylogenetic analyses. *Bioinformatics* **25**, 1972-1973 (2009).

203 Jin, H. M. *et al.* Litorimicrobium taeanense gen. nov., sp. nov., isolated from a sandy beach. *International Journal of Systematic and Evolutionary Microbiology* **61**, 1392-1396, doi:https://doi.org/10.1099/ijs.0.025007-0 (2011).
204 Alex, A. & Antunes, A. Comparative Genomics Reveals Metabolic Specificity of Endozoicomonas Isolated from a Marine Sponge and the Genomic Repertoire for Host-Bacteria Symbioses. *Microorganisms* **7**, 635 (2019).
205 Kim, Y.-O. *et al.* Litoreibacter ascidiaceicola sp. nov., isolated from the golden sea squirt Halocynthiaaurantium. *Int. J. Syst. Evol. Microbiol.* **64**, 2545-2550, doi:https://doi.org/10.1099/ijs.0.064196-0 (2014).
206 Kupper, F. C. *et al.* Iodide accumulation provides kelp with an inorganic antioxidant impacting atmospheric chemistry. *Proceedings of the National Academy of Sciences, USA* **105**, 6954-6958, doi:10.1073/pnas.0709959105 (2008).
207 Jung, H. S., Jeong, S. E., Chun, B. H., Quan, Z.-X. & Jeon, C. O. Rhodophyticola porphyridii gen. nov., sp. nov., isolated from a red alga, Porphyridium marinum. *International Journal of Systematic and Evolutionary Microbiology* **69**, 1656-1661, doi:https://doi.org/10.1099/ijsem.0.003371 (2019).
208 Lachkar, Z., Lévy, M. & Smith, K. S. Strong intensification of the Arabian Sea oxygen minimum zone in response to Arabian Gulf warming. *Geophysical Research Letters* **46**, 5420-5429, doi:10.1029/2018gl081631 (2019).
209 Farrenkopf, A. M. & Luther, G. W. Iodine chemistry reflects productivity and denitrification in the Arabian Sea: evidence for flux of dissolved species from sediments of western India into the OMZ. *Deep-Sea Res Pt II* **49**, 2303-2318 (2002).
210 Bertagnolli, A. D. & Stewart, F. J. Microbial niches in marine oxygen minimum zones. *Nature Reviews Microbiology* **16**, 723-729, doi:10.1038/s41579-018-0087-z (2018).
211 Cutter, G. A., Moffett, J. W., Nielsdóttir, M. C. & Sanial, V. Multiple oxidation state trace elements in suboxic waters off Peru: In situ redox processes and advective/diffusive horizontal transport. *Marine Chemistry* **201**, 77-89, doi:10.1016/J.MARCHEM.2018.01.003 (2018).
212 Karstensen, J., Stramma, L. & Visbeck, M. Oxygen minimum zones in the eastern tropical Atlantic and Pacific oceans. *Progress in Oceanography* **77**, 331-350, doi:https://doi.org/10.1016/j.pocean.2007.05.009 (2008).
213 Farrenkopf, A. M., Luther, G. W., Truesdale, V. W. & Van Der Weijden, C. H. Sub-surface iodide maxima: evidence for biologically catalyzed redox cycling in Arabian Sea OMZ during the SW intermonsoon. *Deep-Sea Res Pt II.* **44**, 1391-1409, doi:https://doi.org/10.1016/S0967-0645(97)00013-1 (1997).
214 Kalvelage, T. *et al.* Aerobic microbial respiration in oceanic oxygen minimum zones. *PLoS One* **10**, e0133526-e0133526, doi:10.1371/journal.pone.0133526 (2015).
215 Howarth, R. W. Nutrient limitation of net primary production in marine ecosystems. *Annual review of ecology and systematics* **19**, 89-110 (1988).
216 Wright, J. J., Konwar, K. M. & Hallam, S. J. Microbial ecology of expanding oxygen minimum zones. *Nature Reviews Microbiology* **10**, 381-394, doi:10.1038/nrmicro2778 (2012).
217 Hardisty, D. S. *et al.* Limited iodate reduction in shipboard seawater incubations from the Eastern Tropical North Pacific oxygen deficient zone. *Earth and Planetary Science Letters.* **554**, 116676, doi:https://doi.org/10.1016/j.epsl.2020.116676 (2021).
218 Reysenbach, A.-L., Banta, A. B., Boone, D. R., Cary, S. C. & Luther, G. W. Microbial essentials at hydrothermal vents. *Nature* **404**, 835-835, doi:10.1038/35009029 (2000).
219 Amend, J. P. & Teske, A. in *Geobiology: Objectives, Concepts, Perspectives* (ed N. Noffke) 131-155 (Elsevier, 2005).
220 Khan, M., Rhew, R., Whelan, M., Zhou, K. & Deverel, S. Methyl halide and chloroform emissions from a subsiding Sacramento–San Joaquin delta island converted to rice fields. *Atmospheric environment* **45**, 977-985 (2011).

221 Roulier, M. *et al.* Iodine budget in forest soils: Influence of environmental conditions and soil physicochemical properties. *Chemosphere* **224**, 20-28, doi:10.1016/J.CHEMOSPHERE.2019.02.060 (2019).
222 Bowman, J. P., McCammon, S. A., Brown, M. V., Nichols, D. S. & McMeekin, T. A. Diversity and association of psychrophilic bacteria in Antarctic sea ice. *Applied and Environmental Microbiology* **63**, 3068-3078 (1997).
223 Zhang, D.-C. *et al.* Marinobacter psychrophilus sp. nov., a psychrophilic bacterium isolated from the Arctic. *International Journal of Systematic and Evolutionary Microbiology* **58**, 1463-1466, doi:https://doi.org/10.1099/ijs.0.65690-0 (2008).
224 Zaikova, E. *et al.* Microbial community dynamics in a seasonally anoxic fjord: Saanich Inlet, British Columbia. *Environmental Microbiology* **12**, 172-191, doi:https://doi.org/10.1111/j.1462-2920.2009.02058.x (2010).
225 Sheik, C. S., Jain, S. & Dick, G. J. Metabolic flexibility of enigmatic SAR324 revealed through metagenomics and metatranscriptomics. *Environmental Microbiology* **16**, 304-317, doi:https://doi.org/10.1111/1462-2920.12165 (2014).
226 Swan, B. K. *et al.* Potential for chemolithoautotrophy among ubiquitous bacteria lineages in the dark ocean. *Science* **333**, 1296-1300 (2011).
227 Mizuno, C. M., Rodriguez-Valera, F., Ghai, R. & Giovannoni, S. J. Genomes of Planktonic Acidimicrobiales: Widening Horizons for Marine Actinobacteria by Metagenomics. *mBio* **6**, e02083-02014, doi:doi:10.1128/mBio.02083-14 (2015).
228 Parks, D. H. *et al.* Recovery of nearly 8,000 metagenome-assembled genomes substantially expands the tree of life. *Nature Microbiology* **2**, 1533-1542, doi:10.1038/s41564-017-0012-7 (2017).
229 Ettwig, K. F. *et al.* Nitrite-driven anaerobic methane oxidation by oxygenic bacteria. *Nature* **464**, 543-548, doi:10.1038/nature08883 (2010).
230 Mise, K., Masuda, Y., Senoo, K., Itoh, H. & Tringe, S. G. Undervalued Pseudo-nifH Sequences in Public Databases Distort Metagenomic Insights into Biological Nitrogen Fixers. *mSphere* **0**, e00785-00721, doi:doi:10.1128/msphere.00785-21.
231 Fuge, R. & Johnson, C. C. Iodine and human health, the role of environmental geochemistry and diet, a review. *Applied Geochemistry* **63**, 282-302, doi:10.1016/j.apgeochem.2015.09.013 (2015).
232 Saiz-Lopez, A. *et al.* Atmospheric Chemistry of Iodine. *Chemical Reviews* **112**, 1773-1804, doi:10.1021/cr200029u (2012).
233 Baker, A. R., Tunnicliffe, C. & Jickells, T. D. Iodine speciation and deposition fluxes from the marine atmosphere. *Journal of Geophysical Research: Atmospheres* **106**, 28743-28749, doi:https://doi.org/10.1029/2000JD000004 (2001).
234 Coates, J. D. *et al.* Ubiquity and diversity of dissimilatory (per)chlorate-reducing bacteria. *Appl. Environ. Microbiol.* **65**, 5234-5241 (1999).
235 Farby, M. (ed San Mateo Countywide Water Pollution Prevention Program) (EOA Inc, Oakland, CA, 2020).
236 Song, B., Häggblom, M. M., Zhou, J., Tiedje, J. M. & Palleroni, N. J. Taxonomic characterization of denitrifying bacteria that degrade aromatic compounds and description of Azoarcus toluvorans sp. nov. and Azoarcus toluclasticus sp. nov. *Int. J. Syst. Evol. Microbiol.* **49**, 1129-1140 (1999).
237 Rabus, R. *et al.* Aromatoleum gen. nov., a novel genus accommodating the phylogenetic lineage including Azoarcus evansii and related species, and proposal of Aromatoleum aromaticum sp. nov., Aromatoleum petrolei sp. nov., Aromatoleum bremense sp. nov., Aromatoleum toluolicum sp. nov. and Aromatoleum diolicum sp. nov. *Int. J. Syst. Evol. Microbiol.* **69**, 982-997 (2019).
238 Martín-Moldes, Z. *et al.* Whole-genome analysis of Azoarcus sp. strain CIB provides genetic insights to its different lifestyles and predicts novel metabolic features. *Syst. Appl. Microbiol.* **38**, 462-471, doi:https://doi.org/10.1016/j.syapm.2015.07.002 (2015).
239 Reinhold-Hurek, B., Tan, Z. & Hurek, T. Azoarcus. *Bergey's Manual of Systematics of Archaea and Bacteria*, 1-19 (2015).

240 Bankevich, A. *et al.* SPAdes: a new genome assembly algorithm and its applications to single-cell sequencing. *Journal of computational biology : a journal of computational molecular cell biology* **19**, 455-477, doi:10.1089/cmb.2012.0021 (2012).
241 Durrant, M. G., Li, M. M., Siranosian, B. A., Montgomery, S. B. & Bhatt, A. S. A Bioinformatic Analysis of Integrative Mobile Genetic Elements Highlights Their Role in Bacterial Adaptation. *Cell Host & Microbe* **27**, 140-153.e149, doi:10.1016/j.chom.2019.10.022 (2020).
242 Price, M. N., Dehal, P. S. & Arkin, A. P. FastTree 2–approximately maximum-likelihood trees for large alignments. *PloS one* **5**, e9490 (2010).
243 Letunic, I. & Bork, P. Interactive tree of life (iTOL) v3: an online tool for the display and annotation of phylogenetic and other trees. *Nucleic Acids Research* **44**, W242-W245, doi:10.1093/nar/gkw290 (2016).
244 Benson, G. Tandem repeats finder: a program to analyze DNA sequences. *Nucleic Acids Research* **27**, 573-580, doi:10.1093/nar/27.2.573 (1999).
245 Schwarz, G. & Mendel, R. R. MOLYBDENUM COFACTOR BIOSYNTHESIS AND MOLYBDENUM ENZYMES. *Annual Review of Plant Biology* **57**, 623-647, doi:10.1146/annurev.arplant.57.032905.105437 (2006).
246 Clark, I. C., Melnyk, R. A., Engelbrektson, A. & Coates, J. D. Structure and evolution of chlorate reduction composite transposons. *mBio* **4**, e00379-00313, doi:10.1128/mBio.00379-13 (2013).
247 Woese, C. R. *et al.* Conservation of primary structure in 16S ribosomal RNA. *Nature* **254**, 83-86, doi:10.1038/254083a0 (1975).
248 Federhen, S. The NCBI Taxonomy database. *Nucleic Acids Research* **40**, D136-D143, doi:10.1093/nar/gkr1178 (2012).
249 Achenbach, L. A. & Coates, J. D. Disparity between bacterial phylogeny and physiology. *ASM news* **66**, 714-715 (2000).
250 Wang, Z., Li, W., Li, H., Zheng, W. & Guo, F. Phylogenomics of Rhodocyclales and its distribution in wastewater treatment systems. *Scientific Reports* **10**, 3883, doi:10.1038/s41598-020-60723-x (2020).
251 Reinhold-Hurek, B. & Hurek, T. Reassessment of the taxonomic structure of the diazotrophic genus Azoarcus sensu lato and description of three new genera and new species, Azovibrio restrictus gen. nov., sp. nov., Azospira oryzae gen. nov., sp. nov. and Azonexus fungiphilus gen. nov., sp. nov. *Int. J. Syst. Evol. Microbiol.* **50**, 649-659 (2000).
252 Hurek, T. & Reinhold-Hurek, B. Azoarcus sp. strain BH72 as a model for nitrogen-fixing grass endophytes. *J. Biotechnol.* **106**, 169-178, doi:https://doi.org/10.1016/j.jbiotec.2003.07.010 (2003).
253 Egener, T., Martin, D., Hurek, T. & Reinhold-Hurek, B. in *Biological Nitrogen Fixation for the 21st Century* 377-378 (Springer, 1998).
254 Raittz, R. T. *et al.* Comparative Genomics Provides Insights into the Taxonomy of Azoarcus and Reveals Separate Origins of Nif Genes in the Proposed Azoarcus and Aromatoleum Genera. *Genes* **12**, 71 (2021).
255 Lueders, T. The ecology of anaerobic degraders of BTEX hydrocarbons in aquifers. *FEMS Microbiol. Ecol.* **93**, fiw220 (2017).
256 Kasai, Y., Takahata, Y., Manefield, M. & Watanabe, K. RNA-Based Stable Isotope Probing and Isolation of Anaerobic Benzene-Degrading Bacteria from Gasoline-Contaminated Groundwater. *Applied and Environmental Microbiology* **72**, 3586-3592, doi:10.1128/aem.72.5.3586-3592.2006 (2006).
257 Orla-Jensen, S. The Main Lines of the Natural Bacterial System. *J. Bacteriol.* **6**, 263-273, doi:10.1128/JB.6.3.263-273.1921 (1921).
258 Buchanan, R. E., Breed, R. S. & Rettger, L. F. A DIAGRAMMATIC SUMMARY OF VARIOUS BACTERIAL CLASSIFICATIONS. *J. Bacteriol.* **16**, 387-396, doi:10.1128/JB.16.6.387-396.1928 (1928).

259 Barnum, T. P. *et al.* Identification of a parasitic symbiosis between respiratory metabolisms in the biogeochemical chlorine cycle. *The ISME Journal* **14**, 1194-1206, doi:10.1038/s41396-020-0599-1 (2020).
260 De Vos, P. & Truper, H. Judicial commission of the international committee on systematic bacteriology; IXth international (IUMS) congress of bacteriology and applied microbiology. *International Journal of Systematic and Evolutionary Microbiology* **50**, 2239-2244, doi:https://doi.org/10.1099/00207713-50-6-2239 (2000).
261 Parte, A. C., Sardà Carbasse, J., Meier-Kolthoff, J. P., Reimer, L. C. & Göker, M. List of Prokaryotic names with Standing in Nomenclature (LPSN) moves to the DSMZ. *International Journal of Systematic and Evolutionary Microbiology* **70**, 5607-5612, doi:https://doi.org/10.1099/ijsem.0.004332 (2020).
262 Olm, M. R. *et al.* Consistent metagenome-derived metrics verify and delineate bacterial species boundaries. *Msystems* **5**, e00731-00719 (2020).
263 Chaumeil, P. A., Mussig, A. J., Hugenholtz, P. & Parks, D. H. GTDB-Tk: a toolkit to classify genomes with the Genome Taxonomy Database. *Bioinformatics* **36**, 1925-1927, doi:10.1093/bioinformatics/btz848 (2019).
264 Barco, R. A. *et al.* A Genus Definition for Bacteria and Archaea Based on a Standard Genome Relatedness Index. *mBio* **11**, e02475-02419, doi:10.1128/mBio.02475-19 (2020).
265 Jain, C., Rodriguez-R, L. M., Phillippy, A. M., Konstantinidis, K. T. & Aluru, S. High throughput ANI analysis of 90K prokaryotic genomes reveals clear species boundaries. *Nature Communications* **9**, 5114, doi:10.1038/s41467-018-07641-9 (2018).
266 Méheust, R., Burstein, D., Castelle, C. J. & Banfield, J. F. The distinction of CPR bacteria from other bacteria based on protein family content. *Nature communications* **10**, 1-12 (2019).
267 Ren, H. *et al.* A high power density miniaturized microbial fuel cell having carbon nanotube anodes. *Journal of Power Sources* **273**, 823-830, doi:https://doi.org/10.1016/j.jpowsour.2014.09.165 (2015).
268 Ramos-Padrón, E. *et al.* Carbon and sulfur cycling by microbial communities in a gypsum-treated oil sands tailings pond. *Environ. Sci. Technol.* **45**, 439-446 (2011).
269 McDonald, D. *et al.* An improved Greengenes taxonomy with explicit ranks for ecological and evolutionary analyses of bacteria and archaea. *The ISME Journal* **6**, 610-618, doi:10.1038/ismej.2011.139 (2012).
270 Inc., S. G. *The Greengenes Database*, <https://greengenes.secondgenome.com/> (2021).
271 Pruesse, E. *et al.* SILVA: a comprehensive online resource for quality checked and aligned ribosomal RNA sequence data compatible with ARB. *Nucleic acids research* **35**, 7188-7196 (2007).
272 Whitman, W. B. Genome sequences as the type material for taxonomic descriptions of prokaryotes. *Syst. Appl. Microbiol.* **38**, 217-222, doi:https://doi.org/10.1016/j.syapm.2015.02.003 (2015).
273 Boden, R., Hutt, L. P. & Rae, A. W. Reclassification of Thiobacillus aquaesulis (Wood & Kelly, 1995) as Annwoodia aquaesulis gen. nov., comb. nov., transfer of Thiobacillus (Beijerinck, 1904) from the Hydrogenophilales to the Nitrosomonadales, proposal of Hydrogenophilalia class. nov. within the 'Proteobacteria', and four new families within the orders Nitrosomonadales and Rhodocyclales. *International Journal of Systematic and Evolutionary Microbiology* **67**, 1191-1205, doi:https://doi.org/10.1099/ijsem.0.001927 (2017).
274 Parks, D. H. *et al.* A standardized bacterial taxonomy based on genome phylogeny substantially revises the tree of life. *Nature Biotechnology* **36**, 996-1004, doi:10.1038/nbt.4229 (2018).
275 Lau, C. K., Krewulak, K. D. & Vogel, H. J. Bacterial ferrous iron transport: the Feo system. *FEMS Microbiol. Rev.* **40**, 273-298, doi:10.1093/femsre/fuv049 (2016).

276 Carlson, H. K., Clark, I. C., Blazewicz, S. J., Iavarone, A. T. & Coates, J. D. Fe(II) oxidation is an innate capability of nitrate-reducing bacteria that involves abiotic and biotic reactions. *Journal of bacteriology* **195**, 3260-3268, doi:10.1128/JB.00058-13 (2013).
277 Higgins, S., Gualdi, S., Pinto-Carbó, M. & Eberl, L. Copper resistance genes of Burkholderia cenocepacia H111 identified by transposon sequencing. *Environmental Microbiology Reports* **12**, 241-249, doi:https://doi.org/10.1111/1758-2229.12828 (2020).
278 Zimniak, P. & Barnes Jr, E. M. Characterization of a calcium/proton antiporter and an electrogenic calcium transporter in membrane vesicles from Azotobacter vinelandii. *Journal of Biological Chemistry* **255**, 10140-10143 (1980).
279 Nakamura, T., Hsu, C. & Rosen, B. P. Cation/proton antiport systems in Escherichia coli. Solubilization and reconstitution of delta pH-driven sodium/proton and calcium/proton antiporters. *Journal of Biological Chemistry* **261**, 678-683, doi:https://doi.org/10.1016/S0021-9258(17)36146-X (1986).
280 Domínguez, D. C., Guragain, M. & Patrauchan, M. Calcium binding proteins and calcium signaling in prokaryotes. *Cell Calcium* **57**, 151-165, doi:https://doi.org/10.1016/j.ceca.2014.12.006 (2015).
281 Waditee, R. *et al.* Isolation and functional characterization of Ca2+/H+ antiporters from cyanobacteria. *Journal of Biological Chemistry* **279**, 4330-4338 (2004).
282 Tortell, P. D., Maldonado, M. T. & Price, N. M. The role of heterotrophic bacteria in iron-limited ocean ecosystems. *Nature* **383**, 330-332, doi:10.1038/383330a0 (1996).
283 Morel, F. M. M. & Price, N. M. The biogeochemical cycles of trace metals in the oceans. *Science* **300**, 944-947, doi:10.1126/science.1083545 (2003).
284 Kogure, K. Bioenergetics of marine bacteria. *Curr. Opin. Biotechnol.* **9**, 278-282, doi:https://doi.org/10.1016/S0958-1669(98)80059-1 (1998).
285 Verkhovsky, M. I. & Bogachev, A. V. Sodium-translocating NADH:quinone oxidoreductase as a redox-driven ion pump. *Biochim. Biophys. Acta* **1797**, 738-746, doi:https://doi.org/10.1016/j.bbabio.2009.12.020 (2010).
286 Mertens, J., Aliyu, H. & Cowan, D. A. LEA Proteins and the Evolution of the WHy Domain. *Appl. Environ. Microbiol.* **84**, e00539-00518, doi:10.1128/aem.00539-18 (2018).
287 Comfort, D. & Clubb, R. T. A comparative genome analysis identifies distinct sorting pathways in gram-positive bacteria. *Infect. Immun.* **72**, 2710-2722, doi:10.1128/iai.72.5.2710-2722.2004 (2004).
288 Sakamaki, T., Nishimura, O. & Sudo, R. Tidal time-scale variation in nutrient flux across the sediment–water interface of an estuarine tidal flat. *Estuar. Coast. Shelf Sci.* **67**, 653-663, doi:https://doi.org/10.1016/j.ecss.2006.01.005 (2006).
289 Sturtevant, W. C. *Handbook of North American Indians: California*. 485-495 (Smithsonian Institution, 1978).
290 Richter, M. & Rosselló-Móra, R. Shifting the genomic gold standard for the prokaryotic species definition. *Proceedings of the National Academy of Sciences* **106**, 19126-19131, doi:10.1073/pnas.0906412106 (2009).